

Helicity Evolution at Small x : Quark to Gluon and Gluon to Quark Transition Operators

Jeremy Borden,^{*} Yuri V. Kovchegov,[†] and Ming Li[‡]

Department of Physics, The Ohio State University, Columbus, OH 43210, USA

We include the quark to gluon and gluon to quark shock-wave transition operators into the small Bjorken- x evolution equations for helicity in the flavor-singlet channel derived earlier in [1–3]. While such transitions do not affect the large- N_c version of the evolution equations for helicity, the large- $N_c&N_f$ equations are affected. (N_c and N_f are the numbers of quark colors and flavors, respectively.) We derive the corresponding corrected large- $N_c&N_f$ equations for the polarized dipole amplitudes contributing to the flavor-singlet quark and gluon helicity distributions in the double-logarithmic approximation (DLA), resumming powers of $\alpha_s \ln^2(1/x)$ with α_s the strong coupling constant. We solve these equations iteratively and extract the polarized splitting functions up to four loops. We show that our splitting functions agree with the fixed-order perturbative calculations up to and including the existing three-loops results [4–7]. Similar to the large- N_c helicity evolution in the shock-wave approach [8], our large- $N_c&N_f$ small- x splitting functions agree with those obtained in the infrared evolution equations framework from [9, 10] up to three loops, but appear to slightly disagree at four loops.

PACS numbers: 12.38.-t, 12.38.Bx, 12.38.Cy

CONTENTS

I. Introduction	2
II. Polarized Wilson lines: a recap	3
III. Derivation of the Quark to Gluon and Gluon to Quark Contribution to Helicity Evolution	6
A. Quark to Gluon and Gluon to Quark Transition Operators	6
B. Contribution to the evolution of the adjoint dipole amplitude of the first type	8
1. Diagrams calculation	8
2. Simplifications in the DLA and at large $N_c&N_f$	10
C. Evolution for \tilde{Q}	12
1. The DLA evolution equation for \tilde{Q}	12
2. A relation between \tilde{Q} and the quark helicity TMD and PDF	15
D. Contribution to the evolution for the dipole amplitude Q	16
E. A new version of the large- $N_c&N_f$ evolution equations	18
IV. Iterative Solution	20
A. Step 1	20
B. Step 2	21
C. Step 3	22
D. Summary of our results up to three loops	23
E. Step 4	24
V. Conclusions and Outlook	24
Acknowledgments	25
A. Derivation of the large- $N_c&N_f$ Evolution Equations using Light-Cone Perturbation Theory	25
1. Light-cone Wavefunctions	25
2. Contribution to the evolution of the adjoint dipole amplitude of the first type	26
3. Evolution for \tilde{Q}	30

^{*} Email: borden.75@buckeyemail.osu.edu

[†] Email: kovchegov.1@osu.edu

[‡] Email: li.13449@osu.edu

I. INTRODUCTION

In the past decade significant advances have been achieved toward constructing small- x evolution equations for helicity parton distribution functions (hPDFs) and related to them g_1 structure function of a nucleon [1–3, 8, 11–23]. Most of this work was carried out using the s -channel evolution/shock wave formalism [24–36], which had been developed earlier to address the problem of gluon saturation in the proton and nuclear wave functions. The aim of developing small- x evolution for helicity distributions and observables is to help solve the proton spin puzzle [37–48] by theoretically and phenomenologically constraining the amount of the proton spin carried by small- x partons. Phenomenological implementation of the formalism from [1–3, 8, 11–16, 18–20, 22, 23] to describe the polarized deep inelastic scattering (DIS) and semi-inclusive DIS (SIDIS) small- x data has been recently carried out in [49, 50].

Derivation of the helicity evolution equations at small x [1–3, 12] utilizes the sub-eikonal corrections to the eikonal shock wave formalism computed in [2, 15, 51–66]. The first step is to simplify the distribution functions, such as the flavor-singlet quark and gluon hPDFs $\Delta\Sigma(x, Q^2)$ and $\Delta G(x, Q^2)$, at small x by rewriting them in terms of the dipole scattering amplitudes on the target proton. These dipole amplitudes are different from the case of the eikonal spin-independent scattering of [24–36], where the dipole amplitudes are correlators of pairs of infinite light-cone Wilson lines. Since Wilson lines do not couple to the target proton helicity, for helicity observables one needs to improve the precision of the calculation by employing the sub-eikonal corrections to the Wilson lines: these corrections are suppressed by one power of energy compared to the eikonal terms. The sub-eikonal corrections come in the form of insertions of one or two local sub-eikonal operators into the infinite light-cone Wilson line [2, 15, 51–57, 60–66]. We will call the resulting objects ‘polarized Wilson lines’: they are detailed in Sec. II below. When a polarized Wilson line is combined in a color trace with the regular infinite light-cone Wilson line (with one of them conjugated) and the resulting operator is evaluated in the polarized nucleon state, one obtains the so-called ‘polarized dipole scattering amplitude’. Since there exist different types of polarized Wilson lines, there exist different types of polarized dipole amplitudes [3], in contrast to the single unpolarized dipole amplitude in the eikonal scattering case (for a given color representation of the partons). The hPDFs $\Delta\Sigma$ and ΔG , along with the g_1 structure function, can all be expressed at small x in terms of the polarized dipole amplitudes [1–3, 12].

In the shock wave formalism, the small- x evolution equations for helicity are written for the polarized Wilson lines correlators with the regular light-cone Wilson lines [1–3, 12, 21]. At the leading order, the equations re-sum powers of the double-logarithmic parameters $\alpha_s \ln^2(1/x)$ and $\alpha_s \ln(1/x) \ln(Q^2/\Lambda^2)$, with α_s the strong coupling constant, Q the hard momentum scale, and Λ the infrared (IR) cutoff. This is the double logarithmic approximation (DLA). The equations are not closed in general (cf. [27]). They close in the large- N_c limit [67] and, unlike the unpolarized case, in the large- N_c & N_f limit [68] as well. The large- N_c equations, whose current version was derived in [3], were solved numerically in the same reference, and analytically in [8]. The gluon–gluon polarized anomalous dimension for the polarized Dokshitzer-Gribov-Lipatov-Altarelli-Parisi (DGLAP) evolution equations [4, 5, 69] obtained in [8] was shown to agree with the small- x large- N_c limit of the existing perturbative calculations [4–7, 70–77] to the three known loops. The same three-loop agreement with the known gluon–gluon splitting function was observed by iteratively solving the large- N_c helicity evolution equations in [3]. The gluon–gluon polarized anomalous dimension from [8] appears to differ from that extracted out of the work by Bartels, Ermolaev and Ryskin (BER) [9]. The latter reference used the infrared evolution equations (IREE) approach [78–82] to extract small- x expressions for quark and gluon hPDFs. The gluon–gluon polarized anomalous dimensions of [3] and [9], when expanded as power series in α_s , agree to the three known loops, and disagree beyond that.

The large- N_c & N_f helicity evolution equations from [3] were solved numerically in [23]. In the latter reference an iterative solution of these large- N_c & N_f equations was constructed, resulting in the polarized splitting functions, which, in the terms containing N_f , appeared to deviate from the existing known finite-order $\overline{\text{MS}}$ results [4–7] at the next-to-leading order (NLO). The disagreement could not be attributed to a scheme dependence [23]. In addition, an analytic solution of the large- N_c & N_f helicity evolution equations from [3] was constructed by a subset of the authors using the same general approach as that used in [8], also exhibiting a deviation in N_f -dependent terms from the NLO fixed-order calculations [4–7]. A possible explanation of this disagreement is that a contribution is missing in the large- N_c & N_f helicity evolution equations from [3]: this is the possibility we will explore in this work, ultimately identifying the missing contribution and correcting the evolution equations by including it.

The helicity evolution derived in [1–3, 12] only involved the polarized Wilson lines where the incoming quark becomes an outgoing quark after interacting with the shock wave, or an incoming gluon becomes an outgoing gluon. The *transition* operators, where the incoming (anti-)quark interacts with the shock wave and becomes an outgoing gluon, and, vice versa, an incoming gluon becomes the outgoing (anti-)quark (see Fig. 1 below) were considered in

[1, 12], but were not included in the calculation since they were perceived to cancel for the flavor-singlet quantities [1, 12], not contributing to the flavor-singlet helicity evolution equations in the DLA analysis performed there. The contribution of such transition operators was extensively studied by Chirilli in [21]: they enter the DLA helicity evolution equations derived in that reference. Note that the flavor-singlet versus non-singlet decomposition is done differently in [21] from [1, 3, 12]. The importance of the transition operators for the flavor non-singlet helicity evolution was also recognized in [12], but the contribution of these operators was (correctly) neglected in that reference as sub-leading in the large- N_c limit employed there, leading to the same small- x asymptotics as that obtained by BER in [83] for the flavor non-singlet case (if one takes the large- N_c limit of the latter).

In this work we show that the $q/\bar{q} \rightarrow G$ and $G \rightarrow q/\bar{q}$ shock-wave transition operators do indeed generate DLA terms and contribute to helicity evolution equations in the flavor-singlet channel. We explicitly derive and include the correction due to the transition operators into the large- N_c & N_f helicity evolution equations derived in [3]. The large- N_c helicity evolution equations from [3] remain unchanged, since they include the gluon contributions only. We verify the corrected large- N_c & N_f helicity evolution equations we obtain below by solving them iteratively: this results in the polarized DGLAP splitting functions agreeing with BER [9] to three loops. Our splitting functions also agree with the (small- x and large- N_c & N_f limit of the) fixed-order $\overline{\text{MS}}$ polarized splitting functions [4–7] at one and two loops. The agreement at three loops is achieved after a minor scheme transformation: the same is true for BER splitting functions [7]. The observed agreement applies to all N_c - and N_f -dependent terms in the splitting functions. We also predict the 4-loop polarized DGLAP splitting functions at small- x and large- N_c & N_f .

Our paper is structured as follows. In Sec. II we list the polarized Wilson lines and polarized dipole amplitudes employed in [1–3]. We derive the corrected helicity evolution equations in Sec. III using the light-cone operator treatment (LCOT) method [2, 3, 15, 60]. We first derive the $q/\bar{q} \rightarrow G$ and $G \rightarrow q/\bar{q}$ shock-wave transition operators in Sec. III A. The correction to the evolution of the adjoint type-1 dipole amplitude (in the notation of [3]) is derived in Sec. III B. This correction contains an expectation value of a new operator, which we denote \tilde{Q} . This operator is proportional to the quark helicity transverse momentum-dependent (TMD) PDF and, hence, cannot be called a (polarized) dipole amplitude. The evolution of \tilde{Q} is derived in Sec. III C, and it is found to be related to the quark helicity TMD and the flavor-singlet PDF $\Delta\Sigma$. For completeness, we also find the contribution of the transition operators to the evolution of the type-1 fundamental dipole amplitude Q in Sec. III D: such contribution is suppressed in the large- N_c & N_f limit. The corrected large- N_c & N_f helicity evolution equations are summarized in Sec. III E. (These corrected equations are re-derived in Appendix A using the light-cone perturbation theory (LCPT) [84, 85].) We cross-check these equations against known polarized DGLAP anomalous dimensions [4–7] by performing an iterative solution in Sec. IV and extracting the anomalous dimension perturbatively, finding a complete agreement at the first three loops with the $\overline{\text{MS}}$ polarized splitting functions [4–7] (modulo a scheme transformation at 3 loops) mentioned above and predicting the 4-loop polarized DGLAP splitting functions at low x . We conclude in Sec. V.

II. POLARIZED WILSON LINES: A RECAP

In this Section we briefly review the main results of the earlier works that we will build on below. For a quark scattering on a quark and gluon background field, the sub-eikonal S -matrix is [2, 15, 51–57, 60–66]

$$V_{\underline{x}, \underline{y}; \sigma', \sigma} \Big|_{\text{sub-eikonal}} \equiv \sigma \delta_{\sigma, \sigma'} \left[V_{\underline{x}}^{\text{G}[1]} + V_{\underline{x}}^{\text{q}[1]} \right] \delta^2(\underline{x} - \underline{y}) + \delta_{\sigma, \sigma'} \left[V_{\underline{x}, \underline{y}}^{\text{G}[2]} + V_{\underline{x}}^{\text{q}[2]} \right] \delta^2(\underline{x} - \underline{y}), \quad (1)$$

where the fundamental polarized Wilson lines of the first and second type (denoted by [1] and [2] in the superscript, respectively) are

$$V_{\underline{x}}^{\text{G}[1]} = \frac{igp_1^+}{s} \int_{-\infty}^{\infty} dx^- V_{\underline{x}}[\infty, x^-] F^{12}(x^-, \underline{x}) V_{\underline{x}}[x^-, -\infty], \quad (2a)$$

$$V_{\underline{x}}^{\text{q}[1]} = \frac{g^2 p_1^+}{2s} \int_{-\infty}^{\infty} dx_1^- \int_{x_1^-}^{\infty} dx_2^- V_{\underline{x}}[\infty, x_2^-] t^b \psi_\beta(x_2^-, \underline{x}) U_{\underline{x}}^{ba}[x_2^-, x_1^-] [\gamma^+ \gamma^5]_{\alpha\beta} \bar{\psi}_\alpha(x_1^-, \underline{x}) t^a V_{\underline{x}}[x_1^-, -\infty], \quad (2b)$$

$$V_{\underline{x}, \underline{y}}^{\text{G}[2]} = -\frac{ip_1^+}{s} \int_{-\infty}^{\infty} dz^- d^2z V_{\underline{x}}[\infty, z^-] \delta^2(\underline{x} - \underline{z}) \bar{D}^i(z^-, \underline{z}) D^i(z^-, \underline{z}) V_{\underline{y}}[z^-, -\infty] \delta^2(\underline{y} - \underline{z}), \quad (2c)$$

$$V_{\underline{x}}^{\text{q}[2]} = -\frac{g^2 p_1^+}{2s} \int_{-\infty}^{\infty} dx_1^- \int_{x_1^-}^{\infty} dx_2^- V_{\underline{x}}[\infty, x_2^-] t^b \psi_\beta(x_2^-, \underline{x}) U_{\underline{x}}^{ba}[x_2^-, x_1^-] [\gamma^+]_{\alpha\beta} \bar{\psi}_\alpha(x_1^-, \underline{x}) t^a V_{\underline{x}}[x_1^-, -\infty]. \quad (2d)$$

We employ the light-cone coordinates defined as $x^\pm = (x^0 \pm x^3)/\sqrt{2}$, the transverse position vectors are $\underline{x} = (x^1, x^2)$, the Latin index $i = 1, 2$ labels transverse components, and g is the QCD coupling. Our target nucleon is moving with large momentum p_1^+ in the light-cone x^+ -direction, while s is the center-of-mass energy squared of the projectile-target system. The incoming quark has polarization σ , while the outgoing quark has polarization σ' . The background gluon field A^μ brings in two sub-eikonal operators: the transverse-transverse component of the field strength tensor F^{12} and the $\tilde{D}^i D^i$ operator, with the right- and left-acting covariant derivatives defined by $D^i = \partial^i - igA^i$ and $\tilde{D}^i = \tilde{\partial}^i + igA^i$, respectively. The background quark fields ψ and $\bar{\psi}$ bring in the vector (γ^+) and the axial vector ($\gamma^+ \gamma^5$) current operators, both of which are also sub-eikonal: the vector current operator $V_{\underline{x}}^{\text{q}[2]}$ does not contribute to the helicity evolution constructed in [1–3, 12, 15]. We have also employed the fundamental (V) and adjoint (U) light-cone Wilson lines,

$$V_{\underline{x}}[x_f^-, x_i^-] = \mathcal{P} \exp \left[ig \int_{x_i^-}^{x_f^-} dx^- A^+(0^+, x^-, \underline{x}) \right], \quad U_{\underline{x}}[x_f^-, x_i^-] = \mathcal{P} \exp \left[ig \int_{x_i^-}^{x_f^-} dx^- \mathcal{A}^+(0^+, x^-, \underline{x}) \right]. \quad (3)$$

For the gluon scattering on the same background fields with the initial helicity λ and the final helicity λ' we have the following sub-eikonal S -matrix,

$$(U_{\underline{x}, \underline{y}; \lambda', \lambda})^{\text{ba}} \Big|_{\text{sub-eikonal}} \equiv \lambda \delta_{\lambda, \lambda'} \left(U_{\underline{x}}^{\text{G}[1]} + U_{\underline{x}}^{\text{q}[1]} \right)^{\text{ba}} \delta^2(\underline{x} - \underline{y}) + \delta_{\lambda, \lambda'} \left(U_{\underline{x}, \underline{y}}^{\text{G}[2]} + U_{\underline{x}}^{\text{q}[2]} \delta^2(\underline{x} - \underline{y}) \right)^{\text{ba}} \quad (4)$$

with the polarized Wilson lines

$$(U_{\underline{x}}^{\text{G}[1]})^{\text{ba}} = \frac{2igp_1^+}{s} \int_{-\infty}^{\infty} dx^- (U_{\underline{x}}[\infty, x^-])^{\text{bb}'} (\mathcal{F}^{12})^{\text{b}'\text{a}'}(x^-, \underline{x}) (U_{\underline{x}}[x^-, -\infty])^{\text{a}'\text{a}}, \quad (5\text{a})$$

$$(U_{\underline{x}}^{\text{q}[1]})^{\text{ba}} = \frac{g^2 p_1^+}{2s} \int_{-\infty}^{\infty} dx_1^- \int_{x_1^-}^{\infty} dx_2^- (U_{\underline{x}}[\infty, x_2^-])^{\text{bb}'} \bar{\psi}(x_2^-, \underline{x}) t^{\text{b}'} V_{\underline{x}}[x_2^-, x_1^-] \gamma^+ \gamma^5 t^{\text{a}'} \psi(x_1^-, \underline{x}) (U_{\underline{x}}[x_1^-, -\infty])^{\text{a}'\text{a}} + \text{c.c.}, \quad (5\text{b})$$

$$(U_{\underline{x}, \underline{y}}^{\text{G}[2]})^{\text{ba}} = -\frac{ip_1^+}{s} \int_{-\infty}^{\infty} dz^- d^2z (U_{\underline{x}}[\infty, z^-])^{\text{bb}'} \delta^2(\underline{x} - \underline{z}) \tilde{\mathcal{D}}^{\text{b}'\text{c}}(z^-, \underline{z}) \cdot \mathcal{D}^{\text{ca}'}(z^-, \underline{z}) (U_{\underline{y}}[z^-, -\infty])^{\text{a}'\text{a}} \delta^2(\underline{y} - \underline{z}), \quad (5\text{c})$$

$$(U_{\underline{x}}^{\text{q}[2]})^{\text{ba}} = -\frac{g^2 p_1^+}{2s} \int_{-\infty}^{\infty} dx_1^- \int_{x_1^-}^{\infty} dx_2^- (U_{\underline{x}}[\infty, x_2^-])^{\text{bb}'} \bar{\psi}(x_2^-, \underline{x}) t^{\text{b}'} V_{\underline{x}}[x_2^-, x_1^-] \gamma^+ t^{\text{a}'} \psi(x_1^-, \underline{x}) (U_{\underline{x}}[x_1^-, -\infty])^{\text{a}'\text{a}} - \text{c.c.}, \quad (5\text{d})$$

where \mathcal{F}^{12} and $\tilde{\mathcal{D}} \cdot \mathcal{D}$ are now in the adjoint representation. Again, $U_{\underline{x}}^{\text{q}[2]}$ does not contribute to helicity evolution in [1–3, 12, 15].

The polarized dipole amplitudes needed to construct the large- N_c & N_f helicity evolution equations are

$$Q_{10}(s) = \frac{1}{2N_c} \text{Re} \left\langle \left\langle \text{T tr} \left[V_{\underline{0}} V_{\underline{1}}^{\text{pol}[1] \dagger} \right] + \text{T tr} \left[V_{\underline{1}}^{\text{pol}[1]} V_{\underline{0}}^\dagger \right] \right\rangle \right\rangle (s), \quad (6\text{a})$$

$$G_{10}^i(s) = \frac{1}{2N_c} \text{Re} \left\langle \left\langle \text{T tr} \left[V_{\underline{0}} V_{\underline{1}}^{i\text{G}[2] \dagger} \right] + \text{T tr} \left[V_{\underline{1}}^{i\text{G}[2]} V_{\underline{0}}^\dagger \right] \right\rangle \right\rangle (s), \quad (6\text{b})$$

with

$$V_{\underline{x}}^{\text{pol}[1]} = V_{\underline{x}}^{\text{G}[1]} + V_{\underline{x}}^{\text{q}[1]} \quad (7)$$

and with the new polarized Wilson line

$$V_{\underline{z}}^{i\text{G}[2]} \equiv \frac{p_1^+}{2s} \int_{-\infty}^{\infty} dz^- V_{\underline{z}}[\infty, z^-] \left[D^i(z^-, \underline{z}) - \tilde{D}^i(z^-, \underline{z}) \right] V_{\underline{z}}[z^-, -\infty] \quad (8)$$

related to the one in Eq. (2c) (see [3]). Here T stands for time-ordering. The double angle brackets are defined as the usual saturation physics averaging in the (now, polarized) target wave function, denoted by single angle brackets, with the result multiplied by a power of the center-of-mass energy squared s [1],

$$\left\langle \left\langle \dots \right\rangle \right\rangle \equiv s \left\langle \dots \right\rangle. \quad (9)$$

We also use the abbreviated notation for infinite Wilson lines $V_{\underline{x}} = V_{\underline{x}}[\infty, -\infty]$ and $V_{\underline{1}} = V_{\underline{x}_1}$, $V_{\underline{0}} = V_{\underline{x}_0}$, such that, for instance, $Q_{10}(s)$ depends on the transverse positions \underline{x}_1 , \underline{x}_0 in addition to its dependence on energy s .

Since the g_1 structure function and hPDFs $\Delta\Sigma$ and ΔG at small x depend on the polarized dipole amplitudes integrated over all impact parameters, we can integrate the amplitudes over the impact parameters while keeping the dipole transverse separation $\underline{x}_{10} \equiv \underline{x}_1 - \underline{x}_0$ fixed, defining

$$Q(x_{10}^2, s) \equiv \int d^2 \left(\frac{x_0 + x_1}{2} \right) Q_{10}(s) \quad (10)$$

for the dipole amplitude Q . (We will use the notation where $\underline{x}_{ij} = \underline{x}_i - \underline{x}_j$ and $x_{ij} = |\underline{x}_{ij}|$.) Integrating Eq. (6b) over the impact parameters we write the most general transverse tensor decomposition for the result of such integration as [3, 15]

$$\int d^2 \left(\frac{x_1 + x_0}{2} \right) G_{10}^i(s) = (x_{10})_{\perp}^i G_1(x_{10}^2, s) + \epsilon^{ij} (x_{10})_{\perp}^j G_2(x_{10}^2, s), \quad (11)$$

obtaining two new dipole amplitudes G_1 and G_2 : only G_2 contributes to helicity evolution [3].

The adjoint dipole amplitude of the first (Q) kind is defined by analogy to Eq. (6a) as

$$G_{10}^{\text{adj}}(s) \equiv \frac{1}{2(N_c^2 - 1)} \text{Re} \left\langle \left\langle \text{T Tr} \left[U_{\underline{0}} U_{\underline{1}}^{\text{pol}[1]\dagger} \right] + \text{T Tr} \left[U_{\underline{1}}^{\text{pol}[1]} U_{\underline{0}}^{\dagger} \right] \right\rangle \right\rangle (s) \quad (12)$$

with

$$U_{\underline{x}}^{\text{pol}[1]} = U_{\underline{x}}^{\text{G}[1]} + U_{\underline{x}}^{\text{q}[1]}. \quad (13)$$

In the large- N_c & N_f limit this dipole amplitude reduces to [2, 3]

$$G_{10}^{\text{adj}}(s) = 4 S_{10}(s) \tilde{G}_{10}(s) \quad (14)$$

where

$$S_{10}(s) = \frac{1}{N_c} \left\langle \text{T tr} \left[V_{\underline{0}} V_{\underline{1}}^{\dagger} \right] \right\rangle (s) \quad (15)$$

is the eikonal (unpolarized) dipole S -matrix and

$$\tilde{G}_{10}(s) = \frac{1}{2N_c} \text{Re} \left\langle \left\langle \text{T tr} \left[V_{\underline{0}} W_{\underline{1}}^{\text{pol}[1]\dagger} \right] + \text{T tr} \left[W_{\underline{1}}^{\text{pol}[1]} V_{\underline{0}}^{\dagger} \right] \right\rangle \right\rangle (s) \quad (16)$$

with

$$W_{\underline{x}}^{\text{pol}[1]} = V_{\underline{x}}^{\text{G}[1]} - \frac{g^2 p_1^+}{4s} \int_{-\infty}^{\infty} dx_1^- \int_{x_1^-}^{\infty} dx_2^- V_{\underline{x}}[\infty, x_2^-] \psi_{\alpha}(x_2^-, \underline{x}) \left(\frac{1}{2} \gamma^+ \gamma_5 \right)_{\beta\alpha} \bar{\psi}_{\beta}(x_1^-, \underline{x}) V_{\underline{x}}[x_1^-, -\infty]. \quad (17)$$

(Note that the relative sign is different on the right-hand side of Eq. (17) as compared to Eq. (137) of [3]: the difference is due to fermionic field ordering. The typo in Eq. (137) of [3] does not propagate.)

The large- N_c & N_f helicity evolution equations are written for the dipole amplitudes Q , G_2 and \tilde{G} , along with their ‘‘neighbor’’ dipole amplitudes $\bar{\Gamma}$, Γ_2 , and $\tilde{\Gamma}$, introduced to properly account for the light-cone lifetime ordering [1–3].

For completeness, we list the expressions for the flavor-singlet hPDFs obtained in [1–3, 12, 15] in the DLA limit:

$$\Delta\Sigma(x, Q^2) = -\frac{N_c N_f}{2\pi^3} \int_{\Lambda^2/s}^1 \frac{dz}{z} \int_{\frac{1}{zs}}^{\min\left\{\frac{1}{zQ^2}, \frac{1}{\Lambda^2}\right\}} \frac{dx_{10}^2}{x_{10}^2} [Q(x_{10}^2, zs) + 2 G_2(x_{10}^2, zs)], \quad (18a)$$

$$\Delta G(x, Q^2) = \frac{2N_c}{\alpha_s \pi^2} G_2 \left(x_{10}^2 = \frac{1}{Q^2}, s = \frac{Q^2}{x} \right). \quad (18b)$$

Here z is the minus momentum fraction carried by the anti-quark (or quark) line in the definition of the quark (anti-quark) PDF. Below we will find a correction to the integration limits of Eq. (18a).

The g_1 structure function is [1, 3]

$$g_1(x, Q^2) = - \sum_f \frac{N_c Z_f^2}{4\pi^3} \int_{\Lambda^2/s}^1 \frac{dz}{z} \int_{\frac{1}{zs}}^{\min\{\frac{1}{zQ^2}, \frac{1}{\Lambda^2}\}} \frac{dx_{10}^2}{x_{10}^2} [Q(x_{10}^2, zs) + 2G_2(x_{10}^2, zs)], \quad (19)$$

with z the minus momentum fraction of the virtual photon's momentum carried by the (longitudinally) softer line between the quark and the anti-quark the virtual photon splits into.

III. DERIVATION OF THE QUARK TO GLUON AND GLUON TO QUARK CONTRIBUTION TO HELICITY EVOLUTION

In this Section we derive corrections to the large- N_c & N_f helicity evolution equations due to the $q/\bar{q} \rightarrow G$ and $G \rightarrow q/\bar{q}$ shock-wave transition operators using LCOT [2, 3, 15, 60]. In Appendix A we re-derive the same corrections to the helicity evolution equations using LCPT [84, 85].

A. Quark to Gluon and Gluon to Quark Transition Operators

We begin the calculation by constructing the (anti-)quark to gluon and gluon to (anti-)quark transition operators. They are shown diagrammatically in Fig. 1. The background gluon and quark fields in Fig. 1 are represented by vertical corkscrew and straight lines, respectively. The non-eikonal interaction is due to the quark background field: the interactions with the gluon background field in Fig. 1 are, therefore, assumed to be eikonal, and will be described by light-cone Wilson lines in the appropriate (adjoint or fundamental) color representations.

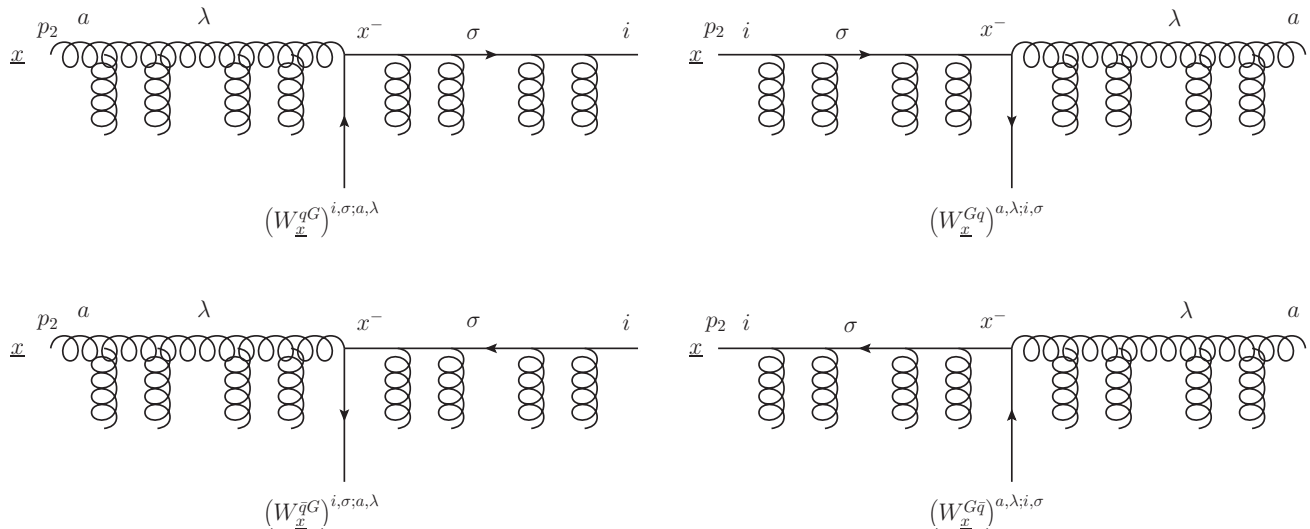


FIG. 1. A diagrammatic representation of the $q/\bar{q} \rightarrow G$ and $G \rightarrow q/\bar{q}$ transition operators. The incoming particle's momentum p_2 has a large light-cone minus component. The polarizations and colors of the incoming and outgoing partons are labeled explicitly.

A straightforward calculation along the lines of those done in [2, 15, 60] yields for the transition operators defined

in Fig. 1

$$W_{\underline{x}}^{Gq}[\infty, -\infty] = \frac{-ig}{2\sqrt{\sqrt{2}p_2^-}} \delta_{\lambda,\sigma} \int_{-\infty}^{\infty} dx^- U_{\underline{x}}^{ab}[\infty, x^-] \bar{\psi}(x^-, \underline{x}) t^b [\rho(+)+\rho(-)-\sigma(\rho(+)-\rho(-))] V_{\underline{x}}[x^-, -\infty], \quad (20a)$$

$$W_{\underline{x}}^{G\bar{q}}[\infty, -\infty] = \frac{ig}{2\sqrt{\sqrt{2}p_2^-}} \delta_{\lambda,\sigma} \int_{-\infty}^{\infty} dx^- U_{\underline{x}}^{ab}[\infty, x^-] V_{\underline{x}}[-\infty, x^-] [\bar{\rho}(+)+\bar{\rho}(-)+\sigma(\bar{\rho}(+)-\bar{\rho}(-))] t^b \psi(x^-, \underline{x}), \quad (20b)$$

$$W_{\underline{x}}^{qG}[\infty, -\infty] = \frac{-ig}{2\sqrt{\sqrt{2}p_2^-}} \delta_{\lambda,\sigma} \int_{-\infty}^{\infty} dx^- V_{\underline{x}}[\infty, x^-] [\bar{\rho}(+)+\bar{\rho}(-)-\sigma(\bar{\rho}(+)-\bar{\rho}(-))] t^b \psi(x^-, \underline{x}) U_{\underline{x}}^{ba}[x^-, -\infty], \quad (20c)$$

$$W_{\underline{x}}^{\bar{q}G}[\infty, -\infty] = \frac{ig}{2\sqrt{\sqrt{2}p_2^-}} \delta_{\lambda,\sigma} \int_{-\infty}^{\infty} dx^- \bar{\psi}(x^-, \underline{x}) t^b [\rho(+)+\rho(-)+\sigma(\rho(+)-\rho(-))] V_{\underline{x}}[x^-, \infty] U_{\underline{x}}^{ba}[x^-, -\infty]. \quad (20d)$$

We are suppressing the polarization and color indices, shown in Fig. 1. The superscripts of the W -operators in Eq. (20) denote the outgoing and incoming particles: for instance, $W_{\underline{x}}^{Gq}$ denotes the transition operator for the incoming quark and outgoing gluon, as shown in the upper right panel of Fig. 1. Here we are working in $A^- = 0$ gauge for the gluons; an incoming or outgoing gluon with momentum k is described by the polarization four-vector $\epsilon_{\lambda}^{\mu} = (\epsilon_{\lambda} \cdot \underline{k}/k^-, 0, \epsilon_{\lambda})$ with $\epsilon_{\lambda} = -(1/\sqrt{2})(\lambda, i)$ [84]. The external quark and anti-quark lines are described by the ‘‘anti’’-Brody-Lepage spinors [2, 84]

$$u_{\sigma}(p) = \frac{1}{\sqrt{\sqrt{2}p^-}} [\sqrt{2}p^- + m\gamma^0 + \gamma^0 \underline{\gamma} \cdot \underline{p}] \rho(\sigma), \quad v_{\sigma}(p) = \frac{1}{\sqrt{\sqrt{2}p^-}} [\sqrt{2}p^- - m\gamma^0 + \gamma^0 \underline{\gamma} \cdot \underline{p}] \rho(-\sigma), \quad (21)$$

with $p^{\mu} = \left(\frac{p^2+m^2}{2p^-}, p^-, \underline{p}\right)$ and

$$\rho(+1) = \frac{1}{\sqrt{2}} \begin{pmatrix} 1 \\ 0 \\ -1 \\ 0 \end{pmatrix}, \quad \rho(-1) = \frac{1}{\sqrt{2}} \begin{pmatrix} 0 \\ 1 \\ 0 \\ 1 \end{pmatrix}. \quad (22)$$

Relations between the transition operators are

$$\left(W_{\underline{x}}^{Gq}[\infty, -\infty]\right)^{\dagger} = W_{\underline{x}}^{qG}[-\infty, \infty], \quad \left(W_{\underline{x}}^{G\bar{q}}[\infty, -\infty]\right)^{\dagger} = W_{\underline{x}}^{\bar{q}G}[-\infty, \infty]. \quad (23)$$

Defining

$$W_{\underline{x}}^{a;i[1]}[b^-, a^-] = \frac{ig}{2\sqrt{\sqrt{2}p^-}} \int_{a^-}^{b^-} dx^- U_{\underline{x}}^{ab}[b^-, x^-] \bar{\psi}^{i'}(x^-, \underline{x}) t^b [\rho(+)-\rho(-)] (V_{\underline{x}}[x^-, a^-])^{i'i}, \quad (24a)$$

$$W_{\underline{x}}^{a;i[2]}[b^-, a^-] = -\frac{ig}{2\sqrt{\sqrt{2}p^-}} \int_{a^-}^{b^-} dx^- U_{\underline{x}}^{ab}[b^-, x^-] \bar{\psi}^{i'}(x^-, \underline{x}) t^b [\rho(+)+\rho(-)] (V_{\underline{x}}[x^-, a^-])^{i'i}, \quad (24b)$$

which are rows in quark color space, we rewrite Eqs. (20) as

$$\left(W_{\underline{x}}^{Gq}[\infty, -\infty]\right)^{a,\lambda;i,\sigma} = \sigma \delta_{\lambda,\sigma} W_{\underline{x}}^{a;i[1]}[\infty, -\infty] + \delta_{\lambda,\sigma} W_{\underline{x}}^{a;i[2]}[\infty, -\infty], \quad (25a)$$

$$\left(W_{\underline{x}}^{G\bar{q}}[\infty, -\infty]\right)^{a,\lambda;i,\sigma} = -\sigma \delta_{\lambda,\sigma} \left(W_{\underline{x}}^{a;i[1]}[\infty, -\infty]\right)^{\dagger} + \delta_{\lambda,\sigma} \left(W_{\underline{x}}^{a;i[2]}[\infty, -\infty]\right)^{\dagger}, \quad (25b)$$

$$\left(W_{\underline{x}}^{qG}[\infty, -\infty]\right)^{i,\sigma;a,\lambda} = \sigma \delta_{\lambda,\sigma} \left(W_{\underline{x}}^{a;i[1]}[-\infty, \infty]\right)^{\dagger} + \delta_{\lambda,\sigma} \left(W_{\underline{x}}^{a;i[2]}[-\infty, \infty]\right)^{\dagger}, \quad (25c)$$

$$\left(W_{\underline{x}}^{\bar{q}G}[\infty, -\infty]\right)^{i,\sigma;a,\lambda} = -\sigma \delta_{\lambda,\sigma} W_{\underline{x}}^{a;i[1]}[-\infty, \infty] + \delta_{\lambda,\sigma} W_{\underline{x}}^{a;i[2]}[-\infty, \infty]. \quad (25d)$$

Having constructed the shock-wave transition operators, we are now ready to calculate their contributions to the flavor-singlet helicity evolution.

B. Contribution to the evolution of the adjoint dipole amplitude of the first type

1. Diagrams calculation

The shock-wave transition operators (25) may contribute to the flavor-singlet helicity evolution of the adjoint type-1 polarized dipole amplitude G_{10}^{adj} defined in Eq. (12). The diagrams in the shock wave formalism are shown in Fig. 2, with the shock wave represented by a vertical shaded rectangle. These diagrams arise due to the contribution of the polarized Wilson line operator $(U_{\underline{x}}^{q[1]})^{ba}$ to G_{10}^{adj} . The diagrams in Fig. 2 include two transition operators from Eqs. (25): they were not included in the analysis of [1–3].

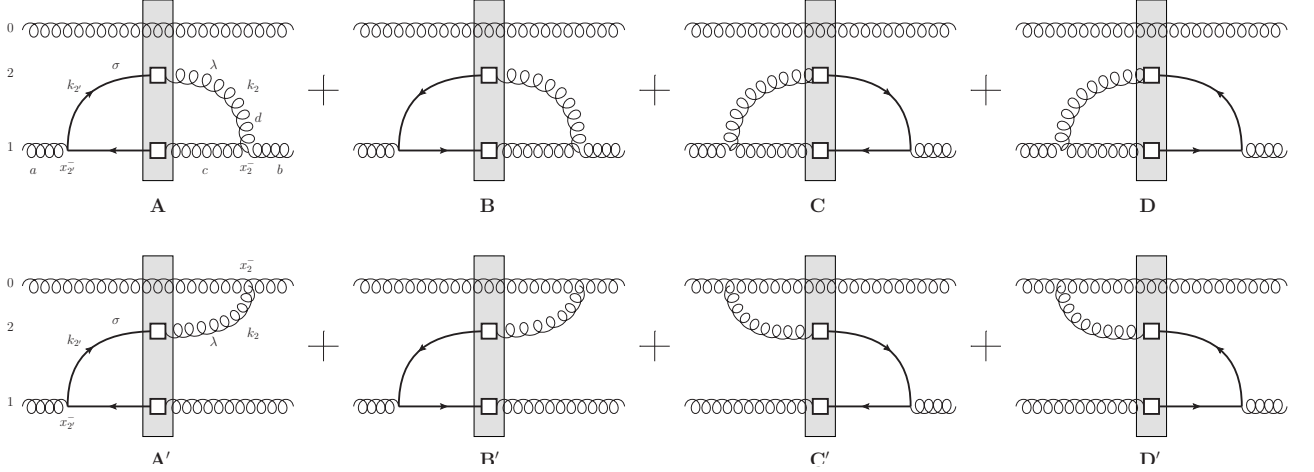


FIG. 2. The diagrams for the evolution of G_{10}^{adj} due to the $q/\bar{q} \rightarrow G$ and $G \rightarrow q/\bar{q}$ shock-wave transition operators calculated here. The shaded rectangle denotes the shock wave, while the white square denotes the non-eikonal interaction with the shock wave mediated by the transition operators from Fig. 1.

To calculate diagrams A and A' from Fig. 2 we will need the following background-field propagator, which can be constructed along the lines of [2, 3, 15, 60] (quarks are assumed to be massless):

$$\begin{aligned} \int_{-\infty}^0 dx_{2'}^- \int_0^{\infty} dx_2^- \overline{\psi}_\alpha^i(x_{2'}, \underline{x}_1) a^{+d}(x_2^-, \underline{x}_0) &= \frac{1}{4\pi^3} \int_0^{p_2^-} dk^- \int d^2x_2 \frac{x_{20}^m}{x_{20}^2} \\ &\times \left[(\epsilon_+^m \bar{\rho}(+)_{\beta} - \epsilon_-^m \bar{\rho}(-)_{\beta}) W_2^{d;i[1]}[\infty, -\infty] + (\epsilon_+^m \bar{\rho}(+)_{\beta} + \epsilon_-^m \bar{\rho}(-)_{\beta}) W_2^{d;i[2]}[\infty, -\infty] \right] \\ &\times \left[i\sqrt{2k^-} \ln\left(\frac{1}{x_{21}\Lambda}\right) + \frac{1}{\sqrt{2k^-}} \frac{x_{21}^l}{x_{21}^2} \gamma^0 \gamma^l \right]_{\beta\alpha}. \end{aligned} \quad (26)$$

The notations used in Eq. (26) are defined in Fig. 2, with the typical (large) minus momentum of the original (parent) dipole being p_2^- . The first term in the last square brackets of Eq. (26) does not contribute to the evolution at hand. The second term gives, after some algebra,

$$\begin{aligned} A + A' &= \frac{1}{N_c^2 - 1} \frac{\alpha_s}{2\pi^2} \sum_f \int_0^{p_2^-} \frac{dk^-}{k^-} \int d^2x_2 \left\langle \left\langle (U_0^\dagger)^{ab} f^{dbc} \left[iW_2^{d[1]}[\infty, -\infty] t^a \left(W_1^{c[2]}[\infty, -\infty] \right)^\dagger \frac{x_{20}}{x_{20}^2} \cdot \frac{x_{21}}{x_{21}^2} \right. \right. \right. \\ &+ W_2^{d[1]}[\infty, -\infty] t^a \left(W_1^{c[1]}[\infty, -\infty] \right)^\dagger \frac{x_{20}}{x_{20}^2} \times \frac{x_{21}}{x_{21}^2} + iW_2^{d[2]}[\infty, -\infty] t^a \left(W_1^{c[1]}[\infty, -\infty] \right)^\dagger \frac{x_{20}}{x_{20}^2} \cdot \frac{x_{21}}{x_{21}^2} \\ &\left. \left. \left. + W_2^{d[2]}[\infty, -\infty] t^a \left(W_1^{c[2]}[\infty, -\infty] \right)^\dagger \frac{x_{20}}{x_{20}^2} \times \frac{x_{21}}{x_{21}^2} \right] \right\rangle - (\underline{x}_{20} \rightarrow \underline{x}_{21}), \end{aligned} \quad (27)$$

where we have suppressed the quark color indices on the W 's.

Here, the double angle brackets are defined as

$$\left\langle \left\langle W_2^{d[k]} \dots \left(W_1^{c[l]} \right)^\dagger \right\rangle \right\rangle \equiv \sqrt{2k^- p_1^+} \sqrt{2p_2^- p_1^+} \left\langle W_2^{d[k]} \dots \left(W_1^{c[l]} \right)^\dagger \right\rangle \quad (28)$$

with $k, l = 1, 2$, which is a generalization of Eq. (9) to the case of two non-eikonal interactions considered in Fig. 2.

Next we move on to diagrams B and B'. We now need another propagator, which one can also readily construct,

$$\begin{aligned} \int_{-\infty}^0 dx_{2'}^- \int_0^{\infty} dx_2^- \overbrace{\psi_{\alpha}^i(x_{2'}, \underline{x}_1)} a^{+d}(x_2^-, \underline{x}_0) &= \frac{1}{4\pi^3} \int_0^{p_2^-} dk^- \int d^2x_2 \frac{x_{20}^m}{x_{20}^2} \\ &\times \left[i \sqrt{\sqrt{2}k^-} \ln \left(\frac{1}{x_{21}\Lambda} \right) + \frac{1}{\sqrt{\sqrt{2}k^-}} \frac{x_{21}^l}{x_{21}^2} \gamma^l \gamma^0 \right]_{\alpha\beta} \\ &\times \left[(\epsilon_+^m \rho(-)_{\beta} - \epsilon_-^m \rho(+)_{\beta}) \left(W_{\underline{2}}^{d;i[1]}[\infty, -\infty] \right)^{\dagger} - (\epsilon_+^m \rho(-)_{\beta} + \epsilon_-^m \rho(+)_{\beta}) \left(W_{\underline{2}}^{d;i[2]}[\infty, -\infty] \right)^{\dagger} \right]. \end{aligned} \quad (29)$$

Again the first term in the (now) first square brackets does not contribute to evolution. The second term yields

$$\begin{aligned} B + B' &= \frac{1}{N_c^2 - 1} \frac{\alpha_s}{2\pi^2} \sum_f \int_0^{p_2^-} \frac{dk^-}{k^-} \int d^2x_2 \left\langle \left(U_{\underline{0}}^{\dagger} \right)^{ab} f^{dbc} \left[-i W_{\underline{1}}^{c[2]}[\infty, -\infty] t^a \left(W_{\underline{2}}^{d[1]}[\infty, -\infty] \right)^{\dagger} \frac{x_{20}}{x_{20}^2} \cdot \frac{x_{21}}{x_{21}^2} \right. \right. \\ &+ W_{\underline{1}}^{c[1]}[\infty, -\infty] t^a \left(W_{\underline{2}}^{d[1]}[\infty, -\infty] \right)^{\dagger} \frac{x_{20}}{x_{20}^2} \times \frac{x_{21}}{x_{21}^2} - i W_{\underline{1}}^{c[1]}[\infty, -\infty] t^a \left(W_{\underline{2}}^{d[2]}[\infty, -\infty] \right)^{\dagger} \frac{x_{20}}{x_{20}^2} \cdot \frac{x_{21}}{x_{21}^2} \\ &\left. \left. + W_{\underline{1}}^{c[2]}[\infty, -\infty] t^a \left(W_{\underline{2}}^{d[2]}[\infty, -\infty] \right)^{\dagger} \frac{x_{20}}{x_{20}^2} \times \frac{x_{21}}{x_{21}^2} \right] \right\rangle - (\underline{x}_{20} \rightarrow \underline{x}_{21}). \end{aligned} \quad (30)$$

We observe that

$$B + B' = (A + A')^*. \quad (31)$$

Considering diagrams C and C' next, we need the following propagator:

$$\begin{aligned} \int_{-\infty}^0 dx_{2'}^- \int_0^{\infty} dx_2^- \overbrace{\psi_{\alpha}^i(x_{2'}, \underline{x}_1)} a^{+d}(x_2^-, \underline{x}_0) &= -\frac{1}{4\pi^3} \int_0^{p_2^-} dk^- \int d^2x_2 \frac{x_{20}^m}{x_{20}^2} \\ &\times \left[i \sqrt{\sqrt{2}k^-} \ln \left(\frac{1}{x_{21}\Lambda} \right) + \frac{1}{\sqrt{\sqrt{2}k^-}} \frac{x_{21}^l}{x_{21}^2} \gamma^0 \gamma^l \right]_{\alpha\beta} \\ &\times \left[(\epsilon_+^{m*} \rho(+)_{\beta} - \epsilon_-^{m*} \rho(-)_{\beta}) \left(W_{\underline{2}}^{d;i[1]}[-\infty, \infty] \right)^{\dagger} + (\epsilon_+^{m*} \rho(+)_{\beta} + \epsilon_-^{m*} \rho(-)_{\beta}) \left(W_{\underline{2}}^{d;i[2]}[-\infty, \infty] \right)^{\dagger} \right]. \end{aligned} \quad (32)$$

Only the second term in the first square bracket contributes. We obtain

$$\begin{aligned} C + C' &= \frac{1}{N_c^2 - 1} \frac{\alpha_s}{2\pi^2} \sum_f \int_0^{p_2^-} \frac{dk^-}{k^-} \int d^2x_2 \left\langle \left(U_{\underline{0}}^{\dagger} \right)^{ab} f^{dac} \left[-i W_{\underline{1}}^{c[2]}[-\infty, \infty] t^b \left(W_{\underline{2}}^{d[1]}[-\infty, \infty] \right)^{\dagger} \frac{x_{20}}{x_{20}^2} \cdot \frac{x_{21}}{x_{21}^2} \right. \right. \\ &+ W_{\underline{1}}^{c[1]}[-\infty, \infty] t^b \left(W_{\underline{2}}^{d[1]}[-\infty, \infty] \right)^{\dagger} \frac{x_{20}}{x_{20}^2} \times \frac{x_{21}}{x_{21}^2} - i W_{\underline{1}}^{c[1]}[-\infty, \infty] t^b \left(W_{\underline{2}}^{d[2]}[-\infty, \infty] \right)^{\dagger} \frac{x_{20}}{x_{20}^2} \cdot \frac{x_{21}}{x_{21}^2} \\ &\left. \left. + W_{\underline{1}}^{c[2]}[-\infty, \infty] t^b \left(W_{\underline{2}}^{d[2]}[-\infty, \infty] \right)^{\dagger} \frac{x_{20}}{x_{20}^2} \times \frac{x_{21}}{x_{21}^2} \right] \right\rangle - (\underline{x}_{20} \rightarrow \underline{x}_{21}). \end{aligned} \quad (33)$$

One can now guess that

$$D + D' = (C + C')^*, \quad (34)$$

such that

$$\begin{aligned} D + D' &= \frac{1}{N_c^2 - 1} \frac{\alpha_s}{2\pi^2} \sum_f \int_0^{p_2^-} \frac{dk^-}{k^-} \int d^2x_2 \left\langle \left(U_{\underline{0}}^{\dagger} \right)^{ab} f^{dac} \left[i W_{\underline{2}}^{d[1]}[-\infty, \infty] t^b \left(W_{\underline{1}}^{c[2]}[-\infty, \infty] \right)^{\dagger} \frac{x_{20}}{x_{20}^2} \cdot \frac{x_{21}}{x_{21}^2} \right. \right. \\ &+ W_{\underline{2}}^{d[1]}[-\infty, \infty] t^b \left(W_{\underline{1}}^{c[1]}[-\infty, \infty] \right)^{\dagger} \frac{x_{20}}{x_{20}^2} \times \frac{x_{21}}{x_{21}^2} + i W_{\underline{2}}^{d[2]}[-\infty, \infty] t^b \left(W_{\underline{1}}^{c[1]}[-\infty, \infty] \right)^{\dagger} \frac{x_{20}}{x_{20}^2} \cdot \frac{x_{21}}{x_{21}^2} \\ &\left. \left. + W_{\underline{2}}^{d[2]}[-\infty, \infty] t^b \left(W_{\underline{1}}^{c[2]}[-\infty, \infty] \right)^{\dagger} \frac{x_{20}}{x_{20}^2} \times \frac{x_{21}}{x_{21}^2} \right] \right\rangle - (\underline{x}_{20} \rightarrow \underline{x}_{21}). \end{aligned} \quad (35)$$

This is what one indeed obtains by a direct calculation using the propagator

$$\begin{aligned} \int_{-\infty}^0 dx_2^- \int_0^{\infty} dx_2^- \overline{\psi}_\alpha^i(x_2^-, \underline{x}_1) a^{+d}(x_2^-, \underline{x}_0) &= \frac{1}{4\pi^3} \int_0^{p_2^-} dk^- \int d^2x_2 \frac{x_{20}^m}{x_{20}^2} \\ &\times \left[(-\epsilon_+^{m*} \bar{\rho}(-)_\beta + \epsilon_-^{m*} \bar{\rho}(+)_\beta) W_{\underline{2}}^{d;i[1]}[-\infty, \infty] + (\epsilon_+^{m*} \bar{\rho}(-)_\beta + \epsilon_-^{m*} \bar{\rho}(+)_\beta) W_{\underline{2}}^{d;i[2]}[-\infty, \infty] \right] \\ &\times \left[i \sqrt{\sqrt{2}k^-} \ln\left(\frac{1}{x_{21}\Lambda}\right) + \frac{1}{\sqrt{\sqrt{2}k^-}} \frac{x_{21}^l}{x_{21}^2} \gamma^l \gamma^0 \right]_{\beta\alpha}. \end{aligned} \quad (36)$$

The sum of the diagrams from Fig. 2 is obtained by adding the contributions found in Eqs. (27), (30), (33), and (35).

2. Simplifications in the DLA and at large N_c & N_f

Simplifying Eqs. (27), (30), (33), and (35) in the DLA, we neglect the terms with the cross products as not double-logarithmic, and write

$$\begin{aligned} A + A' + B + B' + C + C' + D + D' \Big|_{DLA} &= -\frac{1}{N_c^2 - 1} \frac{\alpha_s}{2\pi} \sum_f \int_0^{p_2^-} \frac{dk^-}{k^-} \int_0^{x_{10}^2} \frac{dx_{21}^2}{x_{21}^2} \\ &\times \left\langle \left\langle \left(U_0^\dagger \right)^{ab} f^{dbc} \left[i W_{\underline{2}}^{d[1]}[\infty, -\infty] t^a \left(W_{\underline{1}}^{c[2]}[\infty, -\infty] \right)^\dagger + i W_{\underline{2}}^{d[2]}[\infty, -\infty] t^a \left(W_{\underline{1}}^{c[1]}[\infty, -\infty] \right)^\dagger + \text{c.c.} \right] \right. \right. \\ &\left. \left. + \left(U_0^\dagger \right)^{ab} f^{dac} \left[i W_{\underline{2}}^{d[1]}[-\infty, \infty] t^b \left(W_{\underline{1}}^{c[2]}[-\infty, \infty] \right)^\dagger + i W_{\underline{2}}^{d[2]}[-\infty, \infty] t^b \left(W_{\underline{1}}^{c[1]}[-\infty, \infty] \right)^\dagger + \text{c.c.} \right] \right\rangle \right\rangle. \end{aligned} \quad (37)$$

Here c.c. stands for complex conjugate.

Using the definitions (24) one can readily show that the expression in the first square brackets of Eq. (37) is

$$\begin{aligned} i W_{\underline{2}}^{d[1]}[\infty, -\infty] t^a \left(W_{\underline{1}}^{c[2]}[\infty, -\infty] \right)^\dagger + i W_{\underline{2}}^{d[2]}[\infty, -\infty] t^a \left(W_{\underline{1}}^{c[1]}[\infty, -\infty] \right)^\dagger + \text{c.c.} &= \\ -i \frac{g^2}{4\sqrt{k^- p_2^-}} \int_{-\infty}^{\infty} dy^- \int_{-\infty}^{\infty} dz^- U_{\underline{2}}^{dd'}[\infty, y^-] U_{\underline{1}}^{cc'}[\infty, z^-] \bar{\psi}(y^-, \underline{x}_2) t^{d'} \gamma^+ \gamma^5 V_2[y^-, -\infty] t^a V_1[-\infty, z^-] t^{c'} \psi(z^-, \underline{x}_1) &+ \text{c.c.} \end{aligned} \quad (38)$$

The expression in the second square brackets of Eq. (37) is obtained from the above by simply interchanging the $\infty \leftrightarrow -\infty$ limits:

$$\begin{aligned} i W_{\underline{2}}^{d[1]}[-\infty, \infty] t^b \left(W_{\underline{1}}^{c[2]}[-\infty, \infty] \right)^\dagger + i W_{\underline{2}}^{d[2]}[-\infty, \infty] t^b \left(W_{\underline{1}}^{c[1]}[-\infty, \infty] \right)^\dagger + \text{c.c.} &= \\ -i \frac{g^2}{4\sqrt{k^- p_2^-}} \int_{-\infty}^{\infty} dy^- \int_{-\infty}^{\infty} dz^- U_{\underline{2}}^{dd'}[-\infty, y^-] U_{\underline{1}}^{cc'}[-\infty, z^-] \bar{\psi}(y^-, \underline{x}_2) t^{d'} \gamma^+ \gamma^5 V_2[y^-, \infty] t^b V_1[\infty, z^-] t^{c'} \psi(z^-, \underline{x}_1) &+ \text{c.c.} \end{aligned} \quad (39)$$

Employing Eq. (38) along with

$$U^{ab} = 2 \text{tr}[t^a V t^b V^\dagger], \quad (40)$$

applying the Fierz identity several times while neglecting the N_c -suppressed terms (either explicitly, or by neglecting the terms with fewer color traces, since each color trace brings in a factor of N_c), we arrive at

$$\begin{aligned} &\left\langle \left\langle \left(U_0^\dagger \right)^{ab} f^{dbc} \left[i W_{\underline{2}}^{d[1]}[\infty, -\infty] t^a \left(W_{\underline{1}}^{c[2]}[\infty, -\infty] \right)^\dagger + i W_{\underline{2}}^{d[2]}[\infty, -\infty] t^a \left(W_{\underline{1}}^{c[1]}[\infty, -\infty] \right)^\dagger + \text{c.c.} \right] \right\rangle \right\rangle \\ &= \int_{-\infty}^{\infty} dy^- \int_{-\infty}^{\infty} dz^- \left\langle \text{tr} \left[V_{\underline{2}} V_0^\dagger \right] \right\rangle \left\langle \text{tr} \left[V_0 V_{\underline{1}}^\dagger \right] \right\rangle \left\langle \left\langle \frac{g^2}{16\sqrt{k^- p_2^-}} \bar{\psi}(y^-, \underline{x}_2) \gamma^+ \gamma^5 V_2[y^-, \infty] V_1[\infty, z^-] \psi(z^-, \underline{x}_1) \right\rangle \right\rangle + \text{c.c.} \end{aligned} \quad (41)$$

Similarly, for the expression (39), we get

$$\begin{aligned} & \left\langle\left\langle \left(U_0^\dagger \right)^{ab} f^{dac} \left[i W_{\underline{2}}^{d[1]}[-\infty, \infty] t^b \left(W_{\underline{1}}^{c[2]}[-\infty, \infty] \right)^\dagger + i W_{\underline{2}}^{d[2]}[-\infty, \infty] t^b \left(W_{\underline{1}}^{c[1]}[-\infty, \infty] \right)^\dagger + \text{c.c.} \right] \right\rangle\right\rangle \quad (42) \\ & = \int_{-\infty}^{\infty} dy^- \int_{-\infty}^{\infty} dz^- \left\langle \text{tr} \left[V_{\underline{2}}^\dagger V_0 \right] \right\rangle \left\langle \text{tr} \left[V_0^\dagger V_{\underline{1}} \right] \right\rangle \left\langle\left\langle \frac{g^2}{16\sqrt{k^- p_2^-}} \bar{\psi}(y^-, \underline{x}_2) \gamma^+ \gamma^5 V_{\underline{2}}[y^-, -\infty] V_{\underline{1}}[-\infty, z^-] \psi(z^-, \underline{x}_1) \right\rangle\right\rangle + \text{c.c.} \end{aligned}$$

Employing Eqs. (41) and (42) in Eq. (37) we obtain (at large N_c & N_f)

$$\begin{aligned} A + A' + B + B' + C + C' + D + D' \Big|_{DLA} &= -\frac{\alpha_s}{2\pi} \sum_f \int_0^{p_2^-} \frac{dk^-}{k^-} \int_0^{x_{10}^2} \frac{dx_{21}^2}{x_{21}^2} S_{20}(2k^- p_1^+) S_{10}(2k^- p_1^+) \quad (43) \\ & \times \left\langle\left\langle \frac{g^2}{16\sqrt{k^- p_2^-}} \int_{-\infty}^{\infty} dy^- \int_{-\infty}^{\infty} dz^- \left[\bar{\psi}(y^-, \underline{x}_2) \gamma^+ \gamma^5 V_{\underline{2}}[y^-, \infty] V_{\underline{1}}[\infty, z^-] \psi(z^-, \underline{x}_1) \right. \right. \right. \\ & \left. \left. \left. + \bar{\psi}(y^-, \underline{x}_2) \gamma^+ \gamma^5 V_{\underline{2}}[y^-, -\infty] V_{\underline{1}}[-\infty, z^-] \psi(z^-, \underline{x}_1) + \text{c.c.} \right] \right\rangle\right\rangle. \end{aligned}$$

By analogy to Eqs. (16) and (17) we define a new object (which one cannot call a dipole scattering amplitude, since it is more like a quark helicity TMD, with one term containing a future-pointing (SIDIS) staple, and another term containing a past-pointing (Drell-Yan (DY)) staple),¹

$$\begin{aligned} \tilde{Q}_{12}(s) &\equiv \left\langle\left\langle \frac{g^2}{16\sqrt{k^- p_2^-}} \int_{-\infty}^{\infty} dy^- \int_{-\infty}^{\infty} dz^- \left[\bar{\psi}(y^-, \underline{x}_2) \left(\frac{1}{2} \gamma^+ \gamma^5 \right) V_{\underline{2}}[y^-, \infty] V_{\underline{1}}[\infty, z^-] \psi(z^-, \underline{x}_1) \right. \right. \right. \quad (44) \\ & \left. \left. \left. + \bar{\psi}(y^-, \underline{x}_2) \left(\frac{1}{2} \gamma^+ \gamma^5 \right) V_{\underline{2}}[y^-, -\infty] V_{\underline{1}}[-\infty, z^-] \psi(z^-, \underline{x}_1) + \text{c.c.} \right] \right\rangle\right\rangle(s). \end{aligned}$$

This gives

$$A + A' + B + B' + C + C' + D + D' \Big|_{DLA} = -\frac{\alpha_s}{\pi} \sum_f \int_0^{p_2^-} \frac{dk^-}{k^-} \int_0^{x_{10}^2} \frac{dx_{21}^2}{x_{21}^2} S_{20}(2k^- p_1^+) S_{10}(2k^- p_1^+) \tilde{Q}_{12}(2k^- p_1^+). \quad (45)$$

In DLA we put $S = 1$, since the unpolarized evolution is single-logarithmic. In addition, for simplicity, we replace $\sum_f \rightarrow N_f$, assuming that all flavors contribute equally (which, indeed, is not the case in phenomenology [50]). Writing $k^- = z' p_2^-$ and generalizing the calculation to the case of the parent dipole not being the original projectile, and rather being produced by previous steps of the evolution and described by the minus momentum fraction $z > z'$ we obtain, after imposing the light-cone lifetime constraints [1, 2, 18],

$$A + A' + B + B' + C + C' + D + D' \Big|_{DLA} = -\frac{\alpha_s N_f}{\pi} \int_{\frac{\Lambda^2}{s}}^z \frac{dz'}{z'} \int_{1/(z's)}^{x_{10}^2} \frac{dx_{21}^2}{x_{21}^2} \tilde{Q}_{12}(z' s). \quad (46)$$

Note that Eq. (46) gives the contribution of the transition operators to the evolution of $G_{10}^{\text{adj}}(zs)$. However, the large- N_c & N_f helicity evolution equations from [3] contain $\tilde{G}_{10}(zs)$ instead of $G_{10}^{\text{adj}}(zs)$. Employing Eq. (14) we write

$$G_{10}^{\text{adj}}(zs) = 4 S_{10}(zs) \tilde{G}_{10}(zs) \approx 4 \tilde{G}_{10}(zs), \quad (47)$$

¹ Note that our normalization here does not have the $1/N_c$ factor of Eqs. (6) or the $1/(N_c^2 - 1)$ factor of Eq. (16). In that respect, our \tilde{Q}_{12} is normalized similar to the dipole amplitude Q from Eq. (6a): the latter, in the quark sector, has a sum over quark fields colors, and not the average. At the same time, \tilde{Q}_{12} is different from the amplitude \tilde{G} in Eq. (16), in which the quark colors (in the quark sector) are averaged over.

with the last step valid in DLA, where $S_{10} = 1$. We see that while Eq. (46) is the contribution to the evolution of $G_{10}^{\text{adj}}(zs)$, the contribution to the evolution of $\tilde{G}_{10}(zs)$ in DLA is 4 times smaller. Combining Eqs. (47) and (46) we arrive at the following contribution of the transition operators to the evolution of the dipole amplitude $\tilde{G}_{10}(zs)$,

$$\tilde{G}_{10}(zs) \supset -\frac{\alpha_s N_f}{4\pi} \int_{\frac{\Lambda^2}{s}}^z \frac{dz'}{z'} \int_{1/(z's)}^{x_{10}^2} \frac{dx_{21}^2}{x_{21}^2} \tilde{Q}_{12}(z's). \quad (48)$$

We conclude that the transition operators do contribute to the evolution of $\tilde{G}_{10}(zs)$. The evolution equation for $\tilde{G}_{10}(zs)$ found in [3] needs to be augmented by including the new additive term from Eq. (48) into its right-hand side. The evolution equation for the corresponding neighbor dipole amplitude $\tilde{\Gamma}$ needs to be modified in a similar way (with a slightly different upper integration limit on the dipole sizes).

To complete the emerging new set of large- N_c & N_f helicity evolution equations we now need to derive an evolution equation for \tilde{Q} . Since \tilde{Q} enters the evolution of \tilde{G} in Eq. (48) in the $x_{21} \ll x_{10}$ regime, it always describes the evolution of the smaller of the two daughter ‘‘dipoles’’ ($x_{21} \ll x_{20} \approx x_{10}$), and the lifetime of the subsequent evolution in $\tilde{Q}_{12}(z's)$ is bounded by $\sim z' x_{21}^2$ from above, a limit dependent on the transverse size of the x_{21} ‘‘dipole’’ and independent of x_{10} . We thus conclude that, unlike for Q, G_2 and \tilde{G} , no ‘‘neighbor dipole amplitude’’ is needed for \tilde{Q} . We will only need to construct the evolution for the \tilde{Q} proper: this is what we will do next.

C. Evolution for \tilde{Q}

1. The DLA evolution equation for \tilde{Q}

Diagrams contributing to the evolution of $\tilde{Q}_{10}(zs)$ are shown in Fig. 3, with only the future-pointing Wilson line staple shown: the diagrams for the past-pointing staple are constructed and calculated by analogy. Since $\tilde{Q}_{10}(zs)$ operator is similar to the quark helicity TMD (SIDIS plus DY), the diagrams in Fig. 3 closely parallel those in Fig. 2 of [2]. The analysis carried out in [2] suggests that only diagrams \mathcal{D} and \mathcal{E} in our Fig. 3 should contribute in the DLA: this is what we will indeed confirm below.

Diagrams \mathcal{A}, \mathcal{B} and \mathcal{C} from Fig. 3 are just the eikonal corrections for a ‘‘half-dipole’’ amplitude [86]. Their contribution is known from the unpolarized small- x evolution [24–36]:

$$\mathcal{A} + \mathcal{B} + \mathcal{C} = -\frac{\alpha_s N_c}{4\pi^2} \int_{\frac{\Lambda^2}{s}}^z \frac{dz'}{z'} \int d^2x_2 \frac{x_{10}^2}{x_{21}^2 x_{20}^2} \tilde{Q}_{10}(z's) \approx -\frac{\alpha_s N_c}{4\pi} \int_{\frac{\Lambda^2}{s}}^z \frac{dz'}{z'} \left[\int_{1/(z's)}^{x_{10}^2} \frac{dx_{21}^2}{x_{21}^2} + \int_{1/(z's)}^{x_{10}^2} \frac{dx_{20}^2}{x_{20}^2} \right] \tilde{Q}_{10}(z's). \quad (49)$$

Here we include the past-pointing (DY) Wilson line staple’s contribution as well to assemble the entire \tilde{Q} object. The last step in Eq. (49) is the simplification in the DLA limit.

Next, let us calculate diagrams \mathcal{F} and \mathcal{G} in Fig. 3. We will need the propagator (29) again. After some algebra we end up with

$$\begin{aligned} \mathcal{F} + \mathcal{G} &= -2P^+ \frac{g^4}{256 \pi^3} \int_0^{p_2^-} \frac{dk^-}{k^-} \int_{-\infty}^{\infty} dy^- \int_{-\infty}^{\infty} dz^- \int d^2x_2 \left\langle \bar{\psi}(y^-, \underline{x}_0) V_0[y^-, \infty] t^a V_1 U_2^{ab}[\infty, z^-] V_2[-\infty, z^-] \right. \\ &\times \left. \left[\frac{x_{20}}{x_{20}^2} \cdot \frac{x_{21}}{x_{21}^2} \gamma^+ \gamma^5 - i \frac{x_{20}}{x_{20}^2} \times \frac{x_{21}}{x_{21}^2} \gamma^+ \right] t^b \psi(z^-, \underline{x}_2) \right\rangle - (x_{20} \rightarrow x_{21}) + \text{c.c.} \end{aligned} \quad (50)$$

Dropping the cross-product term as non-DLA and simplifying the dot-product term in DLA we obtain

$$\begin{aligned} \mathcal{F} + \mathcal{G} &= 2P^+ \frac{g^4}{256 \pi^2} \int_0^{p_2^-} \frac{dk^-}{k^-} \int_{-\infty}^{\infty} dy^- \int_{-\infty}^{\infty} dz^- \int_{x_{21}^2}^{x_{10}^2} \frac{dx_{21}^2}{x_{21}^2} \left\langle \bar{\psi}(y^-, \underline{x}_0) V_0[y^-, \infty] t^a V_1 U_2^{ab}[\infty, z^-] V_2[-\infty, z^-] \right. \\ &\times \left. \gamma^+ \gamma^5 t^b \psi(z^-, \underline{x}_2) \right\rangle + \text{c.c.} \end{aligned} \quad (51)$$

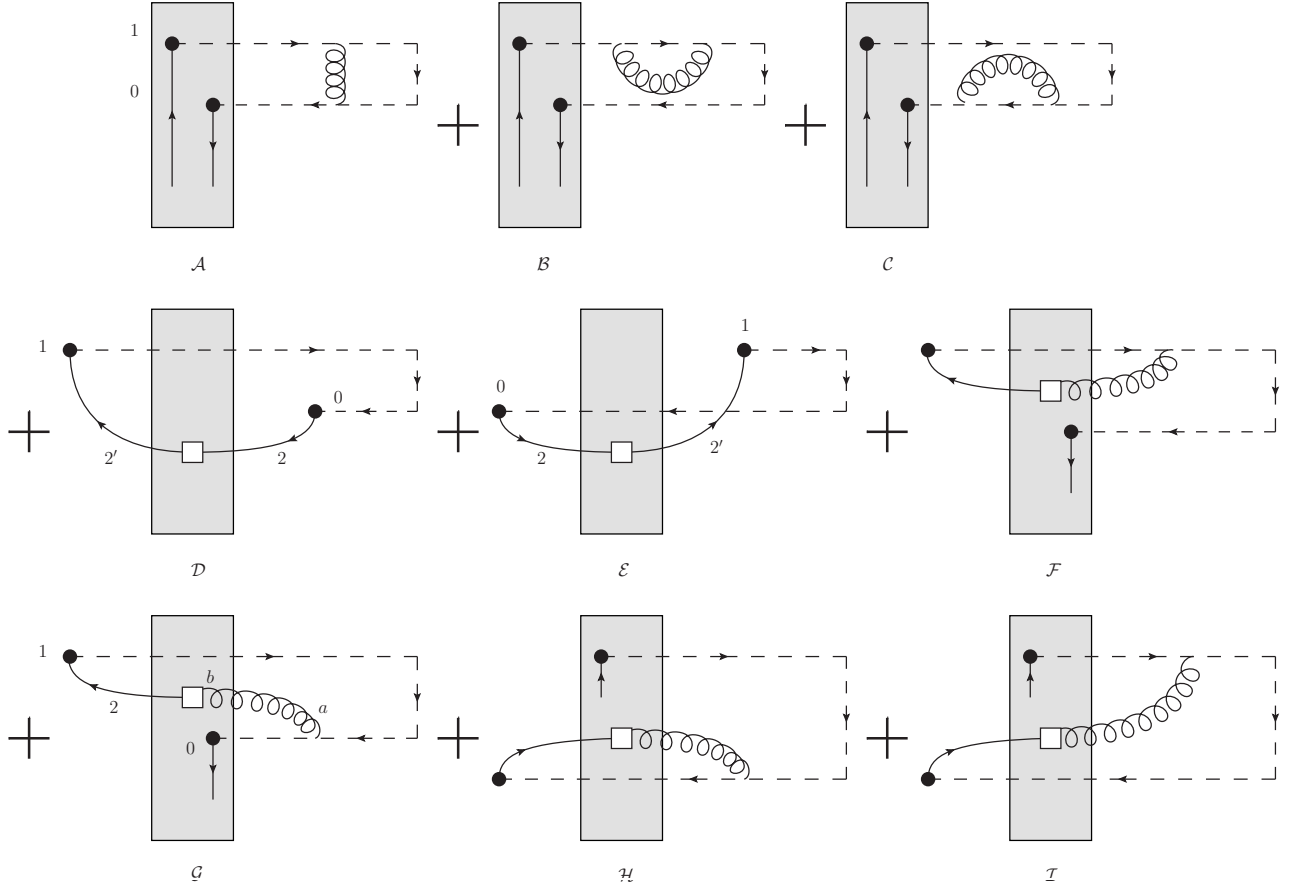


FIG. 3. Diagrams contributing to the DLA evolution of $\tilde{Q}_{10}(zs)$. The shaded rectangle is, again, the shock wave. The white square denotes the non-eikonal interactions, either due to the transition operators (20) or due to the sub-eikonal operators introduced in Sec. II. Vertical straight lines denote the quark and anti-quark fields of the shock wave. The dashed line denotes the (future-pointing) Wilson-line staple.

Taking the large- N_c limit with the help of Eq. (40) and the Fierz identity yields

$$\mathcal{F} + \mathcal{G} = \frac{\alpha_s N_c}{4\pi} \int_{\frac{\Lambda^2}{s}}^z \frac{dz'}{z'} \int_{1/(z's)}^{x_{10}^2} \frac{dx_{21}^2}{x_{21}^2} S_{21}(z's) \tilde{Q}_{20}(z's) \approx \frac{\alpha_s N_c}{4\pi} \int_{\frac{\Lambda^2}{s}}^z \frac{dz'}{z'} \int_{1/(z's)}^{x_{10}^2} \frac{dx_{21}^2}{x_{21}^2} \tilde{Q}_{20}(z's), \quad (52)$$

where in the last step we have put $S = 1$, which is valid in DLA. Again we have included the past-pointing Wilson line staple's contribution by simply interchanging $\infty \leftrightarrow -\infty$ in the above.

Adding Eq. (52) to the first term on the right of Eq. (49) we get

$$\frac{\alpha_s N_c}{4\pi} \int_{\frac{\Lambda^2}{s}}^z \frac{dz'}{z'} \int_{1/(z's)}^{x_{10}^2} \frac{dx_{21}^2}{x_{21}^2} \left[\tilde{Q}_{20}(z's) - \tilde{Q}_{10}(z's) \right] \approx 0. \quad (53)$$

This result, while in general non-zero, is not DLA. Therefore, it can be neglected in our DLA calculation.

It is now straightforward to conclude that diagrams \mathcal{H} and \mathcal{I} from Fig. 3 cancel the second term on the right of Eq. (49) with the same DLA accuracy.

Therefore, only the diagrams \mathcal{D} and \mathcal{E} from Fig. 3, along with their past-pointing Wilson line staple counterparts, contribute to the evolution of the dipole amplitude \tilde{Q} , corresponding to the diagram B and its complex conjugate in Fig. 2 of [2]. We have confirmed the analysis carried out in [2].

Lastly, we need to calculate the diagrams \mathcal{D} and \mathcal{E} . For the diagram \mathcal{E} we will employ the propagator

$$\int_{-\infty}^0 dx_2^- \int_0^\infty dx_{2'}^- \overbrace{\psi_\alpha^i(x_2^-, \underline{x}_0) \psi_\beta^j(x_{2'}^-, \underline{x}_1)} = \frac{1}{\pi} \sum_\sigma \int_0^{p_2^-} dk^- k^- \int d^2 x_2 d^2 x_{2'} \left[\int \frac{d^2 k_{2'}}{(2\pi)^2} e^{-ik_{2'} \cdot \underline{x}_{2'1}} \frac{1}{\underline{k}_{2'}^2} (u_\sigma(k_{2'}))_\beta \right] \quad (54)$$

$$\times \left(\sigma V_{\underline{2}}^{\text{pol}[1]} \delta^2(\underline{x}_{22'}) + V_{\underline{2}, \underline{2}'}^{\text{pol}[2]} \right)^{ji} \left[\int \frac{d^2 k_2}{(2\pi)^2} e^{ik_2 \cdot \underline{x}_{20}} \frac{1}{\underline{k}_2^2} (\bar{u}_\sigma(k_2))_\alpha \right],$$

which includes a minus sign arising due to Wick contractions.

For the diagram \mathcal{D} we need the following propagator,

$$\int_{-\infty}^0 dx_{2'}^- \int_0^\infty dx_2^- \overbrace{\psi_\alpha^i(x_2^-, \underline{x}_0) \psi_\beta^j(x_{2'}^-, \underline{x}_1)} = \frac{1}{\pi} \sum_\sigma \int_0^{p_2^-} dk^- k^- \int d^2 x_2 d^2 x_{2'} \left[\int \frac{d^2 k_{2'}}{(2\pi)^2} e^{ik_{2'} \cdot \underline{x}_{2'1}} \frac{1}{\underline{k}_{2'}^2} (v_\sigma(k_{2'}))_\beta \right] \quad (55)$$

$$\times \left(-\sigma V_{\underline{2}}^{\text{pol}[1] \dagger} \delta^2(\underline{x}_{22'}) + V_{\underline{2}, \underline{2}'}^{\text{pol}[2] \dagger} \right)^{ji} \left[\int \frac{d^2 k_2}{(2\pi)^2} e^{-ik_2 \cdot \underline{x}_{20}} \frac{1}{\underline{k}_2^2} (\bar{v}_\sigma(k_2))_\alpha \right].$$

Note the overall sign difference when comparing our Eq. (55) to Eq. (92) in [3]: this is due to the Wick contraction included in our Eq. (55). There is also a sign difference in front of the σ term in Eq. (55) compared to Eq. (92) in [3]. The typo does not propagate in Sec. IV of [3].

Using these propagators, we arrive at

$$\mathcal{D} + \mathcal{E} = \frac{\alpha_s}{4\pi^2} \int_{\frac{\Lambda^2}{s}}^z \frac{dz'}{z'} \left\{ - \int d^2 x_2 \frac{\underline{x}_{20}}{x_{20}^2} \cdot \frac{\underline{x}_{21}}{x_{21}^2} \left\langle \left\langle \text{tr} \left[V_{\underline{1}} V_{\underline{2}}^{\text{pol}[1] \dagger} \right] \right\rangle \right\rangle + i \int d^2 x_2 d^2 x_{2'} \frac{\underline{x}_{2'1}}{x_{2'1}^2} \times \frac{\underline{x}_{20}}{x_{20}^2} \left\langle \left\langle \text{tr} \left[V_{\underline{1}} V_{\underline{2}, \underline{2}'}^{\text{pol}[2] \dagger} \right] \right\rangle \right\rangle + \text{c.c.} \right\} \quad (56)$$

where we have inserted a factor of 2 to account for the past-pointing Wilson lines. Anticipating the impact-parameter integration, we perform a calculation parallel to that on page 12 of [3], obtaining

$$\mathcal{D} + \mathcal{E} = - \frac{\alpha_s}{4\pi^2} \int_{\frac{\Lambda^2}{s}}^z \frac{dz'}{z'} \int d^2 x_2 \left\{ \frac{\underline{x}_{20}}{x_{20}^2} \cdot \frac{\underline{x}_{21}}{x_{21}^2} \left\langle \left\langle \text{tr} \left[V_{\underline{1}} V_{\underline{2}}^{\text{pol}[1] \dagger} \right] \right\rangle \right\rangle \right. \quad (57)$$

$$\left. - \left[-\epsilon^{ik} \frac{x_{20}^k + x_{21}^k}{x_{21}^2 x_{20}^2} + 2 \frac{\underline{x}_{21} \times \underline{x}_{20}}{x_{21}^2 x_{20}^2} \left(\frac{x_{21}^i}{x_{21}^2} - \frac{x_{20}^i}{x_{20}^2} \right) \right] \left\langle \left\langle \text{tr} \left[V_{\underline{1}} V_{\underline{2}}^{iG[2] \dagger} \right] \right\rangle \right\rangle + \text{c.c.} \right\},$$

or, equivalently,

$$\mathcal{D} + \mathcal{E} = - \frac{\alpha_s N_c}{2\pi^2} \int_{\frac{\Lambda^2}{s}}^z \frac{dz'}{z'} \int d^2 x_2 \left\{ \frac{\underline{x}_{20}}{x_{20}^2} \cdot \frac{\underline{x}_{21}}{x_{21}^2} Q_{21}(z's) \right. \quad (58)$$

$$\left. - \left[-\epsilon^{ik} \frac{x_{20}^k + x_{21}^k}{x_{21}^2 x_{20}^2} + 2 \frac{\underline{x}_{21} \times \underline{x}_{20}}{x_{21}^2 x_{20}^2} \left(\frac{x_{21}^i}{x_{21}^2} - \frac{x_{20}^i}{x_{20}^2} \right) \right] G_{21}^i(z's) \right\}.$$

Integrating Eq. (58) over the impact parameters and extracting the DLA contribution we get

$$\int d^2 \left(\frac{x_0 + x_1}{2} \right) [\mathcal{D} + \mathcal{E}] = - \frac{\alpha_s N_c}{2\pi} \int_{\frac{\Lambda^2}{s}}^z \frac{dz'}{z'} \int_{\max[x_{10}^2, \frac{1}{z's}]}^{\min[\frac{z}{z'} x_{10}^2, \frac{1}{\Lambda^2}]} \frac{dx_{21}^2}{x_{21}^2} [Q(x_{21}^2, z's) + 2 G_2(x_{21}^2, z's)], \quad (59)$$

with the x_{21}^2 -integration limits resulting from the structure of the kernel in Eq. (58), lifetime limits, and from $1/\Lambda$ being the upper cutoff on the dipole sizes (an IR cutoff).

The evolution equation for the impact-parameter integrated \tilde{Q} ,

$$\tilde{Q}(x_{10}^2, zs) \equiv \int d^2 \left(\frac{x_0 + x_1}{2} \right) \tilde{Q}_{10}(zs), \quad (60)$$

is

$$\tilde{Q}(x_{10}^2, zs) = \tilde{Q}^{(0)}(x_{10}^2, zs) - \frac{\alpha_s N_c}{2\pi} \int_{\frac{\Lambda^2}{s}}^z \frac{dz'}{z'} \int_{\max[x_{10}^2, \frac{1}{z's}]}^{\min[\frac{z}{z'}x_{10}^2, \frac{1}{\Lambda^2}]} \frac{dx_{21}^2}{x_{21}^2} [Q(x_{21}^2, z's) + 2G_2(x_{21}^2, z's)]. \quad (61)$$

Here $\tilde{Q}^{(0)}$ denotes the inhomogeneous term in the integral equation, resulting from the initial condition for the evolution of \tilde{Q} .

We have completed augmenting the large- N_c & N_f evolution equations from [3] by the contributions of the transition operators (20): in addition to the correction to the evolution of \tilde{G} and $\tilde{\Gamma}$ resulting from the additional term in Eq. (48), we also have the evolution equation (61) for the new operator \tilde{Q} . Before we summarize the new corrected large- N_c & N_f evolution equations, let us make a few observations.

2. A relation between \tilde{Q} and the quark helicity TMD and PDF

As we have mentioned above, the operator definition of \tilde{Q} in Eq. (44) resembles that for the quark helicity TMD (SIDIS plus DY). Let us try to better quantify this similarity.

We start with Eq. (8) of [2] for the SIDIS quark helicity TMD, in which we un-insert the complete set of states X :

$$g_{1L}^{S, \text{SIDIS}}(x, k_T^2) = 2 \frac{2p^+}{(2\pi)^3} \int d^2\zeta d\zeta^- d^2\xi d\xi^- e^{-ik \cdot (\zeta - \xi)} \langle \bar{\psi}(\xi) (\frac{1}{2}\gamma^+ \gamma^5) V_{\underline{\xi}}[\xi^-, \infty] V_{\underline{\zeta}}[\infty, \zeta^-] \psi(\zeta) \rangle. \quad (62)$$

We have also inserted an overall factor of 2 to account for the anti-quark contribution and approximated $k \cdot (\zeta - \xi) \approx -\underline{k} \cdot (\underline{\zeta} - \underline{\xi})$ in the exponent, which is valid at small x . Fourier-transforming Eq. (62) we arrive at

$$\int d^2k_{\perp} e^{ik \cdot \underline{x}_{10}} g_{1L}^{S, \text{SIDIS}}(x, k_T^2) = \frac{2p^+}{\pi} \int d\zeta^- d\xi^- d^2\xi \langle \bar{\psi}(\xi) (\frac{1}{2}\gamma^+ \gamma^5) V_{\underline{\xi}}[\xi^-, \infty] V_{\underline{\xi} + \underline{x}_{10}}[\infty, \zeta^-] \psi(\xi + x_{10}) \rangle. \quad (63)$$

Similarly, for the DY quark helicity TMD, we write

$$\int d^2k_{\perp} e^{ik \cdot \underline{x}_{10}} g_{1L}^{S, \text{DY}}(x, k_T^2) = \frac{2p^+}{\pi} \int d\zeta^- d\xi^- d^2\xi \langle \bar{\psi}(\xi) (\frac{1}{2}\gamma^+ \gamma^5) V_{\underline{\xi}}[\xi^-, -\infty] V_{\underline{\xi} + \underline{x}_{10}}[-\infty, \zeta^-] \psi(\xi + x_{10}) \rangle. \quad (64)$$

Comparing Eqs. (63) and (64) to the definition of \tilde{Q} in Eq. (44), we readily see that

$$\int d^2k_{\perp} e^{ik \cdot \underline{x}_{10}} [g_{1L}^{S, \text{SIDIS}}(x, k_T^2) + g_{1L}^{S, \text{DY}}(x, k_T^2)] = \frac{1}{\pi} \frac{16}{g^2} \frac{1}{2} \int d^2 \left(\frac{x_0 + x_1}{2} \right) \tilde{Q}_{10}(s = Q^2/x). \quad (65)$$

The factor of 1/2 on the right of Eq. (65) removes the double-counting due to the complex conjugate terms: indeed, since TMDs are real, one can readily show that the expression in Eq. (65) is also real. The factor of $2p^+$ from Eqs. (63) and (64) is present in Eq. (44) owing to the definition of the double angle brackets in Eq. (28).

We thus obtain

$$\tilde{Q}(x_{10}^2, Q^2/x) = \frac{\alpha_s \pi^2}{2} \int d^2k_{\perp} e^{ik \cdot \underline{x}_{10}} [g_{1L}^{S, \text{SIDIS}}(x, k_T^2) + g_{1L}^{S, \text{DY}}(x, k_T^2)]. \quad (66)$$

Since helicity TMDs are PT-even, the DY and SIDIS helicity TMDs are equal, $g_{1L}^{S, \text{SIDIS}}(x, k_T^2) = g_{1L}^{S, \text{DY}}(x, k_T^2) \equiv g_{1L}^S(x, k_T^2)$, such that we can rewrite Eq. (66) as

$$\tilde{Q}(x_{10}^2, Q^2/x) = \alpha_s \pi^2 \int d^2k_{\perp} e^{ik \cdot \underline{x}_{10}} g_{1L}^S(x, k_T^2), \quad (67)$$

or, equivalently,

$$g_{1L}^S(x, k_T^2) = \frac{1}{4\pi^4 \alpha_s} \int d^2x_{10} e^{-ik \cdot \underline{x}_{10}} \tilde{Q}(x_{10}^2, Q^2/x). \quad (68)$$

Equations (67) and (68) provide a relation between the quark helicity TMDs and the new object \tilde{Q} we have introduced in this work.

We can also connect \tilde{Q} to the quark helicity PDFs by writing the flavor-singlet quark helicity PDF as an integral of the corresponding TMD over k_T ,

$$\Delta\Sigma(x, Q^2) = \sum_f \int^{Q^2} d^2k_\perp g_{1L}^S(x, k_T^2) = \frac{N_f}{\alpha_s \pi^2} \tilde{Q}(x_{10}^2, Q^2/x) = \frac{N_f}{\alpha_s \pi^2} \tilde{Q}\left(x_{10}^2 = \frac{1}{Q^2}, s = \frac{Q^2}{x}\right). \quad (69)$$

Here, again, for simplicity we assume that all quark flavors contribute equally.

Using Eq. (61) we write

$$\begin{aligned} \Delta\Sigma(x, Q^2) &= \frac{N_f}{\alpha_s \pi^2} \tilde{Q}^{(0)}\left(x_{10}^2 = \frac{1}{Q^2}, s = \frac{Q^2}{x}\right) - \frac{N_c N_f}{2\pi^3} \int_{\frac{\Lambda^2}{s}}^1 \frac{dz}{z} \int_{\max\left[\frac{1}{Q^2}, \frac{x}{zQ^2}\right]}^{\min\left[\frac{1}{zQ^2}, \frac{1}{\lambda^2}\right]} \frac{dx_{10}^2}{x_{10}^2} [Q(x_{10}^2, zs) + 2G_2(x_{10}^2, zs)] \quad (70) \\ &= \frac{N_f}{\alpha_s \pi^2} \tilde{Q}^{(0)}\left(x_{10}^2 = \frac{1}{Q^2}, s = \frac{Q^2}{x}\right) - \frac{N_c N_f}{2\pi^3} \int_{\frac{1}{Q^2}}^{\frac{1}{\lambda^2}} \frac{dx_{10}^2}{x_{10}^2} \int_{\frac{1}{s x_{10}^2}}^{\frac{1}{Q^2 x_{10}^2}} \frac{dz}{z} [Q(x_{10}^2, zs) + 2G_2(x_{10}^2, zs)]. \end{aligned}$$

Comparing Eq. (18a) to Eq. (70), we see that the latter has the extra inhomogeneous term $\tilde{Q}^{(0)}$ which was neglected in Eq. (18a) (and in [1–3, 12, 13, 50]) as not evolving at small x . In addition, the lower limit of the x_{10} integral is now different in the first line of Eq. (70) as compared to Eq. (18a).

We conclude that equations (69) and (70) result in an expression for $\Delta\Sigma$ at small x with a slight modification as compared to Eq. (18a) used earlier in the literature. As we will see below, the present expression for $\Delta\Sigma$ appears to be close to the $\overline{\text{MS}}$ scheme for calculating the polarized DGLAP splitting functions. (The previous definition (18a) can be thought of corresponding to the “polarized DIS scheme” [23].)

D. Contribution to the evolution for the dipole amplitude Q

For completeness, let us determine the contribution of the transition operators (25) to the DLA evolution of the dipole amplitude Q defined in Eq. (6a) above. (The dipole amplitude G_2 is defined by a purely gluonic operator; therefore, its evolution does not contain quarks and received no contribution from the transition operators.)

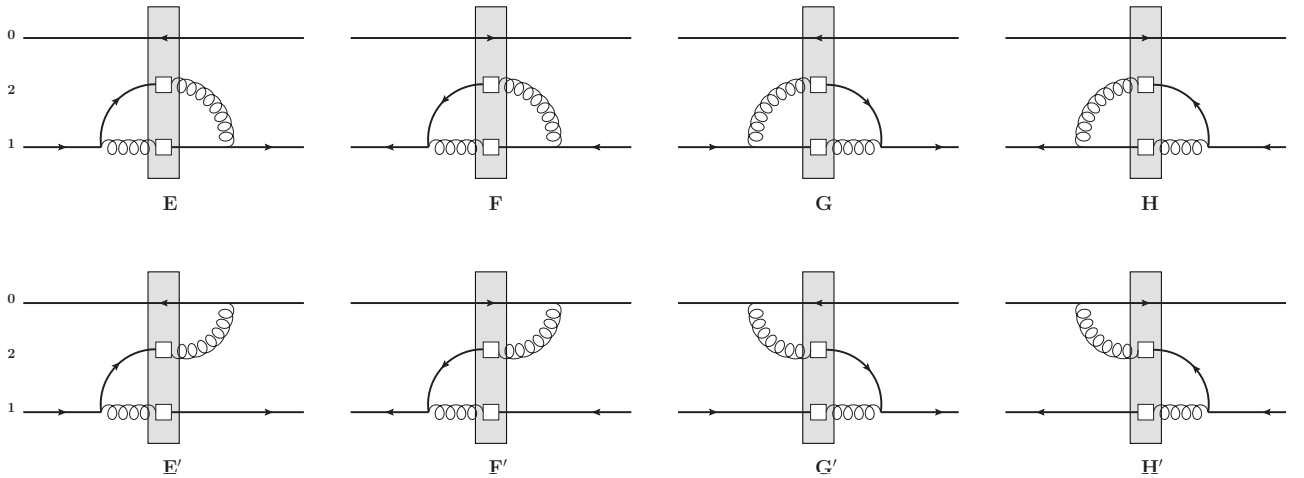


FIG. 4. The diagrams for the evolution of Q_{10} due to the $q/\bar{q} \rightarrow G$ and $G \rightarrow q/\bar{q}$ shock-wave transition operators calculated here. The shaded rectangle denotes the shock wave, while the white square denotes the non-eikonal interaction with the shock wave mediated by the transition operators from Fig. 1.

The relevant diagrams containing contributions of the transition operators to the evolution of the dipole amplitude Q are shown in Fig. 4. Their calculation parallels that in Sec. III B 1 and employs the background field propagators

Employing Eq. (40) and the Fierz identity one can recast Eq. (73) as

$$\begin{aligned}
& \left\langle \left\langle \text{tr} \left[t^a V_0^\dagger t^b \left[\left(W_{\underline{1}}^{a[2]}[-\infty, \infty] \right)^\dagger W_{\underline{2}}^{b[1]}[\infty, -\infty] + \left(W_{\underline{1}}^{a[1]}[-\infty, \infty] \right)^\dagger W_{\underline{2}}^{b[2]}[\infty, -\infty] \right] \right] \right\rangle \right\rangle \quad (75) \\
&= \frac{g^2}{16\sqrt{p_2^-} k^-} \int_{-\infty}^{\infty} dy^- \int_{-\infty}^{\infty} dz^- \left\{ \left\langle \left\langle \bar{\psi}(y^-, \underline{x}_2) \gamma^+ \gamma^5 V_{\underline{2}}[y^-, \infty] V_{\underline{1}} V_0^\dagger V_{\underline{2}} V_{\underline{1}}[-\infty, z^-] \psi(z^-, \underline{x}_1) \right\rangle \right\rangle \right. \\
&- S_{10} \left\langle \left\langle \bar{\psi}(y^-, \underline{x}_2) \gamma^+ \gamma^5 V_{\underline{2}}[y^-, -\infty] V_{\underline{1}}[-\infty, z^-] \psi(z^-, \underline{x}_1) \right\rangle \right\rangle - S_{20} \left\langle \left\langle \bar{\psi}(y^-, \underline{x}_2) \gamma^+ \gamma^5 V_{\underline{2}}[y^-, \infty] V_{\underline{1}}[\infty, z^-] \psi(z^-, \underline{x}_1) \right\rangle \right\rangle \\
&+ \left. \frac{1}{N_c^2} \left\langle \left\langle \bar{\psi}(y^-, \underline{x}_2) \gamma^+ \gamma^5 V_{\underline{2}}[y^-, -\infty] V_0^\dagger V_{\underline{1}}[\infty, z^-] \psi(z^-, \underline{x}_1) \right\rangle \right\rangle \right\}.
\end{aligned}$$

In the second to last line of Eq. (75) we have employed the large- N_c limit to factor out the unpolarized S -matrices S_{10} and S_{20} .

Using Eq. (75) in Eq. (74) we conclude that the contribution of the diagrams in Fig. 4 is sub-leading at large N_c (and at large- $N_c \& N_f$): see the explicit $1/N_c$ overall factor in Eq. (74). We conclude that these diagrams do not contribute to the large- $N_c \& N_f$ (or large- N_c) evolution of the dipole amplitude Q in the DLA. Therefore, we neglect the contribution of the diagrams in Fig. 4 below.

E. A new version of the large- $N_c \& N_f$ evolution equations

Let us now summarize the modified version of the large- $N_c \& N_f$ evolution equations (155) from [3]. Combining our results in Eq. (48) and Eq. (61), along with incorporating Eq. (48) into the evolution for the neighbor dipole amplitude $\tilde{\Gamma}$ from [3], we arrive at

$$Q(x_{10}^2, zs) = Q^{(0)}(x_{10}^2, zs) + \frac{\alpha_s N_c}{2\pi} \int_{1/sx_{10}^2}^z \frac{dz'}{z'} \int_{1/z's}^{x_{10}^2} \frac{dx_{21}^2}{x_{21}^2} \left[2\tilde{G}(x_{21}^2, z's) + 2\tilde{\Gamma}(x_{10}^2, x_{21}^2, z's) \right] \quad (76a)$$

$$+ Q(x_{21}^2, z's) - \bar{\Gamma}(x_{10}^2, x_{21}^2, z's) + 2\Gamma_2(x_{10}^2, x_{21}^2, z's) + 2G_2(x_{21}^2, z's)$$

$$+ \frac{\alpha_s N_c}{4\pi} \int_{\Lambda^2/s}^z \frac{dz'}{z'} \int_{1/z's}^{\min\{x_{10}^2 z'/z', 1/\Lambda^2\}} \frac{dx_{21}^2}{x_{21}^2} [Q(x_{21}^2, z's) + 2G_2(x_{21}^2, z's)],$$

$$\bar{\Gamma}(x_{10}^2, x_{21}^2, z's) = Q^{(0)}(x_{10}^2, z's) + \frac{\alpha_s N_c}{2\pi} \int_{1/sx_{10}^2}^{z'} \frac{dz''}{z''} \int_{1/z''s}^{\min\{x_{10}^2, x_{21}^2 z'/z''\}} \frac{dx_{32}^2}{x_{32}^2} \left[2\tilde{G}(x_{32}^2, z''s) \right] \quad (76b)$$

$$+ 2\tilde{\Gamma}(x_{10}^2, x_{32}^2, z''s) + Q(x_{32}^2, z''s) - \bar{\Gamma}(x_{10}^2, x_{32}^2, z''s) + 2\Gamma_2(x_{10}^2, x_{32}^2, z''s) + 2G_2(x_{32}^2, z''s)$$

$$+ \frac{\alpha_s N_c}{4\pi} \int_{\Lambda^2/s}^{z'} \frac{dz''}{z''} \int_{1/z''s}^{\min\{x_{21}^2 z'/z'', 1/\Lambda^2\}} \frac{dx_{32}^2}{x_{32}^2} [Q(x_{32}^2, z''s) + 2G_2(x_{32}^2, z''s)],$$

$$\tilde{G}(x_{10}^2, zs) = \tilde{G}^{(0)}(x_{10}^2, zs) + \frac{\alpha_s N_c}{2\pi} \int_{1/sx_{10}^2}^z \frac{dz'}{z'} \int_{1/z's}^{x_{10}^2} \frac{dx_{21}^2}{x_{21}^2} \left[3\tilde{G}(x_{21}^2, z's) + \tilde{\Gamma}(x_{10}^2, x_{21}^2, z's) \right] \quad (76c)$$

$$+ 2G_2(x_{21}^2, z's) + \left(2 - \frac{N_f}{2N_c} \right) \Gamma_2(x_{10}^2, x_{21}^2, z's) - \frac{N_f}{4N_c} \bar{\Gamma}(x_{10}^2, x_{21}^2, z's) - \frac{N_f}{2N_c} \tilde{Q}(x_{21}^2, z's)$$

$$- \frac{\alpha_s N_f}{8\pi} \int_{\Lambda^2/s}^z \frac{dz'}{z'} \int_{\max\{x_{10}^2, 1/z's\}}^{\min\{x_{10}^2 z'/z', 1/\Lambda^2\}} \frac{dx_{21}^2}{x_{21}^2} [Q(x_{21}^2, z's) + 2G_2(x_{21}^2, z's)],$$

$$\tilde{\Gamma}(x_{10}^2, x_{21}^2, z's) = \tilde{G}^{(0)}(x_{10}^2, z's) + \frac{\alpha_s N_c}{2\pi} \int_{1/sx_{10}^2}^{z'} \frac{dz''}{z''} \int_{1/z''s}^{\min\{x_{10}^2, x_{21}^2 z'/z''\}} \frac{dx_{32}^2}{x_{32}^2} \left[3\tilde{G}(x_{32}^2, z''s) \right] \quad (76d)$$

$$+ \tilde{\Gamma}(x_{10}^2, x_{32}^2, z''s) + 2G_2(x_{32}^2, z''s) + \left(2 - \frac{N_f}{2N_c} \right) \Gamma_2(x_{10}^2, x_{32}^2, z''s) - \frac{N_f}{4N_c} \bar{\Gamma}(x_{10}^2, x_{32}^2, z''s) - \frac{N_f}{2N_c} \tilde{Q}(x_{32}^2, z''s)$$

$$- \frac{\alpha_s N_f}{8\pi} \int_{\Lambda^2/s}^{z'} \frac{dz''}{z''} \int_{\max\{x_{10}^2, 1/z''s\}}^{\min\{x_{21}^2 z'/z'', 1/\Lambda^2\}} \frac{dx_{32}^2}{x_{32}^2} [Q(x_{32}^2, z''s) + 2G_2(x_{32}^2, z''s)],$$

$$G_2(x_{10}^2, zs) = G_2^{(0)}(x_{10}^2, zs) + \frac{\alpha_s N_c}{\pi} \int_{\frac{\Lambda^2}{s}}^z \frac{dz'}{z'} \int_{\max[x_{10}^2, \frac{1}{z's}]}^{\min\{\frac{z}{z'} x_{10}^2, 1/\Lambda^2\}} \frac{dx_{21}^2}{x_{21}^2} \left[\tilde{G}(x_{21}^2, z's) + 2G_2(x_{21}^2, z's) \right], \quad (76e)$$

$$\Gamma_2(x_{10}^2, x_{21}^2, z's) = G_2^{(0)}(x_{10}^2, z's) + \frac{\alpha_s N_c}{\pi} \int_{\frac{\Lambda^2}{s}}^{z'} \frac{dz''}{z''} \int_{\max[x_{10}^2, \frac{1}{z''s}]}^{\min\{\frac{z'}{z''} x_{21}^2, 1/\Lambda^2\}} \frac{dx_{32}^2}{x_{32}^2} \left[\tilde{G}(x_{32}^2, z''s) + 2G_2(x_{32}^2, z''s) \right], \quad (76f)$$

$$\tilde{Q}(x_{10}^2, zs) = \tilde{Q}^{(0)}(x_{10}^2, zs) - \frac{\alpha_s N_c}{2\pi} \int_{\frac{\Lambda^2}{s}}^z \frac{dz'}{z'} \int_{\max[x_{10}^2, \frac{1}{z's}]}^{\min\{\frac{z}{z'} x_{10}^2, 1/\Lambda^2\}} \frac{dx_{21}^2}{x_{21}^2} [Q(x_{21}^2, z's) + 2G_2(x_{21}^2, z's)]. \quad (76g)$$

The new terms and the new equation are shown in blue. The equations (76) are written in the form treating Λ as the infrared cutoff (and not as a semi-perturbative scale characterizing the target, like the target saturation scale, see [3, 19] for a discussion of this issue). The equations (76) are re-derived in Appendix B using LCPT.

For completeness, let us re-state the expressions for helicity PDFs at small x :

$$\Delta G(x, Q^2) = \frac{2N_c}{\alpha_s \pi^2} G_2 \left(x_{10}^2 = \frac{1}{Q^2}, s = \frac{Q^2}{x} \right), \quad (77a)$$

$$\Delta \Sigma(x, Q^2) = \frac{N_f}{\alpha_s \pi^2} \tilde{Q} \left(x_{10}^2 = \frac{1}{Q^2}, s = \frac{Q^2}{x} \right). \quad (77b)$$

While the expression for ΔG was obtained earlier [15], the result for $\Delta \Sigma$ is new, slightly correcting the older result [1–3, 12].

IV. ITERATIVE SOLUTION

In this Section, we solve Eqs. (76) iteratively, similar to what was done in [3, 23]. We assume non-vanishing constant (independent of x and Q^2) initial conditions $\Delta\Sigma^{(0)}$ and $\Delta G^{(0)}$ for the respective flavor-singlet quark and gluon helicity PDFs. The (also constant) initial conditions for the polarized dipole amplitudes are

$$G_2^{(0)} = \frac{\alpha_s \pi^2}{2N_c} \Delta G^{(0)}, \quad \tilde{Q}^{(0)} = \frac{\alpha_s \pi^2}{N_f} \Delta\Sigma^{(0)}, \quad Q^{(0)} = -\frac{1}{2} \tilde{Q}^{(0)}, \quad \tilde{G}^{(0)} = \frac{N_f}{4N_c} \tilde{Q}^{(0)}. \quad (78)$$

The first two conditions follow from Eqs. (77). The last two conditions can be derived from the original definitions of $Q(x_{10}^2, s)$ in Eq. (6a), $\tilde{G}(x_{10}^2, s)$ in Eq. (16) and $\tilde{Q}(x_{10}^2, s)$ in Eq. (44) by taking the zero dipole size limit, $x_{10}^2 \rightarrow 0$. Indeed, we first notice that only $V_{\underline{x}}^{q[1]}$ in $V_{\underline{x}}^{\text{pol}[1]}$ contributes to $Q(x_{10}^2, s)$ in this limit, and only the quark-fields part of $W_{\underline{x}}^{\text{pol}[1]}$ in Eq. (17) contributes to $\tilde{G}(x_{10}^2, s)$. Performing a little algebra and clarifying that the zero dipole size limit corresponds to $x_{10}^2 \rightarrow 1/s$, with the center-of-mass energy squared s being the highest momentum scale in the problem, we arrive at the following relations between the (impact-parameter integrated) polarized dipole amplitudes:

$$\tilde{G}\left(x_{10}^2 = \frac{1}{s}, s\right) = -\frac{N_f}{4C_F} Q\left(x_{10}^2 = \frac{1}{s}, s\right) \approx -\frac{N_f}{2N_c} Q\left(x_{10}^2 = \frac{1}{s}, s\right), \quad (79a)$$

$$\tilde{G}\left(x_{10}^2 = \frac{1}{s}, s\right) = \frac{N_f}{4N_c} \tilde{Q}\left(x_{10}^2 = \frac{1}{s}, s\right). \quad (79b)$$

Here we have summed over flavors in \tilde{G} , assuming that all flavors contribute equally. (Otherwise, one would have to replace $N_f Q \rightarrow \sum_f Q_f$ in Eq. (79a) and $N_f \tilde{Q} \rightarrow \sum_f \tilde{Q}_f$ in Eq. (79b), with the flavor-dependent dipole amplitudes Q_f and \tilde{Q}_f .) The last transition in Eq. (79a) is valid in the large- N_c and large- $N_c \& N_f$ limits. Equations (79) are otherwise exact. Since all the integral kernels in Eqs. (76) vanish in the $x_{10}^2 \rightarrow 1/s$ limit (which, in those equations, corresponds to the $x_{10}^2 \rightarrow 1/(zs)$ limit), we see that the conditions (79) need to be satisfied by the inhomogeneous terms (the initial conditions) in Eqs. (76), after which they will be always satisfied by the dipole amplitudes solving those evolution equations.

Equations (79) allowed us to fix the initial amplitudes $Q^{(0)}$ and $\tilde{G}^{(0)}$ in Eq. (78).

In what follows, we will solve Eqs. (76) iteratively, using Eqs. (77) to obtain order-by-order in α_s expansion for hPDFs,

$$\Delta\Sigma(x, Q^2) = \Delta\Sigma^{(0)} + \Delta\Sigma^{(1)}(x, Q^2) + \Delta\Sigma^{(2)}(x, Q^2) + \dots, \quad (80a)$$

$$\Delta G(x, Q^2) = \Delta G^{(0)} + \Delta G^{(1)}(x, Q^2) + \Delta G^{(2)}(x, Q^2) + \dots, \quad (80b)$$

where the index in the superscript parenthesis matches the power of α_s correction to $\Delta\Sigma^{(0)}$ and $\Delta G^{(0)}$. The iterative expansion of the dipole amplitudes and DGLAP splitting functions is labeled in the same way.

A. Step 1

After one step of evolution, using the dipole amplitudes from Eq. (78) in Eqs. (76), one obtains

$$G_2^{(1)}(x_{10}^2, zs) = \frac{\alpha_s N_c}{\pi} \ln(zs x_{10}^2) \ln\left(\frac{1}{\Lambda^2 x_{10}^2}\right) \left[\frac{N_f}{4N_c} \tilde{Q}^{(0)} + 2G_2^{(0)}\right], \quad (81a)$$

$$\tilde{Q}^{(1)}(x_{10}^2, zs) = -\frac{\alpha_s N_c}{2\pi} \ln(zs x_{10}^2) \ln\left(\frac{1}{\Lambda^2 x_{10}^2}\right) \left[-\frac{1}{2} \tilde{Q}^{(0)} + 2G_2^{(0)}\right]. \quad (81b)$$

The hPDFs follow from Eq. (77)

$$\Delta G^{(1)}(x, Q^2) = \frac{\alpha_s N_c}{4\pi} \ln \frac{1}{x} \ln \frac{Q^2}{\Lambda^2} \left[2\Delta\Sigma^{(0)} + 8\Delta G^{(0)}\right], \quad (82a)$$

$$\Delta\Sigma^{(1)}(x, Q^2) = \frac{\alpha_s N_c}{4\pi} \ln \frac{1}{x} \ln \frac{Q^2}{\Lambda^2} \left[\Delta\Sigma^{(0)} - 2\frac{N_f}{N_c} \Delta G^{(0)}\right]. \quad (82b)$$

Having these two expressions for hPDFs, one can employ the spin-dependent DGLAP evolution equations

$$\frac{\partial}{\partial \ln Q^2} \begin{pmatrix} \Delta\Sigma(x, Q^2) \\ \Delta G(x, Q^2) \end{pmatrix} = \int_x^1 \frac{dz}{z} \begin{pmatrix} \Delta P_{qq}(z) & \Delta P_{qG}(z) \\ \Delta P_{Gq}(z) & \Delta P_{GG}(z) \end{pmatrix} \begin{pmatrix} \Delta\Sigma\left(\frac{x}{z}, Q^2\right) \\ \Delta G\left(\frac{x}{z}, Q^2\right) \end{pmatrix} \equiv \left[\Delta\mathbf{P} \otimes \begin{pmatrix} \Delta\Sigma \\ \Delta G \end{pmatrix} \right] (x, Q^2) \quad (83)$$

to readily read out the polarized small- x large- N_c & N_f splitting functions at the one-loop order

$$\Delta\mathbf{P}^{(0)}(x) = \frac{\alpha_s N_c}{4\pi} \begin{pmatrix} 1 & -2\frac{N_f}{N_c} \\ 2 & 8 \end{pmatrix}. \quad (84)$$

We also calculated other polarized dipole amplitudes and the neighbor dipole amplitudes after one step of the evolution, obtaining

$$Q^{(1)}(x_{10}^2, zs) = \frac{\alpha_s N_c}{4\pi} \ln^2(zsx_{10}^2) \left[\left(\frac{N_f}{N_c} - \frac{1}{4} \right) \tilde{Q}^{(0)} + 5G_2^{(0)} \right] + \frac{\alpha_s N_c}{4\pi} \ln(zsx_{10}^2) \ln \frac{1}{\Lambda^2 x_{10}^2} \left[-\frac{1}{2} \tilde{Q}^{(0)} + 2G_2^{(0)} \right], \quad (85a)$$

$$\begin{aligned} \tilde{G}^{(1)}(x_{10}^2, zs) &= \frac{\alpha_s N_c}{4\pi} \ln^2(zsx_{10}^2) \left[\frac{5N_f}{8N_c} \tilde{Q}^{(0)} + 4 \left(1 - \frac{N_f}{8N_c} \right) G_2^{(0)} \right] \\ &\quad - \frac{\alpha_s N_c}{4\pi} \ln(zsx_{10}^2) \ln \left(\frac{1}{\Lambda^2 x_{10}^2} \right) \frac{N_f}{2N_c} \left[-\frac{1}{2} \tilde{Q}^{(0)} + 2G_2^{(0)} \right], \end{aligned} \quad (85b)$$

$$\begin{aligned} \bar{\Gamma}^{(1)}(x_{10}^2, x_{21}^2, z's) &= \frac{\alpha_s N_c}{4\pi} \ln^2(z'sx_{21}^2) \left[\left(\frac{N_f}{N_c} - \frac{1}{4} \right) \tilde{Q}^{(0)} + 5G_2^{(0)} \right] \\ &\quad + \frac{\alpha_s N_c}{4\pi} \ln(z'sx_{21}^2) \ln \frac{1}{\Lambda^2 x_{21}^2} \left[\left(\frac{2N_f}{N_c} - \frac{1}{2} \right) \tilde{Q}^{(0)} + 10G_2^{(0)} \right] - \frac{\alpha_s N_c}{4\pi} \ln(z'sx_{21}^2) \ln \frac{1}{\Lambda^2 x_{10}^2} \left[\frac{2N_f}{N_c} \tilde{Q}^{(0)} + 8G_2^{(0)} \right], \end{aligned} \quad (85c)$$

$$\begin{aligned} \tilde{\Gamma}^{(1)}(x_{10}^2, x_{21}^2, z's) &= \frac{\alpha_s N_c}{4\pi} \ln^2(z'sx_{21}^2) \left[\frac{5N_f}{8N_c} \tilde{Q}^{(0)} + \left(4 - \frac{N_f}{2N_c} \right) G_2^{(0)} \right] \\ &\quad + \frac{\alpha_s N_c}{4\pi} \ln(z'sx_{21}^2) \ln \frac{1}{\Lambda^2 x_{21}^2} \left[\frac{5N_f}{4N_c} \tilde{Q}^{(0)} + \left(8 - \frac{N_f}{N_c} \right) G_2^{(0)} \right] - \frac{\alpha_s N_c}{4\pi} \ln(z'sx_{21}^2) \ln \frac{1}{\Lambda^2 x_{10}^2} \left[\frac{N_f}{N_c} \tilde{Q}^{(0)} + 8G_2^{(0)} \right], \end{aligned} \quad (85d)$$

$$\Gamma_2^{(1)}(x_{10}^2, x_{21}^2, z's) = 4 \frac{\alpha_s N_c}{4\pi} \ln(z'sx_{21}^2) \ln \left(\frac{1}{\Lambda^2 x_{10}^2} \right) \left[\frac{N_f}{4N_c} \tilde{Q}^{(0)} + 2G_2^{(0)} \right]. \quad (85e)$$

B. Step 2

After two steps of the evolution, one gets

$$\begin{aligned} G_2^{(2)}(x_{10}^2, zs) &= \left(\frac{\alpha_s N_c}{4\pi} \right)^2 \frac{1}{3} \ln^3(zsx_{10}^2) \ln \left(\frac{1}{\Lambda^2 x_{10}^2} \right) \left[\frac{5N_f}{2N_c} \tilde{Q}^{(0)} + 2 \left(8 - \frac{N_f}{N_c} \right) G_2^{(0)} \right] \\ &\quad + \left(\frac{\alpha_s N_c}{4\pi} \right)^2 \ln^2(zsx_{10}^2) \ln^2 \left(\frac{1}{\Lambda^2 x_{10}^2} \right) \left[\frac{9N_f}{4N_c} \tilde{Q}^{(0)} + \left(16 - \frac{N_f}{N_c} \right) G_2^{(0)} \right], \end{aligned} \quad (86a)$$

$$\begin{aligned} \tilde{Q}^{(2)}(x_{10}^2, zs) &= - \left(\frac{\alpha_s N_c}{4\pi} \right)^2 \frac{2}{3} \ln^3(zsx_{10}^2) \ln \frac{1}{\Lambda^2 x_{10}^2} \left[\left(\frac{N_f}{N_c} - \frac{1}{4} \right) \tilde{Q}^{(0)} + 5G_2^{(0)} \right] \\ &\quad - \left(\frac{\alpha_s N_c}{4\pi} \right)^2 \ln^2(zsx_{10}^2) \ln^2 \left(\frac{1}{\Lambda^2 x_{10}^2} \right) \left[\left(-\frac{1}{4} + \frac{N_f}{N_c} \right) \tilde{Q}^{(0)} + 9G_2^{(0)} \right]. \end{aligned} \quad (86b)$$

The hPDFs from the second iteration are

$$\begin{aligned} \Delta G^{(2)}(x, Q^2) &= \left(\frac{\alpha_s N_c}{4\pi} \right)^2 \frac{1}{3} \ln^3 \frac{1}{x} \ln \left(\frac{Q^2}{\Lambda^2} \right) \left[5\Delta\Sigma^{(0)} + 2 \left(8 - \frac{N_f}{N_c} \right) \Delta G^{(0)} \right] \\ &\quad + \left(\frac{\alpha_s N_c}{4\pi} \right)^2 \ln^2 \frac{1}{x} \ln^2 \left(\frac{Q^2}{\Lambda^2} \right) \left[\frac{9}{2} \Delta\Sigma^{(0)} + \left(16 - \frac{N_f}{N_c} \right) \Delta G^{(0)} \right], \end{aligned} \quad (87a)$$

$$\begin{aligned} \Delta\Sigma^{(2)}(x, Q^2) &= \left(\frac{\alpha_s N_c}{4\pi} \right)^2 \frac{1}{3} \ln^3 \frac{1}{x} \ln \frac{Q^2}{\Lambda^2} \left[\left(\frac{1}{2} - \frac{2N_f}{N_c} \right) \Delta\Sigma^{(0)} - \frac{5N_f}{N_c} \Delta G^{(0)} \right] \\ &\quad + \left(\frac{\alpha_s N_c}{4\pi} \right)^2 \ln^2 \frac{1}{x} \ln^2 \frac{Q^2}{\Lambda^2} \left[\left(\frac{1}{4} - \frac{N_f}{N_c} \right) \Delta\Sigma^{(0)} - \frac{9N_f}{2N_c} \Delta G^{(0)} \right]. \end{aligned} \quad (87b)$$

From the terms containing $\ln^3 \frac{1}{x} \ln \frac{Q^2}{\Lambda^2}$, one can read out the polarized small- x large- N_c & N_f splitting functions at the two-loop order

$$\Delta \mathbf{P}^{(1)}(x) = \left(\frac{\alpha_s N_c}{4\pi} \right)^2 \ln^2 \frac{1}{x} \begin{pmatrix} \frac{1}{2} - \frac{2N_f}{N_c} & -\frac{5N_f}{N_c} \\ 5 & 16 - \frac{2N_f}{N_c} \end{pmatrix}. \quad (88)$$

Other polarized dipole amplitudes after two steps of the evolution that we will need for the next iteration of the solution are

$$Q^{(2)}(x_{10}^2, zs) = \frac{1}{6} \left(\frac{\alpha_s N_c}{4\pi} \right)^2 \ln^4(zsx_{10}^2) \left[\left(\frac{5N_f}{N_c} - \frac{1}{4} \right) \tilde{Q}^{(0)} + \left(35 - \frac{4N_f}{N_c} \right) G_2^{(0)} \right] \quad (89a)$$

$$+ \frac{1}{3} \left(\frac{\alpha_s N_c}{4\pi} \right)^2 \ln^3(zsx_{10}^2) \ln \frac{1}{\Lambda^2 x_{10}^2} \left[\left(\frac{7N_f}{N_c} - \frac{1}{2} \right) \tilde{Q}^{(0)} + \left(46 - \frac{4N_f}{N_c} \right) G_2^{(0)} \right]$$

$$+ \frac{1}{4} \left(\frac{\alpha_s N_c}{4\pi} \right)^2 \ln^2(zsx_{10}^2) \ln^2 \left(\frac{1}{\Lambda^2 x_{10}^2} \right) \left[\left(\frac{2N_f}{N_c} - \frac{1}{2} \right) \tilde{Q}^{(0)} + 18G_2^{(0)} \right],$$

$$\tilde{G}^{(2)}(x_{10}^2, zs) = \frac{1}{6} \left(\frac{\alpha_s N_c}{4\pi} \right)^2 \ln^4(zsx_{10}^2) \left[\frac{N_f}{N_c} \left(-\frac{N_f}{2N_c} + \frac{35}{8} \right) \tilde{Q}^{(0)} + \left(28 - \frac{11N_f}{2N_c} \right) G_2^{(0)} \right] \quad (89b)$$

$$+ \frac{1}{6} \left(\frac{\alpha_s N_c}{4\pi} \right)^2 \ln^3(zsx_{10}^2) \ln \frac{1}{\Lambda^2 x_{10}^2} \left[\frac{N_f}{N_c} \left(\frac{19}{2} - \frac{2N_f}{N_c} \right) \tilde{Q}^{(0)} + \left(64 - \frac{18N_f}{N_c} \right) G_2^{(0)} \right]$$

$$- \frac{1}{8} \left(\frac{\alpha_s N_c}{4\pi} \right)^2 \ln^2(zsx_{10}^2) \ln^2 \frac{1}{\Lambda^2 x_{10}^2} \left[\frac{N_f}{N_c} \left(\frac{2N_f}{N_c} - \frac{1}{2} \right) \tilde{Q}^{(0)} + \frac{18N_f}{N_c} G_2^{(0)} \right].$$

C. Step 3

After three steps of the evolution, the polarized dipole amplitudes that we need to find hPDFs become

$$G_2^{(3)}(x_{10}^2, zs) = \frac{1}{30} \left(\frac{\alpha_s N_c}{4\pi} \right)^3 \ln^5(zsx_{10}^2) \ln \frac{1}{\Lambda^2 x_{10}^2} \left[\frac{N_f}{N_c} \left(-\frac{2N_f}{N_c} + \frac{35}{2} \right) \tilde{Q}^{(0)} + \left(112 - \frac{22N_f}{N_c} \right) G_2^{(0)} \right] \quad (90a)$$

$$+ \frac{1}{24} \left(\frac{\alpha_s N_c}{4\pi} \right)^3 \ln^4(zsx_{10}^2) \ln^2 \frac{1}{\Lambda^2 x_{10}^2} \left[\frac{N_f}{N_c} \left(39 - \frac{4N_f}{N_c} \right) \tilde{Q}^{(0)} + 2 \left(128 - \frac{26N_f}{N_c} \right) G_2^{(0)} \right]$$

$$+ \frac{1}{36} \left(\frac{\alpha_s N_c}{4\pi} \right)^3 \ln^3(zsx_{10}^2) \ln^3 \frac{1}{\Lambda^2 x_{10}^2} \left[\frac{N_f}{N_c} \left(73 - \frac{4N_f}{N_c} \right) \tilde{Q}^{(0)} + 2 \left(256 - \frac{34N_f}{N_c} \right) G_2^{(0)} \right],$$

$$\tilde{Q}^{(3)}(x_{10}^2, zs) = -\frac{1}{30} \left(\frac{\alpha_s N_c}{4\pi} \right)^3 \ln^5(zsx_{10}^2) \ln \frac{1}{\Lambda^2 x_{10}^2} \left[\left(\frac{10N_f}{N_c} - \frac{1}{2} \right) \tilde{Q}^{(0)} + 2 \left(35 - \frac{4N_f}{N_c} \right) G_2^{(0)} \right] \quad (90b)$$

$$- \frac{1}{24} \left(\frac{\alpha_s N_c}{4\pi} \right)^3 \ln^4(zsx_{10}^2) \ln^2 \frac{1}{\Lambda^2 x_{10}^2} \left[\left(\frac{24N_f}{N_c} - 1 \right) \tilde{Q}^{(0)} + 2 \left(78 - \frac{8N_f}{N_c} \right) G_2^{(0)} \right]$$

$$- \frac{1}{36} \left(\frac{\alpha_s N_c}{4\pi} \right)^3 \ln^3(zsx_{10}^2) \ln^3 \frac{1}{\Lambda^2 x_{10}^2} \left[\left(\frac{40N_f}{N_c} - 1 \right) \tilde{Q}^{(0)} + 2 \left(146 - \frac{8N_f}{N_c} \right) G_2^{(0)} \right].$$

The corresponding hPDFs are

$$\begin{aligned} \Delta G^{(3)}(x, Q^2) &= \frac{1}{30} \left(\frac{\alpha_s N_c}{4\pi} \right)^3 \ln^5 \frac{1}{x} \ln \frac{Q^2}{\Lambda^2} \left[\left(35 - \frac{4N_f}{N_c} \right) \Delta \Sigma^{(0)} + 2 \left(56 - \frac{11N_f}{N_c} \right) \Delta G^{(0)} \right] \\ &\quad + \frac{1}{24} \left(\frac{\alpha_s N_c}{4\pi} \right)^3 \ln^4 \frac{1}{x} \ln^2 \frac{Q^2}{\Lambda^2} \left[2 \left(39 - \frac{4N_f}{N_c} \right) \Delta \Sigma^{(0)} + 4 \left(64 - \frac{13N_f}{N_c} \right) \Delta G^{(0)} \right] \\ &\quad + \frac{1}{36} \left(\frac{\alpha_s N_c}{4\pi} \right)^3 \ln^3 \frac{1}{x} \ln^3 \frac{Q^2}{\Lambda^2} \left[2 \left(73 - \frac{4N_f}{N_c} \right) \Delta \Sigma^{(0)} + 4 \left(128 - \frac{17N_f}{N_c} \right) \Delta G^{(0)} \right], \end{aligned} \quad (91a)$$

$$\begin{aligned} \Delta \Sigma^{(3)}(x, Q^2) &= -\frac{1}{30} \left(\frac{\alpha_s N_c}{4\pi} \right)^3 \ln^5 \frac{1}{x} \ln \frac{Q^2}{\Lambda^2} \left[\left(\frac{10N_f}{N_c} - \frac{1}{2} \right) \Delta \Sigma^{(0)} + \frac{N_f}{N_c} \left(35 - \frac{4N_f}{N_c} \right) \Delta G^{(0)} \right] \\ &\quad - \frac{1}{24} \left(\frac{\alpha_s N_c}{4\pi} \right)^3 \ln^4 \frac{1}{x} \ln^2 \frac{Q^2}{\Lambda^2} \left[\left(\frac{24N_f}{N_c} - 1 \right) \Delta \Sigma^{(0)} + \frac{N_f}{N_c} \left(78 - \frac{8N_f}{N_c} \right) \Delta G^{(0)} \right] \\ &\quad - \frac{1}{36} \left(\frac{\alpha_s N_c}{4\pi} \right)^3 \ln^3 \frac{1}{x} \ln^3 \frac{Q^2}{\Lambda^2} \left[\left(\frac{40N_f}{N_c} - 1 \right) \Delta \Sigma^{(0)} + \frac{N_f}{N_c} \left(146 - \frac{8N_f}{N_c} \right) \Delta G^{(0)} \right]. \end{aligned} \quad (91b)$$

Again, from the terms containing $\ln^5 \frac{1}{x} \ln \frac{Q^2}{\Lambda^2}$, one reads out the polarized small- x large- N_c & N_f splitting functions at the three-loop order

$$\Delta \mathbf{P}^{(2)}(x) = \frac{1}{6} \left(\frac{\alpha_s N_c}{4\pi} \right)^3 \ln^4 \frac{1}{x} \begin{pmatrix} \left(\frac{1}{2} - \frac{10N_f}{N_c} \right) & -\frac{N_f}{N_c} \left(35 - \frac{4N_f}{N_c} \right) \\ 35 - \frac{4N_f}{N_c} & 2 \left(56 - \frac{11N_f}{N_c} \right) \end{pmatrix}. \quad (92)$$

D. Summary of our results up to three loops

To summarize the above results, we note that we obtained the splitting functions up to three loops by iteratively solving the small- x helicity evolution equations. Collecting Eqs. (84), (88) and (92), we have the following expressions

$$\Delta P_{qq}(x) = \frac{\alpha_s N_c}{4\pi} + \left(\frac{\alpha_s N_c}{4\pi} \right)^2 \left(\frac{1}{2} - 2 \frac{N_f}{N_c} \right) \ln^2 \frac{1}{x} + \left(\frac{\alpha_s N_c}{4\pi} \right)^3 \frac{1}{12} \left(1 - 20 \frac{N_f}{N_c} \right) \ln^4 \frac{1}{x} + \mathcal{O}(\alpha_s^4), \quad (93a)$$

$$\Delta P_{qG}(x) = -\left(\frac{\alpha_s N_c}{4\pi} \right) \frac{2N_f}{N_c} - \left(\frac{\alpha_s N_c}{4\pi} \right)^2 \frac{5N_f}{N_c} \ln^2 \frac{1}{x} - \left(\frac{\alpha_s N_c}{4\pi} \right)^3 \frac{1}{6} \frac{N_f}{N_c} \left(35 - 4 \frac{N_f}{N_c} \right) \ln^4 \frac{1}{x} + \mathcal{O}(\alpha_s^4), \quad (93b)$$

$$\Delta P_{Gq}(x) = 2 \left(\frac{\alpha_s N_c}{4\pi} \right) + 5 \left(\frac{\alpha_s N_c}{4\pi} \right)^2 \ln^2 \frac{1}{x} + \left(\frac{\alpha_s N_c}{4\pi} \right)^3 \frac{1}{6} \left(35 - 4 \frac{N_f}{N_c} \right) \ln^4 \frac{1}{x} + \mathcal{O}(\alpha_s^4), \quad (93c)$$

$$\Delta P_{GG}(x) = 8 \left(\frac{\alpha_s N_c}{4\pi} \right) + \left(\frac{\alpha_s N_c}{4\pi} \right)^2 \left(16 - 2 \frac{N_f}{N_c} \right) \ln^2 \frac{1}{x} + \left(\frac{\alpha_s N_c}{4\pi} \right)^3 \frac{1}{3} \left(56 - 11 \frac{N_f}{N_c} \right) \ln^4 \frac{1}{x} + \mathcal{O}(\alpha_s^4). \quad (93d)$$

These splitting functions completely agree with the results of BER IREE expansion (obtained by applying the large- N_c & N_f limit to Eq. (14) in [10]).

For comparison, in the $\overline{\text{MS}}$ scheme, the small- x limits of the polarized splitting functions at large- N_c & N_f are [4–7],

$$\Delta \overline{P}_{qq}(x) = \left(\frac{\alpha_s N_c}{4\pi} \right) + \left(\frac{\alpha_s N_c}{4\pi} \right)^2 \left(\frac{1}{2} - 2 \frac{N_f}{N_c} \right) \ln^2 \frac{1}{x} + \left(\frac{\alpha_s N_c}{4\pi} \right)^3 \frac{1}{12} \left(1 - 20 \frac{N_f}{N_c} \right) \ln^4 \frac{1}{x} + \mathcal{O}(\alpha_s^4), \quad (94a)$$

$$\Delta \overline{P}_{qG}(x) = -\left(\frac{\alpha_s N_c}{4\pi} \right) \frac{2N_f}{N_c} - \left(\frac{\alpha_s N_c}{4\pi} \right)^2 \frac{5N_f}{N_c} \ln^2 \frac{1}{x} - \left(\frac{\alpha_s N_c}{4\pi} \right)^3 \frac{1}{6} \frac{N_f}{N_c} \left(34 - 4 \frac{N_f}{N_c} \right) \ln^4 \frac{1}{x} + \mathcal{O}(\alpha_s^4), \quad (94b)$$

$$\Delta \overline{P}_{Gq}(x) = 2 \left(\frac{\alpha_s N_c}{4\pi} \right) + 5 \left(\frac{\alpha_s N_c}{4\pi} \right)^2 \ln^2 \frac{1}{x} + \left(\frac{\alpha_s N_c}{4\pi} \right)^3 \frac{1}{6} \left(36 - 4 \frac{N_f}{N_c} \right) \ln^4 \frac{1}{x} + \mathcal{O}(\alpha_s^4), \quad (94c)$$

$$\Delta \overline{P}_{GG}(x) = 8 \left(\frac{\alpha_s N_c}{4\pi} \right) + \left(\frac{\alpha_s N_c}{4\pi} \right)^2 \left(16 - 2 \frac{N_f}{N_c} \right) \ln^2 \frac{1}{x} + \left(\frac{\alpha_s N_c}{4\pi} \right)^3 \frac{1}{3} \left(56 - 11 \frac{N_f}{N_c} \right) \ln^4 \frac{1}{x} + \mathcal{O}(\alpha_s^4). \quad (94d)$$

We see that our (and BER) polarized splitting functions ΔP_{qq} and ΔP_{GG} agree with the $\overline{\text{MS}}$ ones, while ΔP_{qG} and ΔP_{Gq} appear to disagree slightly at the order- α_s^3 with their $\overline{\text{MS}}$ counterparts. The same disagreement between

the BER 3-loop results and $\overline{\text{MS}}$ was attributed to scheme dependence of splitting functions in [7]: in Appendix B we construct the scheme transformation relating Eqs. (93) and (94) explicitly. Here we note that the three-loop calculation [7] was carried out in the Larin scheme [87, 88], and the results were then transformed into the $\overline{\text{MS}}$ scheme (see [89] for a recent comparison of the two schemes).

Let us also note that it was pointed out in [10] that the splitting functions obtained from solving BER IREE evolution equations have the property that

$$\Delta P_{qG}(x) = -\frac{N_f}{N_c} \Delta P_{Gq}(x) \quad (95)$$

to all orders in α_s . The same property seem to be true for our splitting functions (93) to three loops and, as we will see below, at four loops as well. However, the relation (95) is not obeyed by the polarized splitting functions (94) in the $\overline{\text{MS}}$ scheme. It is violated at the order- α_s^3 as can be seen from Eqs. (94b) and (94c).

E. Step 4

One can continue iteratively solving the evolution equations (for simplicity further iteration was done while setting $\Delta\Sigma^{(0)} = 0$). The resulting four-loop splitting functions we obtain this way are

$$\Delta P_{qq}^{(3)}(x) = \left(\frac{\alpha_s N_c}{4\pi}\right)^4 \frac{1}{720} \left(5 - 748 \frac{N_f}{N_c} + 80 \frac{N_f^2}{N_c^2}\right) \ln^6 \frac{1}{x}, \quad (96a)$$

$$\Delta P_{qG}^{(3)}(x) = -\left(\frac{\alpha_s N_c}{4\pi}\right)^4 \frac{1}{360} \frac{N_f}{N_c} \left(1213 - 224 \frac{N_f}{N_c}\right) \ln^6 \frac{1}{x}, \quad (96b)$$

$$\Delta P_{Gq}^{(3)}(x) = \left(\frac{\alpha_s N_c}{4\pi}\right)^4 \frac{1}{360} \left(1213 - 224 \frac{N_f}{N_c}\right) \ln^6 \frac{1}{x}, \quad (96c)$$

$$\Delta P_{GG}^{(3)}(x) = \left(\frac{\alpha_s N_c}{4\pi}\right)^4 \frac{1}{180} \left(1984 - 549 \frac{N_f}{N_c} + 20 \frac{N_f^2}{N_c^2}\right) \ln^6 \frac{1}{x}. \quad (96d)$$

This is our prediction for the small- x large- N_c & N_f polarized splitting functions at four loops. It obeys the property (95) stated above. We hope to be able to compare it to the appropriate limit of the finite-order four-loop result, when the latter is calculated.

The four-loop splitting functions (96) are to be compared with the four loop predictions from the BER IREE expansion. Taking Eq. (15) in [10] and applying the large- N_c & N_f limit, these are

$$\Delta P_{qq}^{(3)\text{(BER)}}(x) = \left(\frac{\alpha_s N_c}{4\pi}\right)^4 \frac{1}{720} \left(5 - 764 \frac{N_f}{N_c} + 80 \frac{N_f^2}{N_c^2}\right) \ln^6 \frac{1}{x}, \quad (97a)$$

$$\Delta P_{qG}^{(3)\text{(BER)}}(x) = -\left(\frac{\alpha_s N_c}{4\pi}\right)^4 \frac{1}{360} \frac{N_f}{N_c} \left(1229 - 224 \frac{N_f}{N_c}\right) \ln^6 \frac{1}{x}, \quad (97b)$$

$$\Delta P_{Gq}^{(3)\text{(BER)}}(x) = \left(\frac{\alpha_s N_c}{4\pi}\right)^4 \frac{1}{360} \left(1229 - 224 \frac{N_f}{N_c}\right) \ln^6 \frac{1}{x}, \quad (97c)$$

$$\Delta P_{GG}^{(3)\text{(BER)}}(x) = \left(\frac{\alpha_s N_c}{4\pi}\right)^4 \frac{1}{180} \left(2016 - 557 \frac{N_f}{N_c} + 20 \frac{N_f^2}{N_c^2}\right) \ln^6 \frac{1}{x}. \quad (97d)$$

By comparing Eqs. (96) to Eqs. (97) we see that evidently the polarized splitting functions we obtain exhibit a very minor disagreement with those from the BER IREE expansion beginning at four loops. This is consistent with [8], where an analytic all-orders in α_s prediction for the polarized small- x GG anomalous dimension at large- N_c was derived from the large- N_c version of this small- x helicity evolution and also disagreed with that derived from the BER IREE beginning at four loops. The difference between Eqs. (96) and (97) cannot be accounted for by a scheme transformation since it persists even in the gluons-only large- N_c limit, where there is only one splitting function, ΔP_{GG} [8].

V. CONCLUSIONS AND OUTLOOK

In this paper we have calculated the contribution of the $q/\bar{q} \rightarrow G$ and $G \rightarrow q/\bar{q}$ shock-wave transition operators to the small- x evolution of the flavor-singlet quark and gluon helicity PDFs. These operators were previously considered

in [21] in the framework of helicity evolution: however, a direct comparison with [21] appears to be complicated due to the difference in our decompositions into flavor-singlet and non-singlet components. While the transition operators do not contribute to helicity evolution in the large- N_c limit which contains no quarks, they do contribute in the large- $N_c \& N_f$ limit. The main result of our work is the modified large- $N_c \& N_f$ helicity evolution equations (76). We showed that this evolution agrees with the (small- x and large- $N_c \& N_f$ limit of the) existing polarized DGLAP splitting functions up to the three known loops, indicating that the equations (76) are likely to include all the contributions needed for small- x helicity evolution. In the future, an analytic solution of Eqs. (76) can be found following the approach of [8].

Our calculations can also be used to further correct the helicity version of the Jalilian-Marian–Iancu–McLerran–Weigert–Leonidov–Kovner (JIMWLK) [31–36] evolution equation, which was constructed in [18] using the older version of helicity evolution, not containing the $\bar{D}^i D^i$ operator employed in [3] and the transition operators calculated here. Performing these corrections for the helicity version of JIMWLK evolution is left for the future work.

The new corrections in equations (76) imply that the results of the helicity phenomenology project [50] need to be updated as well. Introducing the new operator \tilde{Q} will lead to more parameters describing the initial conditions (inhomogeneous terms) for Eqs. (76) than in the version of these equations used in [50]. On the other hand, the new relations (79) may help one constrain some of these parameters, by relating the parameters to each other. The simplicity of Eqs. (77) may also help facilitate the future small- x helicity phenomenology.

ACKNOWLEDGMENTS

One of the authors (YK) is grateful to Frank Krauss and IPPP Durham for their hospitality during the final stages of this work.

This material is based upon work supported by the U.S. Department of Energy, Office of Science, Office of Nuclear Physics under Award Number DE-SC0004286 and within the framework of the Saturated Glue (SURGE) Topical Theory Collaboration.

The Feynman diagrams in this work were drawn using JaxoDraw [90].

Appendix A: Derivation of the large- $N_c \& N_f$ Evolution Equations using Light-Cone Perturbation Theory

The contribution of the shock-wave transition operators to the evolution of G_{10}^{adj} and the evolution of the new structure \tilde{Q}_{10} were derived in Sections III B and III C using the LCOT approach [2, 3, 15, 60], resulting in Eqs. (76). The goal of this Appendix is to show that the same evolution equations can be obtained using the tools of light-cone perturbation theory (LCPT), similarly to that done in [1] and in Sec. 4.2 of [91]. As in the main text, we still work in the $A^- = 0$ gauge with the gluon polarization vector still given by the expression in the main text following Eqs. (20). The spirit of the method used in this Appendix is to treat the interactions with the shock wave in terms of operator insertions (this is the same as in LCOT) but to treat everything outside the shock wave in terms of the light-cone wavefunctions of LCPT. To that end we will need expressions for these wavefunctions. To keep this Appendix self-contained, we first reproduce here the necessary elements from Section III of [1].

1. Light-cone Wavefunctions

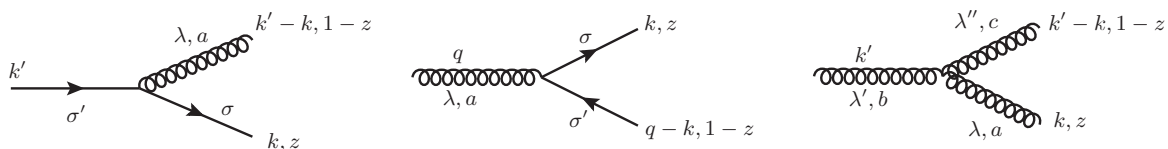


FIG. 5. Leading order contribution to the $q \rightarrow qG$, $G \rightarrow q\bar{q}$, and $G \rightarrow GG$ light-cone wavefunctions.

The leading order in α_s momentum-space expression for the $q \rightarrow qG$ wavefunction shown in Fig. 5 is

$$\psi^{q \rightarrow qG} = -gt^a \delta_{\sigma\sigma'} \sqrt{z} \frac{\epsilon_\lambda^* \cdot (\underline{k} - z\underline{k}')}{|\underline{k} - z\underline{k}'|^2} [1 + z + \sigma\lambda(1 - z)]. \quad (\text{A1})$$

In particular we will need the limits where one of the outgoing particles is soft. These limits, Fourier-transformed to transverse coordinate space, are

$$\psi^{q \rightarrow qG}|_{z \rightarrow 0} \approx -\frac{igt^a}{2\pi} \delta_{\sigma\sigma'} \sqrt{z} \frac{\epsilon_\lambda^* \cdot \underline{x}}{x^2} [1 + \sigma\lambda], \quad (\text{soft quark}), \quad (\text{A2a})$$

$$\psi^{q \rightarrow qG}|_{z \rightarrow 1} \approx \frac{igt^a}{2\pi} \delta_{\sigma\sigma'} \frac{\epsilon_\lambda^* \cdot \underline{x}}{x^2} [2 + \sigma\lambda(1 - z)], \quad (\text{soft gluon}). \quad (\text{A2b})$$

In the above expressions, \underline{x} is the transverse separation between the soft outgoing particle and the incoming particle. In addition, Eq. (A2b) omits some polarization-independent terms that do not contribute to the helicity evolution at hand. Note that we can also use these same expressions, Eqs. (A2a) and (A2b), for $\bar{q} \rightarrow \bar{q}G$ splitting in the diagrams to follow, with the caveat that we need an additional overall minus sign to properly account for the Wick contractions associated with the antiquark fields.

The leading order in α_s momentum-space expression for the $G \rightarrow q\bar{q}$ wavefunction shown in Fig. 5 is

$$\psi^{G \rightarrow q\bar{q}} = gt^a \sqrt{z(1-z)} \frac{\epsilon_\lambda \cdot (\underline{k} - z\underline{q})}{|\underline{k} - z\underline{q}|^2} \delta_{\sigma, -\sigma'} [1 - 2z - \sigma\lambda]. \quad (\text{A3})$$

The transverse coordinate space expressions in the limits where an outgoing particle is soft are

$$\psi^{G \rightarrow q\bar{q}}|_{z \rightarrow 0} \approx \frac{igt^a}{2\pi} \sqrt{z} \frac{\epsilon_\lambda \cdot \underline{x}}{x^2} \delta_{\sigma, -\sigma'} [1 - \sigma\lambda], \quad (\text{soft quark}), \quad (\text{A4a})$$

$$\psi^{G \rightarrow q\bar{q}}|_{z \rightarrow 1} \approx \frac{igt^a}{2\pi} \sqrt{1-z} \frac{\epsilon_\lambda \cdot \underline{x}}{x^2} \delta_{\sigma, -\sigma'} [1 - \sigma'\lambda], \quad (\text{soft antiquark}). \quad (\text{A4b})$$

Finally, the leading order in α_s momentum-space expression for the $G \rightarrow GG$ wavefunction shown in Fig. 5 is

$$\psi^{G \rightarrow GG} = 2igf^{abc} \frac{z(1-z)}{|\underline{k} - z\underline{k}'|^2} \left[\frac{1}{1-z} \epsilon_{\lambda''}^* \cdot (\underline{k} - z\underline{k}') \epsilon_\lambda^* \cdot \epsilon_{\lambda'} + \frac{1}{z} \epsilon_\lambda^* \cdot (\underline{k} - z\underline{k}') \epsilon_{\lambda''}^* \cdot \epsilon_{\lambda'} - \epsilon_{\lambda'} \cdot (\underline{k} - z\underline{k}') \epsilon_{\lambda''}^* \cdot \epsilon_{\lambda'} \right]. \quad (\text{A5})$$

The resulting transverse coordinate space expression for the soft outgoing gluon limit is

$$\psi^{G \rightarrow GG}|_{z \rightarrow 0} \approx \frac{-gf^{abc}}{\pi} \frac{\epsilon_\lambda^* \cdot \underline{x}}{x^2} \delta_{\lambda''\lambda'}, \quad (\text{soft gluon}). \quad (\text{A6})$$

Here again we have kept only the leading sub-eikonal, polarization-dependent terms.

2. Contribution to the evolution of the adjoint dipole amplitude of the first type

In this Subsection we derive the contribution of the shock-wave transition operators to the evolution of G_{10}^{adj} , in order to ultimately reproduce the results of Sec. III B. We begin with diagrams A and A' from Fig. 2, reproduced here with a few modifications to the labels.

We will still treat the interactions with the shock wave in terms of operators, specifically those in Eqs. (20). For everything outside the shock wave, we employ the light cone wavefunctions from Fig. 5. We write for the diagram A:

$$\begin{aligned} A &= \frac{1}{2(N_c^2 - 1)} \left(\frac{1}{2} \sum_{\lambda_1, \lambda_2} \lambda_1 \right) \sum_f \sum_{\sigma, \sigma', \lambda, \lambda'} \int \frac{dz'}{z'} \int \frac{d^2x_2}{4\pi} \theta(x_{10}^2 z - x_{21}^2 z') \\ &\quad \times \left\langle U_{\underline{0}}^{ba} \left[\psi_{dbc; \lambda, \lambda_2, \lambda'}^{G \rightarrow GG} \left(\underline{x}_{21}, \frac{z'}{z} \right) \Big|_{\frac{z'}{z} \rightarrow 0} \right]^* \left(W_{\underline{2}}^{Gq} [\infty, -\infty] \right)^{d, \lambda; i, \sigma} \left[\left(\psi_{a, \lambda_1; \sigma, \sigma'}^{G \rightarrow q\bar{q}} \right)^{ij} \left(\underline{x}_{21}, \frac{z'}{z} \right) \Big|_{\frac{z'}{z} \rightarrow 0} \right] \right. \\ &\quad \left. \times \left(W_{\underline{1}}^{G\bar{q}} [\infty, -\infty] \right)^{c, \lambda'; j, \sigma'} \right\rangle. \end{aligned} \quad (\text{A7})$$

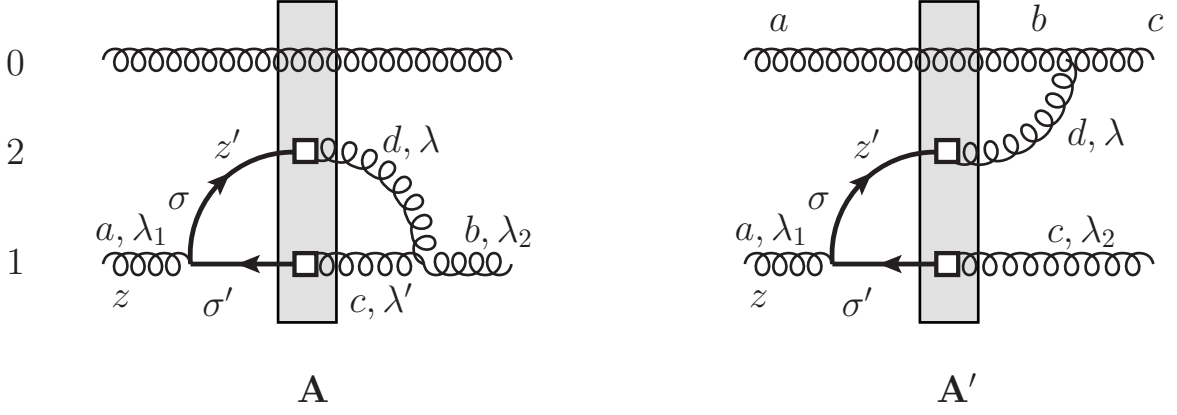


FIG. 6. Diagrams A and A', originally considered in Fig. 2.

The factor of $1/2$ in front averages over incoming helicities. We also weigh our sum by the incoming helicity λ_1 in order to pick out the helicity-dependent term of the sub-eikonal gluon S-matrix, since this is the one that contributes to G_{10}^{adj} (see Eqs. (4), (12), and (13)). Here we have included both adjoint and fundamental color indices as well as polarization arguments for clarity. Note also that we treat both the shock-wave transition operators as being part of the (forward) amplitude rather than one being in the amplitude and another one in the complex conjugate amplitude. Hence we use W^{Gq} and $W^{G\bar{q}}$, both with endpoints running from $-\infty$ to ∞ . In addition, we have a theta function in the first line of Eq. (A7) to enforce light-cone lifetime ordering [1–3].

Now we substitute our splitting wavefunctions and shock-wave transition operators into Eq. (A7). Here we opt to employ the explicit expressions in Eqs. (20) for the transition operators from the outset, obtaining

$$\begin{aligned}
 A = & \frac{1}{2(N_c^2 - 1)} \left(\frac{1}{2} \sum_{\lambda_1, \lambda_2} \lambda_1 \right) \sum_f \sum_{\sigma, \sigma', \lambda, \lambda'} \int \frac{dz'}{z'} \int \frac{d^2 \underline{x}_2}{4\pi} \theta(x_{10}^2 z - x_{21}^2 z') \quad (\text{A8}) \\
 & \times \left\langle U_{\underline{0}}^{ba} \left[\frac{-g}{\pi} f^{abc} \delta_{\lambda_2, \lambda'} \frac{\underline{\epsilon}_{\lambda'} \cdot \underline{x}_{21}}{x_{21}^2} \right]^* \right. \\
 & \left(\int_{-\infty}^{\infty} dw_2^- U_{\underline{2}}^{de} [\infty, w_2^-] \frac{-ig}{2\sqrt{\sqrt{2}k^-}} \bar{\psi}_{\alpha}(w_2^-, \underline{x}_2) t^e \delta_{\sigma, \lambda} [\sigma(\rho_{\alpha}(-) - \rho_{\alpha}(+)) + (\rho_{\alpha}(-) + \rho_{\alpha}(+))] V_{\underline{2}}[w_2^-, -\infty] \right) \\
 & \left[\frac{ig}{2\pi} t^a \delta_{\sigma, -\sigma'} \sqrt{\frac{z'}{z}} (1 - \sigma \lambda_1) \frac{\underline{\epsilon}_{\lambda_1} \cdot \underline{x}_{21}}{x_{21}^2} \right] \\
 & \left. \left(\int_{-\infty}^{\infty} dw_1^- U_{\underline{1}}^{cf} [\infty, w_1^-] \frac{-ig}{2\sqrt{\sqrt{2}p_2^-}} V_{\underline{1}}^{\dagger}[w_1^-, -\infty] \delta_{\sigma', \lambda'} [\sigma'(\bar{\rho}_{\beta}(-) - \bar{\rho}_{\beta}(+)) - (\bar{\rho}_{\beta}(-) + \bar{\rho}_{\beta}(+))] t^f \psi_{\beta}(w_1^-, \underline{x}_1) \right) \right\rangle.
 \end{aligned}$$

We have now suppressed the fundamental color indices but explicitly included the spinor indices α, β . We also suppose that the soft quark entering the shock wave at transverse position 2 comes in with momentum k , while the momentum of the parent dipole is p_2 . Both of these momenta are assumed to have large minus components. With these explicit factors of momentum, and with the factor $\frac{1}{\sqrt{z}}$ from the $G \rightarrow q\bar{q}$ light-cone wave function, we can write

$$\frac{1}{\sqrt{k^- p_2^-}} \frac{1}{\sqrt{z}} \approx \frac{1}{\sqrt{(z' P^-)(z P^-)}} \frac{1}{\sqrt{z}} = \frac{1}{\sqrt{z'}} \frac{2p_1^+}{zs} \quad (\text{A9})$$

where we have taken the projectile to have a large minus component of momentum P^- and the target proton to have a large plus component of momentum p_1^+ with $s = 2p_1^+ P^-$ the center of mass energy squared between them. (The adjoint parent dipole in Fig. 6 need not be the original projectile and could have instead been produced by previous

steps of evolution). Employing this fact and carrying out some algebra we arrive at

$$\begin{aligned}
A &= \frac{1}{z} \frac{1}{2(N_c^2 - 1)} 4i \frac{\alpha_s N_f}{\pi^2} \int \frac{dz'}{z'} \sqrt{z'} \int \frac{d^2 \underline{x}_2}{x_{21}^2} \theta(x_{10}^2 z - x_{21}^2 z') \\
&\quad \times \left\langle \frac{g^2 p_1^+}{8\sqrt{z's}} \int_{-\infty}^{\infty} dw_1^- \int_{-\infty}^{\infty} dw_2^- U_0^{ba} f^{dbc} U_2^{de} [\infty, w_2^-] \bar{\psi}_\alpha(w_2^-, \underline{x}_2) t^e V_2[w_2^-, -\infty] t^a U_1^{cf} [\infty, w_1^-] \right. \\
&\quad \left. \times V_1^\dagger[w_1^-, -\infty] t^f \left(\frac{1}{2} \gamma^+ \gamma^5 \right)_{\alpha\beta} \psi_\beta(w_1^-, \underline{x}_1) \right\rangle.
\end{aligned} \tag{A10}$$

We have replaced \sum_f with N_f for simplicity. Employing the double angle brackets defined in Eq. (28), we obtain

$$\begin{aligned}
A &= \frac{1}{zs} \frac{1}{2(N_c^2 - 1)} 4i \frac{\alpha_s N_f}{\pi^2} \int \frac{dz'}{z'} \int \frac{d^2 \underline{x}_2}{x_{21}^2} \theta(x_{10}^2 z - x_{21}^2 z') \\
&\quad \times \left\langle \left\langle \frac{g^2 p_1^+}{8\sqrt{z's}} \int_{-\infty}^{\infty} dw_1^- \int_{-\infty}^{\infty} dw_2^- U_0^{ba} f^{dbc} U_2^{de} [\infty, w_2^-] \bar{\psi}_\alpha(w_2^-, \underline{x}_2) t^e V_2[w_2^-, -\infty] t^a U_1^{cf} [\infty, w_1^-] \right. \right. \\
&\quad \left. \left. \times V_1^\dagger[w_1^-, -\infty] t^f \left(\frac{1}{2} \gamma^+ \gamma^5 \right)_{\alpha\beta} \psi_\beta(w_1^-, \underline{x}_1) \right\rangle \right\rangle.
\end{aligned} \tag{A11}$$

Diagram A' is similar. We write

$$\begin{aligned}
A' &= \frac{1}{2(N_c^2 - 1)} \left(\frac{1}{2} \sum_{\lambda_1, \lambda_2} \lambda_1 \right) \sum_f \sum_{\sigma, \sigma', \lambda} \int \frac{dz'}{z'} \int \frac{d^2 \underline{x}_2}{4\pi} \theta(x_{10}^2 z - \max\{x_{20}^2, x_{21}^2\} z') \\
&\quad \times \left\langle U_0^{ba} \left[\psi_{dcb; \lambda}^{G \rightarrow GG} \left(\frac{\underline{x}_{20}, z'}{z} \right) \Big|_{\frac{z'}{z} \rightarrow 0} \right]^* \left(W_2^{Gq} [\infty, -\infty] \right)^{d, \lambda; i, \sigma} \left[\left(\psi_{a, \lambda_1; \sigma, \sigma'}^{G \rightarrow q\bar{q}} \right)^{ij} \left(\frac{\underline{x}_{21}, z'}{z} \right) \Big|_{\frac{z'}{z} \rightarrow 0} \right] \right. \\
&\quad \left. \times \left(W_1^{G\bar{q}} [\infty, -\infty] \right)^{c, \lambda_2; j, \sigma'} \right\rangle.
\end{aligned} \tag{A12}$$

Note that the light-cone lifetime-ordering theta function has been modified to account for both resulting (daughter) dipole sizes [1–3]. Following the same steps as with diagram A, we obtain the following result for diagram A',

$$\begin{aligned}
A' &= \frac{1}{zs} \frac{1}{2(N_c^2 - 1)} 4i \frac{\alpha_s N_f}{\pi^2} \int \frac{dz'}{z'} \int d^2 \underline{x}_2 \theta(x_{10}^2 z - \max\{x_{20}^2, x_{21}^2\} z') \frac{\underline{x}_{20} \cdot \underline{x}_{21}}{x_{20}^2 x_{21}^2} \\
&\quad \times \left\langle \left\langle \frac{g^2 p_1^+}{8\sqrt{z's}} \int_{-\infty}^{\infty} dw_1^- \int_{-\infty}^{\infty} dw_2^- U_0^{ba} f^{dcb} U_2^{de} [\infty, w_2^-] \bar{\psi}_\alpha(w_2^-, \underline{x}_2) t^e V_2[w_2^-, -\infty] t^a U_1^{cf} [\infty, w_1^-] V_1^\dagger[w_1^-, -\infty] \right. \right. \\
&\quad \left. \left. \times t^f \left(\frac{1}{2} \gamma^+ \gamma^5 \right)_{\alpha\beta} \psi_\beta(w_1^-, \underline{x}_1) \right\rangle \right\rangle.
\end{aligned} \tag{A13}$$

We have neglected a term proportional to $\underline{x}_{20} \times \underline{x}_{21}$ which does not contribute in DLA.

For diagrams B and B' from Fig. 2 it remains true as in Sec. IIIB that

$$(B + B') = (A + A')^*. \tag{A14}$$

A direct calculation within the framework of this Appendix bears this out, but for brevity we do not show it here.

Next we consider diagrams C and C' from Fig. 2. For diagram C we can write

$$\begin{aligned}
C &= \frac{1}{2(N_c^2 - 1)} \left(\frac{1}{2} \sum_{\lambda_1, \lambda_2} \lambda_1 \right) \sum_f \sum_{\sigma, \sigma', \lambda, \lambda'} \int \frac{dz'}{z'} \int \frac{d^2 \underline{x}_2}{4\pi} \theta(x_{10}^2 z - x_{21}^2 z') \\
&\quad \times \left\langle U_0^{ba} \left[\psi_{dac; \lambda, \lambda_1, \lambda'}^{G \rightarrow GG} \left(\frac{\underline{x}_{21}, z'}{z} \right) \Big|_{\frac{z'}{z} \rightarrow 0} \right] \left(W_1^{qG} [\infty, -\infty] \right)^{j, \sigma'; c, \lambda'} \left[\left(\psi_{b, \lambda_2; \sigma, \sigma'}^{G \rightarrow q\bar{q}} \right)^{ji} \left(\frac{\underline{x}_{21}, z'}{z} \right) \Big|_{\frac{z'}{z} \rightarrow 0} \right]^* \right. \\
&\quad \left. \times \left(W_2^{qG} [\infty, -\infty] \right)^{i, \sigma; d, \lambda} \right\rangle.
\end{aligned} \tag{A15}$$

Just as we did for diagram A, we substitute the light-cone wave functions and the explicit expressions for the shock-wave transition operators. Some simplification yields

$$\begin{aligned}
C = & -\frac{1}{zs} \frac{1}{2(N_c^2 - 1)} 4i \frac{\alpha_s N_f}{\pi^2} \int \frac{dz'}{z'} \int \frac{d^2 \underline{x}_2}{x_{21}^2} \theta(x_{10}^2 z - x_{21}^2 z') \\
& \times \left\langle \left\langle \frac{g^2 p_1^+}{8\sqrt{z'} s} \int_{-\infty}^{\infty} dw_1^- \int_{-\infty}^{\infty} dw_2^- U_0^{ba} f^{dac} \bar{\psi}_\alpha(w_1^-, \underline{x}_1) t^e V_1^\dagger[\infty, w_1^-] U_1^{ec}[w_1^-, -\infty] t^b V_2[w_2^-, \infty] t^f \right. \right. \\
& \left. \left. \times \left(\frac{1}{2} \gamma^+ \gamma^5 \right)_{\alpha\beta} \psi_\beta(w_2^-, \underline{x}_2) U_2^{fd}[w_2^-, -\infty] \right\rangle \right\rangle.
\end{aligned} \tag{A16}$$

Diagram C' from Fig. 2 is calculated similarly. The result is

$$\begin{aligned}
C' = & -\frac{1}{zs} \frac{1}{2(N_c^2 - 1)} 4i \frac{\alpha_s N_f}{\pi^2} \int \frac{dz'}{z'} \int d^2 \underline{x}_2 \theta(x_{10}^2 z - \max\{x_{20}^2, x_{21}^2\} z') \frac{x_{20} \cdot x_{21}}{x_{20}^2 x_{21}^2} \\
& \times \left\langle \left\langle \frac{g^2 p_1^+}{8\sqrt{z'} s} \int_{-\infty}^{\infty} dw_1^- \int_{-\infty}^{\infty} dw_2^- U_0^{ba} f^{dca} \bar{\psi}_\alpha(w_1^-, \underline{x}_1) t^e V_1^\dagger[\infty, w_1^-] U_1^{ec}[w_1^-, -\infty] t^d V_2[\infty, w_2^-] t^f \right. \right. \\
& \left. \left. \times \left(\frac{1}{2} \gamma^+ \gamma^5 \right)_{\alpha\beta} \psi_\beta(w_2^-, \underline{x}_2) U_2^{fd}[w_2^-, -\infty] \right\rangle \right\rangle.
\end{aligned} \tag{A17}$$

Again a straightforward calculation in the framework of this Appendix shows that

$$(D + D') = (C + C')^* \tag{A18}$$

Adding together all the contributions to the evolution of G_{10}^{adj} we obtain

$$\begin{aligned}
A + A' + B + B' + C + C' + D + D' \Big|_{\text{DLA}} = & \frac{4i}{2(N_c^2 - 1)} \frac{\alpha_s N_f}{\pi} \int_{\Lambda^2/s}^z \frac{dz'}{z'} \int_{1/z's}^{x_{10}^2} \frac{dx_{21}^2}{x_{21}^2} \\
& \times \left\langle \left\langle \frac{g^2 p_1^+}{8\sqrt{z'} s} \int_{-\infty}^{\infty} dw_1^- \int_{-\infty}^{\infty} dw_2^- \left(U_0^{ba} f^{dbc} U_2^{de}[\infty, w_2^-] \bar{\psi}_\alpha(w_2^-, \underline{x}_2) t^e V_2[w_2^-, -\infty] t^a U_1^{ef}[\infty, w_1^-] \right. \right. \\
& \quad \times V_1^\dagger[w_1^-, -\infty] t^f \left(\frac{1}{2} \gamma^+ \gamma^5 \right)_{\alpha\beta} \psi_\beta(w_1^-, \underline{x}_1) \\
& \quad + U_0^{ba} f^{dca} \bar{\psi}_\alpha(w_1^-, \underline{x}_1) t^e V_1^\dagger[\infty, w_1^-] U_1^{ec}[w_1^-, -\infty] t^b V_2[\infty, w_2^-] t^f \\
& \quad \left. \left. \times \left(\frac{1}{2} \gamma^+ \gamma^5 \right)_{\alpha\beta} \psi_\beta(w_2^-, \underline{x}_2) U_2^{fd}[w_2^-, -\infty] + \text{c.c.} \right\rangle \right\rangle
\end{aligned} \tag{A19}$$

where we cancelled the factor of $1/zs$ since the same factor appears on the left hand side of the evolution equation (upon applying the double angle brackets) and we also simplified our kernel in DLA, where the transverse integral is only logarithmic for $x_{21} \ll x_{10} \sim x_{20}$. Next we take the large- N_c limit, using Eq. (40) along with the Fierz identity. We neglect all terms sub-leading in N_c and set the unpolarized S-matrices we obtain to 1 (which is valid at DLA). At large- N_c the structure in double angle brackets in Eq. (A19) becomes \tilde{Q}_{21} from Sec. IIIB (see Eq. (44) and simply use the relations $k^- = z' p_2^-$, $s = 2p_1^+ p_2^-$ from that section to reconcile the prefactors). The result at large N_c & N_f is

$$A + A' + B + B' + C + C' + D + D' \Big|_{\text{DLA}} = -\frac{\alpha_s N_f}{\pi} \int_{\Lambda^2/s}^z \frac{dz'}{z'} \int_{1/z's}^{x_{10}^2} \frac{dx_{21}^2}{x_{21}^2} \tilde{Q}_{12}(z's). \tag{A20}$$

Lastly, to write the evolution equations in terms of the dipole amplitude \tilde{G}_{10} instead of G_{10}^{adj} , we divide the contribution obtained here by 4 (see Eq. (47)). The result is

$$\tilde{G}_{10}(zs) \supset -\frac{\alpha_s N_f}{4\pi} \int_{\Lambda^2/s}^z \frac{dz'}{z'} \int_{1/z's}^{x_{10}^2} \frac{dx_{21}^2}{x_{21}^2} \tilde{Q}_{12}(z's) \tag{A21}$$

in agreement with Eq. (48).

3. Evolution for \tilde{Q}

Next we derive the evolution of the new structure \tilde{Q} , in an effort to reproduce the results of Sec. III C 1. We need to consider the diagrams in Fig. 3. However, in order to use the LCPT light-cone wavefunctions we begin without yet having taken the large- N_c limit. That is, we start from the same diagrams for the evolution of the adjoint dipole we have just calculated in Sec. A 2 and add an additional step of evolution to those diagrams. In this procedure we will obtain two evolution kernels. We can factor out and remove the first kernel, corresponding to the first step of our evolution calculated above, and what remains will be the second step of the evolution that we need to find, the evolution of \tilde{Q} . The diagrams we consider here are shown in Fig. 7. As these diagrams are similar to but distinct from those in Fig. 3, we denote them by the same calligraphic letters but with hats. Upon ultimately taking the large- N_c limit we will obtain the contributions of the diagrams in Fig. 3.

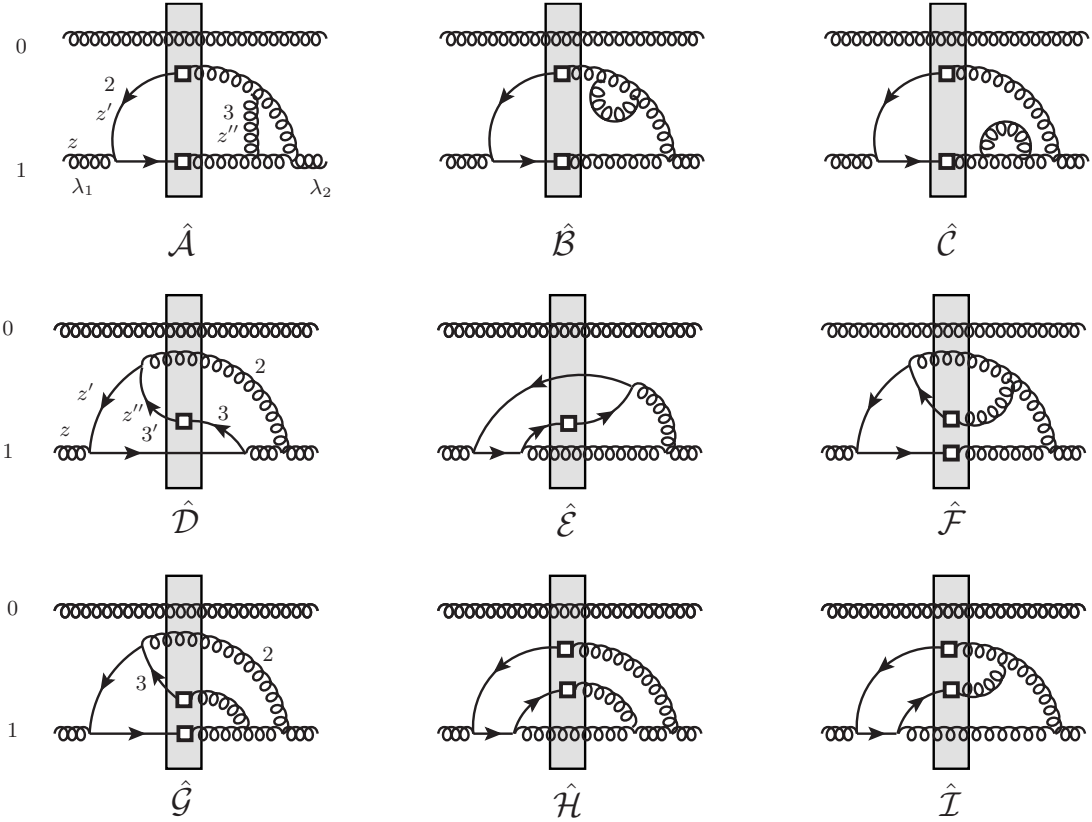


FIG. 7. The diagrams containing two steps of evolution: a step of evolution for G_{10}^{adj} calculated in Sec. A 2 followed by a step of evolution for \tilde{Q}_{21} . Upon taking the large- N_c limit and factoring out the evolution kernel for G_{10}^{adj} found in Sec. A 2, the contributions of these diagrams will reduce to those in Fig. 3.

We begin with the virtual corrections labeled \hat{A} , \hat{B} , and \hat{C} shown in the first row of Fig. 7. To calculate these diagrams we treat the extra emitted gluon (the one at transverse position \underline{x}_3) as real (going through the shock wave, but not interacting with it) and multiply the result of such calculation by an overall factor of $-\frac{1}{2}$, in accordance with the unitarity arguments relating the sum of real and virtual corrections [92] which we use to extract the virtual

contribution. For diagram $\hat{\mathcal{A}}$, which represents the sum of two time-orderings, we write

$$\begin{aligned}
\hat{\mathcal{A}} &= \left(-\frac{1}{2}\right) \frac{1}{2(N_c^2 - 1)} \left(\frac{1}{2} \sum_{\lambda_1, \lambda_2} \lambda_1\right) \sum_f \sum_{\text{internal}} \int \frac{dz'}{z'} \int \frac{d^2 \underline{x}_2}{4\pi} \theta(x_{10}^2 z - x_{21}^2 z') \\
&\times \int \frac{dz''}{z''} \int \frac{d^2 \underline{x}_3}{4\pi} \theta(x_{21}^2 z' - \max\{x_{32}^2, x_{31}^2\} z'') \left\langle \left[\psi_{ebf; \lambda_3, \lambda_2, \lambda_4}^{G \rightarrow GG} \left(\underline{x}_{21}, \frac{z'}{z} \right) \Big|_{\frac{z'}{z} \rightarrow 0} \right]^* \left(W_{\perp}^{Gq} [\infty, -\infty] \right)^{c, \lambda'; j, \sigma'} \right. \\
&\times \left[\left(\psi_{a\lambda_1; \sigma', \sigma}^{G \rightarrow q\bar{q}} \right)^{ji} \left(\underline{x}_{21}, 1 - \frac{z'}{z} \right) \Big|_{1 - \frac{z'}{z} \rightarrow 1} \right] \left(W_{\perp}^{G\bar{q}} [\infty, -\infty] \right)^{d, \lambda; i, \sigma} U_{\underline{0}}^{ba} \\
&\times \left(\left[\psi_{gde; \lambda_5, \lambda, \lambda_3}^{G \rightarrow GG} \left(\underline{x}_{32}, \frac{z''}{z'} \right) \Big|_{\frac{z''}{z'} \rightarrow 0} \right] \left[\psi_{gfc; \lambda_5, \lambda_4, \lambda'}^{G \rightarrow GG} \left(\underline{x}_{31}, \frac{z''}{z'} \right) \Big|_{\frac{z''}{z'} \rightarrow 0} \right]^* \right. \\
&\quad \left. + \left[\psi_{gcf; \lambda_5, \lambda', \lambda_4}^{G \rightarrow GG} \left(\underline{x}_{31}, \frac{z''}{z'} \right) \Big|_{\frac{z''}{z'} \rightarrow 0} \right] \left[\psi_{ged; \lambda_5, \lambda_3, \lambda}^{G \rightarrow GG} \left(\underline{x}_{32}, \frac{z''}{z'} \right) \Big|_{\frac{z''}{z'} \rightarrow 0} \right]^* \right) \left. \right\rangle.
\end{aligned} \tag{A22}$$

Meanwhile, for diagrams $\hat{\mathcal{B}}$ and $\hat{\mathcal{C}}$ we write

$$\begin{aligned}
\hat{\mathcal{B}} + \hat{\mathcal{C}} &= \frac{1}{2} \left(-\frac{1}{2}\right) \frac{1}{2(N_c^2 - 1)} \left(\frac{1}{2} \sum_{\lambda_1, \lambda_2} \lambda_1\right) \sum_f \sum_{\text{internal}} \int \frac{dz'}{z'} \int \frac{d^2 \underline{x}_2}{4\pi} \theta(x_{10}^2 z - x_{21}^2 z') \\
&\times \int \frac{dz''}{z''} \int \frac{d^2 \underline{x}_3}{4\pi} \theta(x_{21}^2 z' - x_{32}^2 z'') \left\langle \left[\psi_{ebf; \lambda_3, \lambda_2, \lambda_4}^{G \rightarrow GG} \left(\underline{x}_{21}, \frac{z'}{z} \right) \Big|_{\frac{z'}{z} \rightarrow 0} \right]^* \left(W_{\perp}^{Gq} [\infty, -\infty] \right)^{c, \lambda'; j, \sigma'} \right. \\
&\times \left[\left(\psi_{a\lambda_1; \sigma', \sigma}^{G \rightarrow q\bar{q}} \right)^{ji} \left(\underline{x}_{21}, 1 - \frac{z'}{z} \right) \Big|_{1 - \frac{z'}{z} \rightarrow 1} \right] \left(W_{\perp}^{G\bar{q}} [\infty, -\infty] \right)^{d, \lambda; i, \sigma} U_{\underline{0}}^{ba} \\
&\times \left[\psi_{gde; \lambda_5, \lambda, \lambda_4}^{G \rightarrow GG} \left(\underline{x}_{32}, \frac{z''}{z'} \right) \Big|_{\frac{z''}{z'} \rightarrow 0} \right] \left[\psi_{gfe; \lambda_5, \lambda_3, \lambda_4}^{G \rightarrow GG} \left(\underline{x}_{32}, \frac{z''}{z'} \right) \Big|_{\frac{z''}{z'} \rightarrow 0} \right]^* \left. \right\rangle + (\underline{x}_{32} \rightarrow \underline{x}_{31}).
\end{aligned} \tag{A23}$$

We have multiplied diagrams $\hat{\mathcal{B}}$ and $\hat{\mathcal{C}}$ by an additional factor of $\frac{1}{2}$. When we eventually take the large- N_c limit, the gluon that connects transverse positions \underline{x}_2 and \underline{x}_1 becomes a quark-antiquark pair and the virtual gluon at transverse position \underline{x}_3 could couple to either of these lines. But only the quark line (in this diagram) becomes a part of the large- N_c structure \tilde{Q}_{21} , and so we only want the contribution where the virtual gluon couples to this line. The factor of $1/2$ gives us this contribution only.

The diagrams we consider here represent an additional step of evolution done to diagram B in Fig. 2. In addition we need to include this same second step of evolution done to all the other diagrams in Fig. 2. This is straightforward as the contribution from diagram A is simply the conjugate of what we have just written, while that from diagrams C and D adds in the contribution to the past-pointing staple (see the second term in parentheses in Eq. (44)) and its conjugate. Meanwhile diagrams A', B', C', and D' simply modify the DLA kernel for the first step of the evolution (the same modification occurred in arriving at Eq. (A19)). Adding in all these contributions, carrying out the algebra, taking the large- N_c limit, and multiplying by an additional factor of $\frac{1}{4}$ to switch from G_{21}^{adj} to \tilde{G}_{21} we obtain

$$\begin{aligned}
\hat{\mathcal{A}} + \hat{\mathcal{B}} + \hat{\mathcal{C}} &= \left(-\frac{\alpha_s N_f}{4\pi} \int_{\Lambda^2/s}^z \frac{dz'}{z'} \int_{1/z's}^{x_{10}^2} \frac{dx_{21}^2}{x_{21}^2} \right) \left(-\frac{\alpha_s N_c}{4\pi^2} \right) \int \frac{dz''}{z''} \int d^2 \underline{x}_3 \\
&\times \left[\frac{1}{x_{32}^2} \theta(x_{21}^2 z' - x_{32}^2 z'') + \frac{1}{x_{31}^2} \theta(x_{21}^2 z' - x_{31}^2 z'') - 2 \frac{x_{32} \cdot x_{31}}{x_{32}^2 x_{31}^2} \theta(x_{21}^2 z' - \max\{x_{32}^2, x_{31}^2\} z'') \right] \tilde{Q}_{21}(z'' s).
\end{aligned} \tag{A24}$$

We have cancelled a factor of $\frac{1}{z's}$ for the same reason stated following Eq. (A19). We also set unpolarized S-matrices to 1. Now the first kernel in Eq. (A24) (the large parentheses in the first line) is simply the kernel for the first step of evolution. So we remove it, leaving just the second step of evolution which, now that we have taken the large- N_c

limit, corresponds to diagrams \mathcal{A} , \mathcal{B} , and \mathcal{C} in Fig. 3. Simplifying the kernel at DLA we obtain

$$\mathcal{A} + \mathcal{B} + \mathcal{C} = -\frac{\alpha_s N_c}{4\pi} \int_{\Lambda^2/s}^{z'} \frac{dz''}{z''} \left[\int_{\frac{1}{z''s}}^{x_{21}^2} \frac{dx_{32}^2}{x_{32}^2} + \int_{\frac{1}{(z''s)}}^{x_{21}^2} \frac{dx_{31}^2}{x_{31}^2} \right] \tilde{Q}_{21}(z''s), \quad (\text{A25})$$

which agrees with Eq. (49) in the main text upon substituting $\underline{x}_1 \rightarrow \underline{x}_2$, $\underline{x}_0 \rightarrow \underline{x}_1$, $\underline{x}_2 \rightarrow \underline{x}_3$, $z' \rightarrow z''$, and $z \rightarrow z''$ in the latter.

The remaining diagrams we need are shown in the last two rows of Fig. 7. We first consider diagrams $\hat{\mathcal{F}}$ and $\hat{\mathcal{G}}$. For diagram $\hat{\mathcal{F}}$ we write

$$\begin{aligned} \hat{\mathcal{F}} &= \frac{1}{2(N_c^2 - 1)} \left(\frac{1}{2} \sum_{\lambda_1, \lambda_2} \lambda_1 \right) \sum_f \sum_{\text{internal}} \int \frac{dz'}{z'} \int \frac{d^2 \underline{x}_2}{4\pi} \int \frac{dz''}{z''} \int \frac{d^2 \underline{x}_3}{4\pi} \\ &\times \left\langle \left[\psi_{fbc; \lambda_4, \lambda_2, \lambda'}^{G \rightarrow GG} \left(\underline{x}_{21}, \frac{z'}{z} \right) \Big|_{\frac{z'}{z} \rightarrow 0} \right]^* \left[\psi_{gfd; \lambda_3, \lambda_4, \lambda}^{G \rightarrow GG} \left(\underline{x}_{32}, \frac{z''}{z'} \right) \Big|_{\frac{z''}{z'} \rightarrow 0} \right]^* U_2^{de} U_0^{ba} \left(W_{\underline{1}}^{Gq} [\infty, -\infty] \right)^{c, \lambda'; j, \sigma'_0} \right. \\ &\times \left. \left[(\psi^{G \rightarrow q\bar{q}})^{ji}{}_{a\lambda_1; \sigma'_0, \sigma_0} \left(\underline{x}_{21}, 1 - \frac{z'}{z} \right) \Big|_{1 - \frac{z'}{z} \rightarrow 1} \right] \left[-(\psi^{q \rightarrow qG})^{ii'}{}_{e, \lambda; \sigma_0, \sigma} \left(\underline{x}_{32}, \frac{z''}{z'} \right) \Big|_{\frac{z''}{z'} \rightarrow 0} \right] \left(W_{\underline{3}}^{G\bar{q}} [\infty, -\infty] \right)^{g, \lambda_3; i', \sigma} \right\rangle. \end{aligned} \quad (\text{A26})$$

Here we have used $-\psi^{q \rightarrow qG}$ for the $\bar{q} \rightarrow \bar{q}G$ splitting, as mentioned in the paragraph just after Eq. (A2b). We have also suppressed the light-cone lifetime-ordering theta functions for brevity. Carrying out the algebra we obtain

$$\begin{aligned} \hat{\mathcal{F}} &= \frac{1}{2(N_c^2 - 1)} \left(-\frac{\alpha_s N_f}{\pi^2} \right) \int \frac{dz'}{z'} \int \frac{d^2 \underline{x}_2}{x_{21}^2} \left(\frac{2\alpha_s}{\pi^2} \right) \int \frac{dz''}{z''} \int \frac{d^2 \underline{x}_3}{x_{32}^2} \\ &\times \left\langle \frac{g^2 P^+}{8\sqrt{z''s}} \int_{-\infty}^{\infty} dw_1^- \int_{-\infty}^{\infty} dw_3^- f^{fbc} f^{gfd} U_{\underline{1}}^{ch} [\infty, w_1^-] \bar{\psi}_\alpha(w_1^-, \underline{x}_1) t^h \left(\frac{1}{2} \gamma^+ \gamma^5 \right)_{\alpha\beta} V_{\underline{1}} [w_1^-, -\infty] t^a t^e \right. \\ &\times \left. U_{\underline{3}}^{gh'} [\infty, w_3^-] V_{\underline{3}}^\dagger [w_3^-, -\infty] t^{h'} \psi_\beta(w_3^-, \underline{x}_3) U_{\underline{2}}^{de} U_{\underline{0}}^{ba} \right\rangle, \end{aligned} \quad (\text{A27})$$

where we have again cancelled a factor of $\frac{1}{z's}$ for the same reason as above. Again, diagram $\hat{\mathcal{F}}$ represents a second step of evolution done to diagram B in Fig. 2, so we need to add in this same step of evolution done to the rest of the diagrams in Fig. 2, just as discussed before Eq. (A24). We again obtain the original kernel from the first step of evolution, which we remove. Doing this, then taking the large- N_c limit, setting the unpolarized S-matrices that result to 1, and including the factor of $\frac{1}{4}$ for the normalization of \tilde{G} , we obtain the contribution of diagram \mathcal{F} . Diagram $\hat{\mathcal{G}}$ is calculated similarly. Simplifying the kernel at DLA, we have for the contributions of diagrams \mathcal{F} and \mathcal{G}

$$\mathcal{F} + \mathcal{G} = \frac{\alpha_s N_c}{4\pi} \int_{\Lambda^2/s}^{z'} \frac{dz''}{z''} \int_{\frac{1}{(z''s)}}^{x_{21}^2} \frac{dx_{32}^2}{x_{32}^2} \tilde{Q}_{31}(z''s). \quad (\text{A28})$$

Eq. (A28) agrees with Eq. (52) upon substituting $\underline{x}_1 \rightarrow \underline{x}_2$, $\underline{x}_0 \rightarrow \underline{x}_1$, $\underline{x}_2 \rightarrow \underline{x}_3$, $z' \rightarrow z''$, and $z \rightarrow z'$ in the latter. Further, Eq. (A28) cancels the first term of Eq. (A25) with the DLA accuracy, just as in Eq. (53). Subsequently diagrams $\hat{\mathcal{H}}$ and $\hat{\mathcal{I}}$ from Fig. 7 yield contributions that cancel the second term of Eq. (A25) with DLA accuracy, just as in Sec. III C 1.

What remains is to calculate the contributions from diagrams $\hat{\mathcal{D}}$ and $\hat{\mathcal{E}}$. We write

$$\begin{aligned} \hat{\mathcal{D}} + \hat{\mathcal{E}} &= (-1) \frac{1}{2(N_c^2 - 1)} \left(\frac{1}{2} \sum_{\lambda_1, \lambda_2} \lambda_1 \right) \sum_f \sum_{\text{internal}} \int \frac{dz'}{z'} \int \frac{d^2 \underline{x}_2}{4\pi} \int \frac{dz''}{z''} \int \frac{d^2 \underline{x}_3 d^2 \underline{x}'_3}{4\pi} \\ &\times \left\langle \left[\psi_{abc; \lambda, \lambda_2, \lambda'}^{G \rightarrow GG} \left(\underline{x}_{21}, \frac{z'}{z} \right) \Big|_{\frac{z'}{z} \rightarrow 0} \right]^* \left[(\psi^{G \rightarrow q\bar{q}})^{j'j''}{}_{c\lambda'; \sigma', \sigma'_0} \left(\underline{x}_{31}, \frac{z''}{z} \right) \Big|_{\frac{z''}{z} \rightarrow 0} \right]^* V_{\underline{1}}^{j''j} \right. \\ &\times \left[(\psi^{G \rightarrow q\bar{q}})^{ji}{}_{a\lambda_1; \sigma'_0, \sigma_0} \left(\underline{x}_{21}, 1 - \frac{z'}{z} \right) \Big|_{1 - \frac{z'}{z} \rightarrow 1} \right] \left[-(\psi^{q \rightarrow qG})^{ii'}{}_{e\lambda; \sigma_0, \sigma} \left(\underline{x}_{3'2}, \frac{z''}{z'} \right) \Big|_{\frac{z''}{z'} \rightarrow 0} \right] \\ &\times \left. \left(-\sigma \delta_{\sigma, \sigma'} V_{\underline{3}}^{\text{pol}[1]\dagger} \delta^2(\underline{x}_3 - \underline{x}_{3'}) + \delta_{\sigma, \sigma'} V_{\underline{3}, \underline{3}'}^{\text{pol}[2]\dagger} \right)^{i'j'} U_{\underline{2}}^{de} U_{\underline{0}}^{ba} + \text{c.c.} \right\rangle. \end{aligned} \quad (\text{A29})$$

As we did for diagrams $\hat{\mathcal{F}}$ and $\hat{\mathcal{G}}$, we again use $-\psi^{q \rightarrow qG}$ for the $\bar{q} \rightarrow \bar{q}G$ splitting. In addition we have an overall minus sign for the fermion loop. This is still required even with an operator insertion mediating the interaction with the shock-wave. We have also once again omitted the lifetime-ordering theta functions. Following the same steps as in the other diagrams and taking the large- N_c limit, we obtain for the contribution of diagrams $\mathcal{D} + \mathcal{E}$:

$$\mathcal{D} + \mathcal{E} = \frac{\alpha_s}{4\pi^2} \int_{\Lambda^2/s}^{z'} \frac{dz''}{z''} \left\{ - \int d^2 \underline{x}_3 \frac{x_{32} \cdot x_{31}}{x_{32}^2 x_{31}^2} \left\langle \left\langle \text{tr} \left[V_{\underline{2}} V_{\underline{3}}^{\text{pol}[1]\dagger} \right] \right\rangle \right\rangle + i \int d^2 \underline{x}_3 d^2 \underline{x}_{3'} \frac{x_{3'2}}{x_{3'2}^2} \times \frac{x_{31}}{x_{31}^2} \left\langle \left\langle \text{tr} \left[V_{\underline{2}} V_{\underline{3},3'}^{\text{pol}[2]\dagger} \right] \right\rangle \right\rangle + \text{c.c} \right\}. \quad (\text{A30})$$

Eq. (A30) agrees with Eq. (56) upon substituting $\underline{x}_0 \rightarrow \underline{x}_1$, $\underline{x}_1 \rightarrow \underline{x}_2$, $\underline{x}_2 \rightarrow \underline{x}_3$, $\underline{x}_{2'} \rightarrow \underline{x}_{3'}$, $z \rightarrow z'$, and $z' \rightarrow z''$ in the latter equation. The rest of the calculation then proceeds exactly as that following Eq. (56) in the main text, resulting in

$$\int d^2 \left(\frac{x_1 + x_2}{2} \right) [\mathcal{D} + \mathcal{E}] = -\frac{\alpha_s N_c}{2\pi} \int_{\Lambda^2/s}^{z'} \frac{dz''}{z''} \int_{\max[x_{21}^2, \frac{1}{z''s}]}^{\min[\frac{z'}{z''} x_{21}^2, \frac{1}{\Lambda^2}]} \frac{dx_{32}^2}{x_{32}^2} [Q(x_{32}^2, z''s) + 2G_2(x_{32}^2, z''s)] \quad (\text{A31})$$

in agreement with Eq. (59) upon making the same substitutions.

To summarize, in this Appendix we have derived the contribution of the shock-wave transition operators to the evolution of the adjoint type-1 polarized dipole amplitude and additionally derived the evolution of the new structure \tilde{Q} itself. While the results of Sec. IIIB and IIIC in the main text were derived using light-cone operator treatment, the derivation in this Appendix employed a slightly different method, making use of the light-cone wave functions of LCPT. We have found complete agreement in the resulting evolution equations.

Appendix B: Scheme Transformation

The differences between the polarized small- x large- N_c & N_f splitting functions in our/BER scheme (93) and in the $\overline{\text{MS}}$ scheme (94) can be accounted for by a scheme transformation. In the following, we explicitly derive the scheme transformation matrix Z that transforms $\Delta \mathbf{P}$ in our/BER scheme to $\Delta \overline{\mathbf{P}}$ in the $\overline{\text{MS}}$ scheme. In our notation, over-lined quantities are understood to be in the $\overline{\text{MS}}$ scheme. The derivation is performed in the Mellin space. In Mellin space, the matrix of anomalous dimensions is

$$\Delta \overline{\gamma}(\omega) = \int_0^1 dx x^{\omega-1} \Delta \mathbf{P}(x). \quad (\text{B1})$$

We follow the method in [7].

Let $\Delta f(\omega, \mu^2) \equiv (\Delta \Sigma(\omega, \mu^2), \Delta G(\omega, \mu^2)^T)$ denote the quark and gluon helicity PDFs in Mellin space. The hPDFs in the two schemes are related by

$$\Delta \overline{f}(\omega, \mu^2) = Z(\omega, \mu^2) \Delta f(\omega, \mu^2). \quad (\text{B2})$$

The polarized DGLAP equations (83) in Mellin space can be formally expressed as a matrix equation

$$\frac{\partial \Delta \overline{f}(\omega, \mu^2)}{\partial \ln \mu^2} = \Delta \overline{\gamma}(\omega) \Delta \overline{f}(\omega, \mu^2), \quad (\text{B3})$$

which can be further written as

$$\frac{\partial Z(\omega, \mu^2)}{\partial \ln \mu^2} \Delta f(\omega, \mu^2) + Z(\omega, \mu^2) \frac{\partial \Delta f(\omega, \mu^2)}{\partial \ln \mu^2} = \Delta \overline{\gamma}(\omega) Z(\omega, \mu^2) \Delta f(\omega, \mu^2), \quad (\text{B4a})$$

$$\implies \frac{\partial Z(\omega, \mu^2)}{\partial \ln \mu^2} \Delta f(\omega, \mu^2) + Z(\omega, \mu^2) \Delta \gamma(\omega) \Delta f(\omega, \mu^2) = \Delta \overline{\gamma}(\omega) Z(\omega, \mu^2) \Delta f(\omega, \mu^2). \quad (\text{B4b})$$

One therefore obtains

$$\Delta \overline{\gamma}(\omega) = Z(\omega, \mu^2) \Delta \gamma(\omega) Z^{-1}(\omega, \mu^2) + \frac{\partial Z(\omega, \mu^2)}{\partial \ln \mu^2} Z^{-1}(\omega, \mu^2). \quad (\text{B5})$$

This is the equation to determine the scheme transformation matrix Z , given $\Delta\gamma$ and $\Delta\bar{\gamma}$. In the following, we solve this equation perturbatively order by order in $a_s = \alpha_s(\mu^2)/4\pi$. The anomalous dimensions have the expansions

$$\Delta\bar{\gamma}(\omega) = a_s\Delta\bar{\gamma}_\omega^{(0)} + a_s^2\Delta\bar{\gamma}_\omega^{(1)} + a_s^3\Delta\bar{\gamma}_\omega^{(2)} + \dots, \quad (\text{B6a})$$

$$\Delta\gamma(\omega) = a_s\Delta\gamma_\omega^{(0)} + a_s^2\Delta\gamma_\omega^{(1)} + a_s^3\Delta\gamma_\omega^{(2)} + \dots \quad (\text{B6b})$$

The scheme transformation matrix Z can also be expanded as

$$Z(\omega, \mu^2) = 1 + a_s Z_\omega^{(1)} + a_s^2 Z_\omega^{(2)} + \dots, \quad (\text{B7a})$$

$$Z^{-1}(\omega, \mu^2) = 1 - a_s Z_\omega^{(1)} - a_s^2 \left(Z_\omega^{(2)} - [Z_\omega^{(1)}]^2 \right) + \mathcal{O}(a_s^3). \quad (\text{B7b})$$

The dependence on μ^2 comes solely from the running coupling constant a_s . We start with the first term on the right-hand side of Eq. (B5).

$$\begin{aligned} Z(\omega, \mu^2)\Delta\gamma(\omega)Z^{-1}(\omega, \mu^2) &= a_s\Delta\gamma_\omega^{(0)} + a_s^2 \left(\Delta\gamma_\omega^{(1)} + [Z_\omega^{(1)}, \Delta\gamma_\omega^{(0)}] \right) \\ &+ a_s^3 \left(\Delta\gamma_\omega^{(2)} + [Z_\omega^{(1)}, \Delta\gamma_\omega^{(1)}] + [Z_\omega^{(2)}, \Delta\gamma_\omega^{(0)}] - [Z_\omega^{(1)}, \Delta\gamma_\omega^{(0)}] Z_\omega^{(1)} \right) + \mathcal{O}(a_s^4). \end{aligned} \quad (\text{B8})$$

We then compute the second term on the right-hand side of Eq. (B5) by first noting that

$$\frac{\partial Z(\omega, \mu^2)}{\partial \ln \mu^2} = \frac{da_s}{d \ln \mu^2} Z_\omega^{(1)} + 2a_s \frac{da_s}{d \ln \mu^2} Z_\omega^{(2)} + \dots \quad (\text{B9})$$

Here running coupling constant satisfies the standard renormalization-group equation

$$\frac{da_s}{d \ln \mu^2} = \beta(a_s) = - \sum_{l=0}^{\infty} a_s^{l+2} \beta_l \quad (\text{B10})$$

with the leading coefficients in the large N_c & N_f limit being

$$\beta_0 = \frac{11}{3}N_c - \frac{2}{3}N_f, \quad (\text{B11a})$$

$$\beta_1 = \frac{34}{3}N_c^2 - \frac{13}{3}N_c N_f. \quad (\text{B11b})$$

One then gets

$$\frac{\partial Z(\omega, \mu^2)}{\partial \ln \mu^2} Z^{-1}(\omega, \mu^2) = -a_s^2 \beta_0 Z_\omega^{(1)} - a_s^3 \left(\beta_1 Z_\omega^{(1)} + 2\beta_0 Z_\omega^{(2)} - \beta_0 [Z_\omega^{(1)}]^2 \right) + \mathcal{O}(a_s^4). \quad (\text{B12})$$

Using the above expressions, Eq. (B5) becomes

$$\begin{aligned} &a_s\Delta\bar{\gamma}_\omega^{(0)} + a_s^2\Delta\bar{\gamma}_\omega^{(1)} + a_s^3\Delta\bar{\gamma}_\omega^{(2)} + \mathcal{O}(a_s^4) \\ &= a_s\Delta\gamma_\omega^{(0)} + a_s^2 \left(\Delta\gamma_\omega^{(1)} + [Z_\omega^{(1)}, \Delta\gamma_\omega^{(0)}] - \beta_0 Z_\omega^{(1)} \right) + a_s^3 \left(\Delta\gamma_\omega^{(2)} + [Z_\omega^{(1)}, \Delta\gamma_\omega^{(1)}] + [Z_\omega^{(2)}, \Delta\gamma_\omega^{(0)}] \right. \\ &\quad \left. - [Z_\omega^{(1)}, \Delta\gamma_\omega^{(0)}] Z_\omega^{(1)} - \left(\beta_1 Z_\omega^{(1)} + 2\beta_0 Z_\omega^{(2)} - \beta_0 [Z_\omega^{(1)}]^2 \right) \right) + \mathcal{O}(a_s^4). \end{aligned} \quad (\text{B13})$$

Comparing the left-hand side and the right-hand side of the equation, one arrives at

$$\Delta\bar{\gamma}_\omega^{(0)} = \Delta\gamma_\omega^{(0)}, \quad (\text{B14a})$$

$$\Delta\bar{\gamma}_\omega^{(1)} = \Delta\gamma_\omega^{(1)} + [Z_\omega^{(1)}, \Delta\gamma_\omega^{(0)}] - \beta_0 Z_\omega^{(1)}, \quad (\text{B14b})$$

$$\begin{aligned} \Delta\bar{\gamma}_\omega^{(2)} &= \Delta\gamma_\omega^{(2)} + [Z_\omega^{(1)}, \Delta\gamma_\omega^{(1)}] + [Z_\omega^{(2)}, \Delta\gamma_\omega^{(0)}] - [Z_\omega^{(1)}, \Delta\gamma_\omega^{(0)}] Z_\omega^{(1)} \\ &\quad - \left(\beta_1 Z_\omega^{(1)} + 2\beta_0 Z_\omega^{(2)} - \beta_0 [Z_\omega^{(1)}]^2 \right). \end{aligned} \quad (\text{B14c})$$

From the explicit expressions for the splitting functions in Eq. (93) and in Eq. (94), we have $\Delta\bar{\gamma}_\omega^{(0)} = \Delta\gamma_\omega^{(0)}$ and $\Delta\bar{\gamma}_\omega^{(1)} = \Delta\gamma_\omega^{(1)}$. Eq. (B14b) becomes

$$[Z_\omega^{(1)}, \Delta\gamma_\omega^{(0)}] - \beta_0 Z_\omega^{(1)} = 0. \quad (\text{B15})$$

One can readily see that the only solution is $Z_\omega^{(1)} = 0$. As a result, Eq. (B14c) reduces to

$$\Delta\bar{\gamma}_\omega^{(2)} - \Delta\gamma_\omega^{(2)} = \left[Z_\omega^{(2)}, \Delta\gamma_\omega^{(0)} \right] - 2\beta_0 Z_\omega^{(2)}. \quad (\text{B16})$$

Let us denote the elements of the scheme transformation matrix at order a_s^2 as

$$Z_\omega^{(2)} = \begin{pmatrix} Z_{qq}^{(2)}(\omega) & Z_{qG}^{(2)}(\omega) \\ Z_{Gq}^{(2)}(\omega) & Z_{GG}^{(2)}(\omega) \end{pmatrix}. \quad (\text{B17})$$

The four component equations from the matrix equation in Eq. (B16) are

$$\Delta\bar{\gamma}_{qq}^{(2)}(\omega) - \Delta\gamma_{qq}^{(2)}(\omega) = Z_{qG}^{(2)}(\omega)\Delta\gamma_{Gq}^{(0)}(\omega) - \Delta\gamma_{qG}^{(0)}(\omega)Z_{Gq}^{(2)}(\omega) - 2\beta_0 Z_{qq}^{(2)}(\omega) = 0, \quad (\text{B18a})$$

$$\Delta\bar{\gamma}_{GG}^{(2)}(\omega) - \Delta\gamma_{GG}^{(2)}(\omega) = Z_{Gq}^{(2)}(\omega)\Delta\gamma_{qG}^{(0)}(\omega) - \Delta\gamma_{GG}^{(0)}(\omega)Z_{qG}^{(2)}(\omega) - 2\beta_0 Z_{GG}^{(2)}(\omega) = 0, \quad (\text{B18b})$$

$$\Delta\bar{\gamma}_{qG}^{(2)}(\omega) - \Delta\gamma_{qG}^{(2)}(\omega) = \Delta\gamma_{qG}^{(0)}(\omega) \left(Z_{qq}^{(2)}(\omega) - Z_{GG}^{(2)}(\omega) \right) + Z_{qG}^{(2)}(\omega) \left(\Delta\gamma_{GG}^{(0)}(\omega) - \Delta\gamma_{qq}^{(0)}(\omega) \right), \quad (\text{B18c})$$

$$\Delta\bar{\gamma}_{Gq}^{(2)}(\omega) - \Delta\gamma_{Gq}^{(2)}(\omega) = \Delta\gamma_{Gq}^{(0)}(\omega) \left(Z_{GG}^{(2)}(\omega) - Z_{qq}^{(2)}(\omega) \right) + Z_{Gq}^{(2)}(\omega) \left(\Delta\gamma_{qq}^{(0)}(\omega) - \Delta\gamma_{GG}^{(0)}(\omega) \right). \quad (\text{B18d})$$

The solutions are

$$Z_{GG}^{(2)}(\omega) = -Z_{qq}^{(2)}(\omega), \quad (\text{B19a})$$

$$Z_{qq}^{(2)}(\omega) = \frac{1}{2\beta_0} \left[\frac{\Delta\gamma_{Gq}^{(0)}(\omega)}{\Delta\gamma_{GG}^{(0)}(\omega) - \Delta\gamma_{qq}^{(0)}(\omega)} (\Delta\bar{\gamma}_{qG}^{(2)}(\omega) - \Delta\gamma_{qG}^{(2)}(\omega)) + \frac{\Delta\gamma_{qG}^{(0)}(\omega)}{\Delta\gamma_{GG}^{(0)}(\omega) - \Delta\gamma_{qq}^{(0)}(\omega)} (\Delta\bar{\gamma}_{Gq}^{(2)}(\omega) - \Delta\gamma_{Gq}^{(2)}(\omega)) \right], \quad (\text{B19b})$$

$$Z_{qG}^{(2)}(\omega) = \frac{\Delta\bar{\gamma}_{qG}^{(2)}(\omega) - \Delta\gamma_{qG}^{(2)}(\omega)}{\Delta\gamma_{GG}^{(0)}(\omega) - \Delta\gamma_{qq}^{(0)}(\omega)} - \frac{2\Delta\gamma_{qG}^{(0)}(\omega)}{\Delta\gamma_{GG}^{(0)}(\omega) - \Delta\gamma_{qq}^{(0)}(\omega)} Z_{qq}^{(2)}(\omega), \quad (\text{B19c})$$

$$Z_{Gq}^{(2)}(\omega) = -\frac{\Delta\bar{\gamma}_{Gq}^{(2)}(\omega) - \Delta\gamma_{Gq}^{(2)}(\omega)}{\Delta\gamma_{GG}^{(0)}(\omega) - \Delta\gamma_{qq}^{(0)}(\omega)} - \frac{2\Delta\gamma_{Gq}^{(0)}(\omega)}{\Delta\gamma_{GG}^{(0)}(\omega) - \Delta\gamma_{qq}^{(0)}(\omega)} Z_{qq}^{(2)}(\omega). \quad (\text{B19d})$$

The relevant anomalous dimensions at fixed orders are

$$\Delta\gamma_{qq}^{(0)}(\omega) = N_c \frac{1}{\omega}, \quad \Delta\gamma_{GG}^{(0)}(\omega) = 8N_c \frac{1}{\omega}, \quad \Delta\gamma_{qG}^{(0)}(\omega) = -2N_f \frac{1}{\omega}, \quad \Delta\gamma_{Gq}^{(0)}(\omega) = 2N_c \frac{1}{\omega} \quad (\text{B20})$$

and

$$\Delta\bar{\gamma}_{qG}^{(2)}(\omega) - \Delta\gamma_{qG}^{(2)}(\omega) = 4N_c^2 N_f \frac{1}{\omega^5}, \quad (\text{B21a})$$

$$\Delta\bar{\gamma}_{Gq}^{(2)}(\omega) - \Delta\gamma_{Gq}^{(2)}(\omega) = 4N_c^3 \frac{1}{\omega}. \quad (\text{B21b})$$

Substituting these expressions into Eq. (B19), one obtains

$$Z_{qq}^{(2)}(\omega) = -Z_{GG}^{(2)}(\omega) = 0, \quad (\text{B22a})$$

$$Z_{qG}^{(2)}(\omega) = \frac{4}{7} N_c N_f \frac{1}{\omega^4}, \quad (\text{B22b})$$

$$Z_{Gq}^{(2)}(\omega) = -\frac{4}{7} N_c^2 \frac{1}{\omega^4}. \quad (\text{B22c})$$

In the matrix form this can be written as

$$Z_\omega^{(2)} = \begin{pmatrix} 0 & \frac{4}{7} N_c N_f \frac{1}{\omega^4} \\ -\frac{4}{7} N_c^2 \frac{1}{\omega^4} & 0 \end{pmatrix}. \quad (\text{B23})$$

Transforming back to the x -space, one gets

$$Z^{(2)}(x) = \begin{pmatrix} 0 & \frac{2}{21} N_c N_f \ln^3 \frac{1}{x} \\ -\frac{2}{21} N_c^2 \ln^3 \frac{1}{x} & 0 \end{pmatrix}. \quad (\text{B24})$$

We conclude that the matrix of the scheme transformation relating the splitting functions (94) to those in (93) up to three loops is given by the following matrix (with $a_s = \alpha_s(\mu^2)/4\pi$):

$$Z(x) = \begin{pmatrix} x \delta(1-x) & \frac{2}{21} a_s^2 N_c N_f \ln^3 \frac{1}{x} \\ -\frac{2}{21} a_s^2 N_c^2 \ln^3 \frac{1}{x} & x \delta(1-x) \end{pmatrix}. \quad (\text{B25})$$

- [1] Y. V. Kovchegov, D. Pitonyak and M. D. Sievert, *Helicity Evolution at Small- x* , *JHEP* **01** (2016) 072, [[1511.06737](#)].
- [2] Y. V. Kovchegov and M. D. Sievert, *Small- x Helicity Evolution: an Operator Treatment*, *Phys. Rev.* **D99** (2019) 054032, [[1808.09010](#)].
- [3] F. Cougoulic, Y. V. Kovchegov, A. Tarasov and Y. Tawabutr, *Quark and gluon helicity evolution at small x : revised and updated*, *JHEP* **07** (2022) 095, [[2204.11898](#)].
- [4] G. Altarelli and G. Parisi, *Asymptotic Freedom in Parton Language*, *Nucl. Phys.* **B126** (1977) 298.
- [5] Y. L. Dokshitzer, *Calculation of the Structure Functions for Deep Inelastic Scattering and e^+e^- Annihilation by Perturbation Theory in Quantum Chromodynamics*, *Sov. Phys. JETP* **46** (1977) 641–653.
- [6] R. Mertig and W. L. van Neerven, *The Calculation of the two loop spin splitting functions $P(ij)(1)(x)$* , *Z. Phys. C* **70** (1996) 637–654, [[hep-ph/9506451](#)].
- [7] S. Moch, J. A. M. Vermaseren and A. Vogt, *The Three-Loop Splitting Functions in QCD: The Helicity-Dependent Case*, *Nucl. Phys. B* **889** (2014) 351–400, [[1409.5131](#)].
- [8] J. Borden and Y. V. Kovchegov, *Analytic solution for the revised helicity evolution at small x and large N_c : New resummed gluon-gluon polarized anomalous dimension and intercept*, *Phys. Rev. D* **108** (2023) 014001, [[2304.06161](#)].
- [9] J. Bartels, B. Ermolaev and M. Ryskin, *Flavor singlet contribution to the structure function $G(1)$ at small x* , *Z. Phys.* **C72** (1996) 627–635, [[hep-ph/9603204](#)].
- [10] J. Blümlein and A. Vogt, *The Singlet contribution to the structure function $g_1(x, Q^{*2})$ at small x* , *Phys. Lett. B* **386** (1996) 350–358, [[hep-ph/9606254](#)].
- [11] Y. Hatta, Y. Nakagawa, F. Yuan, Y. Zhao and B. Xiao, *Gluon orbital angular momentum at small- x* , *Phys. Rev.* **D95** (2017) 114032, [[1612.02445](#)].
- [12] Y. V. Kovchegov, D. Pitonyak and M. D. Sievert, *Helicity Evolution at Small x : Flavor Singlet and Non-Singlet Observables*, *Phys. Rev.* **D95** (2017) 014033, [[1610.06197](#)].
- [13] Y. V. Kovchegov, D. Pitonyak and M. D. Sievert, *Small- x asymptotics of the quark helicity distribution*, *Phys. Rev. Lett.* **118** (2017) 052001, [[1610.06188](#)].
- [14] Y. V. Kovchegov, D. Pitonyak and M. D. Sievert, *Small- x Asymptotics of the Quark Helicity Distribution: Analytic Results*, *Phys. Lett.* **B772** (2017) 136–140, [[1703.05809](#)].
- [15] Y. V. Kovchegov, D. Pitonyak and M. D. Sievert, *Small- x Asymptotics of the Gluon Helicity Distribution*, *JHEP* **10** (2017) 198, [[1706.04236](#)].
- [16] Y. V. Kovchegov, *Orbital Angular Momentum at Small x* , *JHEP* **03** (2019) 174, [[1901.07453](#)].
- [17] R. Boussarie, Y. Hatta and F. Yuan, *Proton Spin Structure at Small- x* , *Phys. Lett.* **B797** (2019) 134817, [[1904.02693](#)].
- [18] F. Cougoulic and Y. V. Kovchegov, *Helicity-dependent generalization of the JIMWLK evolution*, *Phys. Rev.* **D100** (2019) 114020, [[1910.04268](#)].
- [19] Y. V. Kovchegov and Y. Tawabutr, *Helicity at Small x : Oscillations Generated by Bringing Back the Quarks*, *JHEP* **08** (2020) 014, [[2005.07285](#)].
- [20] F. Cougoulic and Y. V. Kovchegov, *Helicity-dependent extension of the McLerran-Venugopalan model*, *Nucl. Phys. A* **1004** (2020) 122051, [[2005.14688](#)].
- [21] G. A. Chirilli, *High-energy operator product expansion at sub-eikonal level*, *JHEP* **06** (2021) 096, [[2101.12744](#)].
- [22] Y. V. Kovchegov, A. Tarasov and Y. Tawabutr, *Helicity evolution at small x : the single-logarithmic contribution*, *JHEP* **03** (2022) 184, [[2104.11765](#)].
- [23] D. Adamiak, Y. V. Kovchegov and Y. Tawabutr, *Helicity evolution at small x : Revised asymptotic results at large N_c and N_f* , *Phys. Rev. D* **108** (2023) 054005, [[2306.01651](#)].
- [24] A. H. Mueller, *Soft gluons in the infinite momentum wave function and the BFKL pomeron*, *Nucl. Phys.* **B415** (1994) 373–385.
- [25] A. H. Mueller and B. Patel, *Single and double BFKL pomeron exchange and a dipole picture of high-energy hard processes*, *Nucl. Phys.* **B425** (1994) 471–488, [[hep-ph/9403256](#)].
- [26] A. H. Mueller, *Unitarity and the BFKL pomeron*, *Nucl. Phys.* **B437** (1995) 107–126, [[hep-ph/9408245](#)].
- [27] I. Balitsky, *Operator expansion for high-energy scattering*, *Nucl. Phys.* **B463** (1996) 99–160, [[hep-ph/9509348](#)].
- [28] I. Balitsky, *Factorization and high-energy effective action*, *Phys. Rev.* **D60** (1999) 014020, [[hep-ph/9812311](#)].

- [29] Y. V. Kovchegov, *Small- x F_2 structure function of a nucleus including multiple pomeron exchanges*, *Phys. Rev.* **D60** (1999) 034008, [hep-ph/9901281].
- [30] Y. V. Kovchegov, *Unitarization of the BFKL pomeron on a nucleus*, *Phys. Rev.* **D61** (2000) 074018, [hep-ph/9905214].
- [31] J. Jalilian-Marian, A. Kovner and H. Weigert, *The Wilson renormalization group for low x physics: Gluon evolution at finite parton density*, *Phys. Rev.* **D59** (1998) 014015, [hep-ph/9709432].
- [32] J. Jalilian-Marian, A. Kovner, A. Leonidov and H. Weigert, *The Wilson renormalization group for low x physics: Towards the high density regime*, *Phys. Rev.* **D59** (1998) 014014, [hep-ph/9706377].
- [33] H. Weigert, *Unitarity at small Bjorken x* , *Nucl. Phys.* **A703** (2002) 823–860, [hep-ph/0004044].
- [34] E. Iancu, A. Leonidov and L. D. McLerran, *The renormalization group equation for the color glass condensate*, *Phys. Lett.* **B510** (2001) 133–144.
- [35] E. Iancu, A. Leonidov and L. D. McLerran, *Nonlinear gluon evolution in the color glass condensate. I*, *Nucl. Phys.* **A692** (2001) 583–645, [hep-ph/0011241].
- [36] E. Ferreiro, E. Iancu, A. Leonidov and L. McLerran, *Nonlinear gluon evolution in the color glass condensate. II*, *Nucl. Phys.* **A703** (2002) 489–538, [hep-ph/0109115].
- [37] EUROPEAN MUON collaboration, J. Ashman et al., *A Measurement of the Spin Asymmetry and Determination of the Structure Function $g(1)$ in Deep Inelastic Muon-Proton Scattering*, *Phys. Lett. B* **206** (1988) 364.
- [38] R. L. Jaffe and A. Manohar, *The $G(1)$ Problem: Fact and Fantasy on the Spin of the Proton*, *Nucl. Phys.* **B337** (1990) 509–546.
- [39] X.-D. Ji, *Gauge-Invariant Decomposition of Nucleon Spin*, *Phys. Rev. Lett.* **78** (1997) 610–613, [hep-ph/9603249].
- [40] D. Boer et al., *Gluons and the quark sea at high energies: Distributions, polarization, tomography*, 1108.1713.
- [41] C. A. Aidala, S. D. Bass, D. Hasch and G. K. Mallot, *The Spin Structure of the Nucleon*, *Rev. Mod. Phys.* **85** (2013) 655–691, [1209.2803].
- [42] A. Accardi et al., *Electron Ion Collider: The Next QCD Frontier*, *Eur. Phys. J.* **A52** (2016) 268, [1212.1701].
- [43] E. Leader and C. Lorcé, *The angular momentum controversy: What’s it all about and does it matter?*, *Phys. Rept.* **541** (2014) 163–248, [1309.4235].
- [44] E. C. Aschenauer et al., *The RHIC Spin Program: Achievements and Future Opportunities*, 1304.0079.
- [45] E.-C. Aschenauer et al., *The RHIC SPIN Program: Achievements and Future Opportunities*, 1501.01220.
- [46] A. Prokudin, Y. Hatta, Y. Kovchegov and C. Marquet, eds., *Proceedings, Probing Nucleons and Nuclei in High Energy Collisions: Dedicated to the Physics of the Electron Ion Collider: Seattle (WA), United States, October 1 - November 16, 2018*, WSP, 2020. 10.1142/11684.
- [47] X. Ji, F. Yuan and Y. Zhao, *What we know and what we don’t know about the proton spin after 30 years*, *Nature Rev. Phys.* **3** (2021) 27–38, [2009.01291].
- [48] R. Abdul Khalek et al., *Science Requirements and Detector Concepts for the Electron-Ion Collider: EIC Yellow Report*, 2103.05419.
- [49] JEFFERSON LAB ANGULAR MOMENTUM collaboration, D. Adamiak, Y. V. Kovchegov, W. Melnitchouk, D. Pitonyak, N. Sato and M. D. Sievert, *First analysis of world polarized DIS data with small- x helicity evolution*, *Phys. Rev. D* **104** (2021) L031501, [2102.06159].
- [50] JEFFERSON LAB ANGULAR MOMENTUM (JAM) collaboration, D. Adamiak, N. Baldonado, Y. V. Kovchegov, W. Melnitchouk, D. Pitonyak, N. Sato et al., *Global analysis of polarized DIS and SIDIS data with improved small- x helicity evolution*, *Phys. Rev. D* **108** (2023) 114007, [2308.07461].
- [51] T. Altinoluk, N. Armesto, G. Beuf, M. Martinez and C. A. Salgado, *Next-to-eikonal corrections in the CGC: gluon production and spin asymmetries in pA collisions*, *JHEP* **07** (2014) 068, [1404.2219].
- [52] I. Balitsky and A. Tarasov, *Rapidity evolution of gluon TMD from low to moderate x* , *JHEP* **10** (2015) 017, [1505.02151].
- [53] I. Balitsky and A. Tarasov, *Gluon TMD in particle production from low to moderate x* , *JHEP* **06** (2016) 164, [1603.06548].
- [54] G. A. Chirilli, *Sub-eikonal corrections to scattering amplitudes at high energy*, *JHEP* **01** (2019) 118, [1807.11435].
- [55] J. Jalilian-Marian, *Quark jets scattering from a gluon field: from saturation to high p_t* , *Phys. Rev.* **D99** (2019) 014043, [1809.04625].
- [56] J. Jalilian-Marian, *Rapidity loss, spin, and angular asymmetries in the scattering of a quark from the color field of a proton or nucleus*, *Phys. Rev. D* **102** (2020) 014008, [1912.08878].
- [57] T. Altinoluk, G. Beuf, A. Czakajka and A. Tymowska, *Quarks at next-to-eikonal accuracy in the CGC: Forward quark-nucleus scattering*, *Phys. Rev. D* **104** (2021) 014019, [2012.03886].
- [58] R. Boussarie and Y. Mehtar-Tani, *Gauge invariance of transverse momentum dependent distributions at small x* , *Phys. Rev. D* **103** (2021) 094012, [2001.06449].
- [59] R. Boussarie and Y. Mehtar-Tani, *A novel formulation of the unintegrated gluon distribution for DIS*, *Phys. Lett. B* **831** (2022) 137125, [2006.14569].
- [60] Y. V. Kovchegov and M. G. Santiago, *Quark sivers function at small x : spin-dependent odderon and the sub-eikonal evolution*, *JHEP* **11** (2021) 200, [2108.03667].
- [61] T. Altinoluk and G. Beuf, *Quark and scalar propagators at next-to-eikonal accuracy in the CGC through a dynamical background gluon field*, *Phys. Rev. D* **105** (2022) 074026, [2109.01620].
- [62] Y. V. Kovchegov and M. G. Santiago, *T -odd leading-twist quark TMDs at small x* , *JHEP* **11** (2022) 098, [2209.03538].
- [63] T. Altinoluk, G. Beuf, A. Czakajka and A. Tymowska, *DIS dijet production at next-to-eikonal accuracy in the CGC*, *Phys. Rev. D* **107** (2023) 074016, [2212.10484].
- [64] T. Altinoluk, N. Armesto and G. Beuf, *Probing quark transverse momentum distributions in the color glass condensate: Quark-gluon dijets in deep inelastic scattering at next-to-eikonal accuracy*, *Phys. Rev. D* **108** (2023) 074023, [2303.12691].

- [65] T. Altinoluk, G. Beuf and J. Jalilian-Marian, *Renormalization of the gluon distribution function in the background field formalism*, 2305.11079.
- [66] M. Li, *Small x physics beyond eikonal approximation: an effective Hamiltonian approach*, *JHEP* **07** (2023) 158, [2304.12842].
- [67] G. 't Hooft, *Can We Make Sense Out of Quantum Chromodynamics?*, *Subnucl. Ser.* **15** (1979) 943.
- [68] G. Veneziano, *Some Aspects of a Unified Approach to Gauge, Dual and Gribov Theories*, *Nucl. Phys. B* **117** (1976) 519–545.
- [69] V. N. Gribov and L. N. Lipatov, *Deep inelastic $e p$ scattering in perturbation theory*, *Sov. J. Nucl. Phys.* **15** (1972) 438–450.
- [70] E. B. Zijlstra and W. L. van Neerven, *Order- α_s^2 corrections to the polarized structure function $g_1(x, Q^2)$* , *Nucl. Phys. B* **417** (1994) 61–100.
- [71] S. Moch and J. A. M. Vermaseren, *Deep inelastic structure functions at two loops*, *Nucl. Phys. B* **573** (2000) 853–907, [hep-ph/9912355].
- [72] W. L. van Neerven and A. Vogt, *NNLO evolution of deep inelastic structure functions: The Singlet case*, *Nucl. Phys. B* **588** (2000) 345–373, [hep-ph/0006154].
- [73] J. A. M. Vermaseren, A. Vogt and S. Moch, *The Third-order QCD corrections to deep-inelastic scattering by photon exchange*, *Nucl. Phys. B* **724** (2005) 3–182, [hep-ph/0504242].
- [74] J. Blümlein, P. Marquard, C. Schneider and K. Schönwald, *The three-loop polarized singlet anomalous dimensions from off-shell operator matrix elements*, *JHEP* **01** (2022) 193, [2111.12401].
- [75] J. Blümlein and M. Saragnese, *The N³LO scheme-invariant QCD evolution of the non-singlet structure functions $F_2NS(x, Q^2)$ and $g_1NS(x, Q^2)$* , *Phys. Lett. B* **820** (2021) 136589, [2107.01293].
- [76] J. Davies, C. H. Kom, S. Moch and A. Vogt, *Resummation of small- x double logarithms in QCD: inclusive deep-inelastic scattering*, *JHEP* **08** (2022) 135, [2202.10362].
- [77] J. Blümlein, P. Marquard, C. Schneider and K. Schönwald, *The massless three-loop Wilson coefficients for the deep-inelastic structure functions F_2 , F_L , xF_3 and g_1* , *JHEP* **11** (2022) 156, [2208.14325].
- [78] V. G. Gorshkov, V. N. Gribov, L. N. Lipatov and G. V. Frolov, *Doubly logarithmic asymptotic behavior in quantum electrodynamics*, *Sov. J. Nucl. Phys.* **6** (1968) 95.
- [79] R. Kirschner and L. Lipatov, *Double Logarithmic Asymptotics and Regge Singularities of Quark Amplitudes with Flavor Exchange*, *Nucl. Phys.* **B213** (1983) 122–148.
- [80] R. Kirschner, *Reggeon interactions in perturbative QCD*, *Z. Phys.* **C65** (1995) 505–510, [hep-th/9407085].
- [81] R. Kirschner, *Regge asymptotics of scattering with flavor exchange in QCD*, *Z. Phys.* **C67** (1995) 459–466, [hep-th/9404158].
- [82] S. Griffiths and D. Ross, *Studying the perturbative Reggeon*, *Eur. Phys. J.* **C12** (2000) 277–286, [hep-ph/9906550].
- [83] J. Bartels, B. Ermolaev and M. Ryskin, *Nonsinglet contributions to the structure function g_1 at small x* , *Z. Phys.* **C70** (1996) 273–280, [hep-ph/9507271].
- [84] G. P. Lepage and S. J. Brodsky, *Exclusive processes in perturbative quantum chromodynamics*, *Phys. Rev.* **D22** (1980) 2157.
- [85] S. J. Brodsky, H.-C. Pauli and S. S. Pinsky, *Quantum chromodynamics and other field theories on the light cone*, *Phys. Rept.* **301** (1998) 299–486, [hep-ph/9705477].
- [86] Y. V. Kovchegov and M. D. Sievert, *Calculating TMDs of a Large Nucleus: Quasi-Classical Approximation and Quantum Evolution*, *Nucl. Phys.* **B903** (2016) 164–203, [1505.01176].
- [87] S. A. Larin and J. A. M. Vermaseren, *The α_s^3 corrections to the Bjorken sum rule for polarized electroproduction and to the Gross-Llewellyn Smith sum rule*, *Phys. Lett. B* **259** (1991) 345–352.
- [88] S. A. Larin, *The Renormalization of the axial anomaly in dimensional regularization*, *Phys. Lett. B* **303** (1993) 113–118, [hep-ph/9302240].
- [89] J. Blümlein and M. Saragnese, *Next-to-Next-to-Leading Order Evolution of Polarized Parton Densities in the Larin Scheme*, 2405.17252.
- [90] D. Binosi and L. Theußl, *Jaxodraw: A graphical user interface for drawing feynman diagrams*, *Computer Physics Communications* **161** (2004) 76–86.
- [91] Y. Tawabutr, *Helicity of Quarks and Gluons at Small Bjorken x* , Ph.D. thesis, The Ohio State University, Ohio State U., 2022. 2306.10361.
- [92] Y. V. Kovchegov and E. Levin, *Quantum chromodynamics at high energy*, vol. 33. Cambridge University Press, 2012.